Summer 2008

Modification of Nitinol Nickel and Titanium Oxides with Self-Assembled Monolayers and POlymers for Corrosion Mitigation in Biomtaerial Applications

Rosalynn Quinones-Fernandez

MODIFICATION OF NITINOL NICKEL AND TITANIUM OXIDES WITH SELF-ASSEMBLED MONOLAYERS AND POLYMERS FOR CORROSION MITIGATION IN BIOMATERIAL APPLICATIONS

A Dissertation

Submitted to Bayer School

of Natural and Environmental Sciences

Duquesne University

In partial fulfillment of the requirements for

the degree of Doctor of Philosophy

By

Rosalynn Quiñones-Fernández

July 2008

MODIFICATION OF NITINOL

NICKEL AND TITANIUM OXIDES

WITH SELF-ASSEMBLED MONOLAYERS AND POLYMERS

FOR CORROSION MITIGATION IN BIOMATERIAL APPLICATIONS

By

Rosalynn Quiñones-Fernández

Approved

_____ Dr. Ellen S. Gawalt Asst. Professor of Chemistry and Biochemistry Duquesne University (Dissertation Advisor)	_____ Dr. Jeffrey D. Evanseck Professor of Chemistry and Biochemistry Duquesne University (Committee Member)
_____ Dr. Jennifer A. Aitken Asst. Professor of Chemistry and Biochemistry Duquesne University (Committee Member)	_____ Dr. Joshua A. Maurer Asst. Professor of Chemistry Washington University in St. Louis (Outside Reader)
_____ Dr. David W. Seybert Dean, Bayer School of Natural & Environmental Science Professor of Chemistry & Biochemistry Duquesne University	_____ Dr. Jeffry D. Madura Chair, Department of Chemistry & Biochemistry Professor of Chemistry & Biochemistry Duquesne University

ABSTRACT

MODIFICATION OF NITINOL

NICKEL AND TITANIUM OXIDES

WITH SELF-ASSEMBLED MONOLAYERS AND POLYMERS

FOR CORROSION MITIGATION IN BIOMATERIAL APPLICATIONS

By:

Rosalynn Quiñones-Fernández

July 2008

Dissertation Supervised by: Dr. Ellen S. Gawalt

For the first time Self-Assembled Monolayers (SAMs) were formed on nitinol and characterized. Factors which can affect the formation of SAMs such as head groups, chain length, and tail groups were varied and analyzed to form the most stable and strongly adhered monolayer on the surface. Since an alloy is being studied, the formation of SAMs was also studied on nickel and titanium oxide, the components of the nitinol surface. After data was collected by infrared spectroscopy (IR), atomic force microscopy (AFM), matrix-assisted laser desorption ionization mass spectrometry (MALDI), and contact angle measurements on the modified substrates. In the long term, the formation of strongly adhered self-assembled monolayers may form an effective interface between the biomaterial, nitinol, and the human body.

DEDICATION

I want to dedicate this dissertation to my family especially my son Jose Antonio Buxó and my husband Jose Francisco Buxó. They are a really important part of my life, dreams and hopes. My son was born while I was studying and he is the one who taught me how to balance my personal and professional life without putting him aside. Without my husband I could not have made this big step because he sacrificed so much by coming to another country leaving his family for me, and also the time that he took care of our son is grateful. Not all men would do something like he did and I really am thankful for it.

I want to also thank my grandmother Ana M. Tirado who comes every couple of months to help, give me support and her company. She has been with me all of my life and I consider her my second mother.

In my time completing my studies I lost my paternal grandmother Cristina Rivera. From her I learned to be humble, and kind hearted and not to forget my heritage. I want to dedicate my thesis to her memory because I was her oldest granddaughter and I know how proud she would be. She is watching and taking care of me from heaven.

Finally last but not least I want to dedicate my dissertation to my friends who were being always supportive of me. Jean C. Sanchez, Milrely and Roberto Aponte, Xaymara Navarrete, Luz I. Garcia, and Antonio Delgado are some of the forever friends we always carry in our heart.

I want to dedicate also this to my family: mom, dad, brothers, grandfather Gerardo and my family in-law as well. God knows how much I miss my family, friends,

and country Puerto Rico although some sacrifices had to be made for me to be where I am now.

ACKNOWLEDMENT

First, I would like to thank my thesis advisor Dr. Ellen S. Gawalt for her dedication, time and persistence with me. Also, I thank my PhD committee member: Dr. Jeffrey Evanseck, Dr. Jennifer Aitken and my outside reader Dr. Joshua Maurer.

I want to thank Dr. Toby Chapman and his student Peter Bell (Department of Chemistry- University of Pittsburgh) for use of the contact angle meter, Dr. Stephanie Wetzel (Department of Chemistry- Duquesne University) for help in using the MALDI-TOF, and Dr. Thomas E. Mallouk (Department of Chemistry- Penn State University) for providing us with undecylphosphonic acid.

Also, I thank Dr. Partha Basu and Dr. Shahed Khan and their students Eranda Perera and Dr. Yasser Shaban (Department of Chemistry- Duquesne University) for the use of the cyclic voltammograms and Dr. X. Tracy Cui and her student Nicholas Alba (Department of Bioengineering- University of Pittsburgh) for the use of the electrochemical impedance spectroscopy. I thank Dr. Aleem Gangjee (Mylan School of Pharmacy-Duquesne University) for the use of the hydrogenator. I show gratitude to Nathan Takas, Kristin Kroniser, Jonathan Lekse and Sarah Johnson for their help and assistance with instruments. Moreover, I thank the instrumentation technicians because without them the instruments would not be up and running when they broke. Lauren Matosziuk thanks for your scheme and figures.

I thank past and present members of Dr. Gawalt's research group for the team work and being like a family in the lab: Dr. Aparna Raman, Kelly Keller, Lisa N.

Barriger, Brian Disalle, Shelby Hott, Anthony Ross and Rachelle Palchesko. Amy Stroyne Sandy Russell and Carolina Martine thank you for your time and dedication.

TABLE OF CONTENT

Page

LIST OF TABLES

Page

LIST OF FIGURES

Page

Chapter 1

Introduction

1.1 Introduction

In 1935, Langmuir published his first work on the study of two-dimensional systems of molecular films at the gas-liquid interface.[1] The Langmuir-Blodgett (LB) was the first technique to provide the capability to construct ordered molecular assemblies.[1-4] However, the process to form LB films can be difficult due to the expense of the equipment involved and the need for meticulous control of atmospheric, temperature, humidity conditions in the laboratory.[5] Over the last 30 years, self-assembled monolayers (SAMs) of octadecyltrichhlorosilane (OTS) were introduced as a possible alternative to LB systems.[4] Subsequently, self-assembled monolayers (SAMs) have been utilized to form organic thin films on surfaces by immersion,[6-11] vapor deposition[12, 13] or aerosol spraying[10, 14-16] on an appropriate substrate with a variety of organics such as thiols and organic acids.[8, 10, 17-32] The major limitation with the self-assembly process is that multilayer films are possible, in contrast to LB films where the monolayer formation is controlled by using constant surface pressure.

A SAM can be divided into three parts: head group, alkyl chain and terminal functional group. (Figure 1.1) The head group provides the chemisorption on the solid

surface. The affinity of the molecule for the surface is dependent upon its interaction with the active site on the surface, such as the hydroxyls or μ-oxo oxygen groups. This part of SAM formation is an exothermic and spontaneous reaction between the head group and the binding sites on the surface.[5] The alkyl chains contribute to SAM formation and stability through van der Waals interactions. Therefore, an ordered, densely packed film with highly oriented molecules is expected with long alkyl chains that can contribute significantly to the energetic stability of the film and offset the entropic penalties of film formation. However, when a bulky head or tail group is used to form SAMs, the packing density of the film can be lower and the alkyl chains can be pushed away from each other and the van der Waals contribution is minimized. In this scenario, the alkyl chains are disordered and contain gauche interactions. [33, 34] Additionally, tail group functionality can be varied to affect SAM formation and stability, and change the surface from being hydrophilic to hydrophobic. Different functional groups are amines,[35-41] methyl,[8, 9, 14, 16, 28, 37, 42-44] carboxylic acid, [11, 14, 15, 24, 30, 37, 45, 46] and hydroxyls.[24, 28, 37, 42, 43, 47, 48] Other intermolecular interactions can be detected among the tail groups, such as hydrogen bonding networks and dipole interactions.[19, 39, 49-52] However, if the tail and the headgroup are hydrophilic, then the two can adsorb on the metal oxide surface or with each other.[46] This can lead to multilayer film formation. Therefore, in order for monolayer formation to be successful, the interactions and identity of the head, tail and alkyl chain length must be carefully chosen and their effects analyzed.

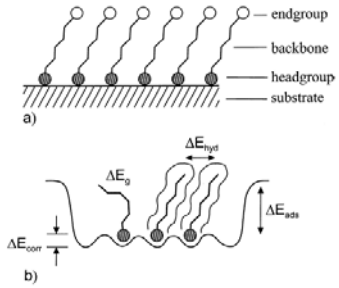

Figure 1.1 (a) Schematic of a SAM. Shaded circles indicate chemisorb headgroup, where open circles endgroups, which can be chosen from variety of chemical functionalities. (b) Schematic of different energies. ΔE_{ads} stands for adsorption energy, ΔE_{corr} corrugation of substrate potential experienced by molecule, ΔE_{hyd} van der Waals interaction of the alkyl chain, and ΔE_g energy of gauche defect or disordered films.[53]

In 1983, Nuzzo and Allara published the first paper using dialkylsulfides to form SAMs on gold.[54] Alkanethiols on gold have been utilized in model systems for various purposes, including corrosion resistance,[48, 55, 56] adhesion,[57, 58] and biosensors.[59-61] Thiols generally do not adhere to metal oxides or are easily removed by rinsing. Alkanethiols are frequently used to study SAMs on gold because of the strong S-Au bond, which generates densely packed arrays of Au thiolates that have an average tilt angle of 27- 48º from the normal of the surface.[7, 19, 21, 48, 59, 62-67] However, the formation of well-ordered and strong alkanethiol monolayers has been limited to metal oxide surfaces.[68] Researchers have used long-chain organic acids (carboxylic, sulfonic, hydroxamic, phosphonic) on some metal oxides, but these acids have been studied far less than alkanethiols on gold.[16, 25, 27, 28, 69-71] Some examples of spontaneous adsorption of long monolayers on metal oxides are carboxylic acids on copper,[23, 72]aluminum, [17, 70, 73] and stainless steel oxides.[8, 9, 74, 75] Phosphonic acids have been used to form robust and

ordered films on relatively inert oxide surfaces, such as titanium and stainless steel.[8, 16, 24, 26, 27, 71, 76] Aside from these systems, new and innovative combination of monolayers and surfaces have been created and analyzed.[27, 44, 48, 60, 61, 77-93] For example, organic thin films have been made that contain benzene, polymers, intramolecular unsaturated chains, salts, gradient surfaces, proteins and carbohydrates on a variety of surfaces.[27, 44, 48, 60, 61, 77-93]

The development of advanced analytical tools for the study of thin organic films has been reported over the last decade.[15, 25, 42, 46, 49, 94-105] Infrared spectroscopy is a routine tool for the study of molecular packing and orientation of organic thin films. Snyder et al. reported that the packing of polyethylene lead to higher stretching frequencies as the length of the alkyl chain decreased.[106, 107] Specifically, Snyder et al. have reported 2920 cm^{-1} for the $\nu_{CH\ asym}$ mode in crystalline polyethylene, which is 8 cm^{-1} lower than the peak position for polyethylene in the liquid state (2928 cm^{-1}).[106] They also reported that 2850 cm^{-1} is the wavenumber for $\nu_{CH\ sym}$ in crystalline polyethylene, which is 6 cm^{-1} lower than the peak value in the liquid state (2856 cm^{-1}). These results have been verified using FTIR on monolayers and thin films.[9, 16, 17, 21, 28, 32, 44, 64, 66, 108] Due to the ease of analysis, the correlation between CH_2 symmetric and asymmetric stretching is the most common method of determining alkyl chain ordering. Changes in order have been found to be due to variations in interactions between the different functional groups, chain length and surfaces.[8, 9, 16-18, 21, 23, 28, 44, 46, 56, 57, 66, 70, 73, 108]

Condensed (ordered) films contain rigid molecules due to more energetically favorable interactions between alkyl chains of each molecule and the molecules resulting in a closely packed monolayer.(Figure 1.2) Alkyl chains in condensed films have all

trans or anti conformations. Tail-tail interactions of the molecules can be strong and aid in aligning the molecules such as by van der Waals and hydrogen bonding interactions. In dilute (disordered) films the alkyl chain may have mobility with in the film and weaker adhesion to the surface. (Figure 1.2) Alkyl chains in dilute films (disordered monolayers) contain *gauche* or cis conformations.

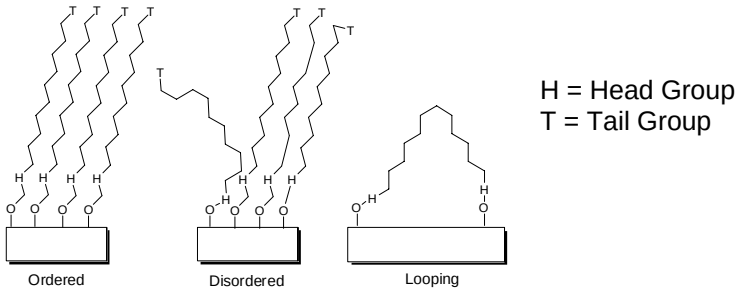

Figure 1.2 How SAMs can be organized on a solid surface: ordered (solid-like) or disordered (liquid-like) or looping.

One of the instruments commonly used to analyze the wettability on the surface is the contact angle goniometer.[8-10, 14, 15, 39, 40, 109, 110] The wettability of the surface relates to the quality of stable organic thin films.[5, 20] This is due to the fact the shape of a liquid drop on a planar, homogenous surface is affected by the free energy of the interactions between the liquid drop at the surface.[111, 112] When a liquid does not wet a surface completely it forms a droplet, an angle θ results, which is the contact angle between the surface beneath the droplet and the tangent to the surface. (Figure 1.3) The angle of a drop is the result of the balance between the cohesive forces in the liquid and the adhesive forces between the liquid and the solid.[5, 34] If there is no interaction between the liquid and the solid, the contact angle will be 180° (ultrahydrophobic) and as the

interaction increases the liquid drop spreads until $\theta = 0°$.[113-115] Usually, the contact angles of methyl terminated group closely packed SAMs from a smooth solid surface with water are $\theta = 105\text{-}115°$.[8, 16, 17, 21, 28, 32, 66, 116, 117] Different techniques can be used to measure the contact angle, but the most common method is the sessile drop.[5, 21, 66] In the sessile drop, a image is recorded after the liquid drop becomes stationary on the surface.[118] In the captive drop method, a needle has to be kept in the drop and if the drop falls, the contact angles values becomes lower and therefore, not accurate. Variability in contact angles may arise due to surface roughness, because it is difficult to compare surfaces that have similar compositions, but different degrees of roughness.[113, 119] Ideally, the solid surface should be smooth to apply the theory of the contact angles and wetting. If the surface is rather rough, the apparent contact angles will be affected by the thermodynamics and kinetics associated with such structures.[34] For example, if the "true" contact angle of a liquid is less than 90° on the smooth surface, the angle will be even smaller on a rough surface. For a true contact angle higher than 90°, roughness could increase the apparent contact angle. [34, 113, 119]

For disordered monolayers the contact angle decreases as the methylene groups are more exposed to the surface.[5] Therefore, as the alkyl chain length is reduced contact angles tend to vary. The contact angle measurements are taken on different areas of the surface at least three times and an average of the values are calculated.

Figure 1.3 Liquid drop in a solid surface using the sessile drop. Methyl terminated group was used in this image.

An important tool to analyze the surface of thin organic films is the atomic force microscope (AFM). AFM can measure the morphology and properties of surfaces on the atomic scale of a wide variety of samples.[120] These include Langmuir-Blodgett (LB) films,[22, 29, 121, 122] SAMs,[6, 123, 124] polymers,[125-127] and biological materials.[122, 128-130] Also, this microscopic technique can be used to measure topography, and surface hardness at the nanometer scale. AFM, in contrast to scanning tunneling microscope (STM), can image both conductor and nonconducting surfaces with atomic resolution.[131] AFM operates by measuring the forces between the sample and the probe. These forces are highly dependent on the nature of the sample, the spring constant of the probe, the distance between the probe and the sample, and any contamination on the sample surface.[131] There are two common modes in AFM imaging; contact and noncontact modes which, if either are known as tapping mode. In contact mode, the tip is in direct contact to the surface and the repulsive forces can be measured due to the interatomic forces that induce bending of the cantilever. This bending is detected by a laser beam that is reflected off the back of the cantilever on the photodiode. This mode also is

known as the repulsive mode.[120, 131, 132] In noncontact mode, the van der Waals interactions act between the tip and the sample and the tip is oscillating close to its resonance frequency during the scans. The advantage of the noncontact mode is that the sample is not damaged during the scan. However, the resolution is lower than in contact mode.[131-133]

SAMs are ideal for AFM studies because the modified surfaces are smooth, structurally ordered and chemically defined at the microscopic scale.[130] The AFM is used to obtain the film height of adsorbed molecules on surfaces. The roughness analysis on the two-dimensional topography image was based on a calculation of the standard deviation of all height values within the given imaged area (root-mean-square-roughness (rms)).[8] Besides this method, using contact mode the surface can be scratched with either an AFM cantilever or a sharp needle in a defined area to reveal the bare surface removing the modification and the film height is subsequently measured. However, if the needle goes deep on the surface it can remove a deeper on the surface to an inner layer. The AFM images also give information about the roughness of the bare surface, the completeness or formation of micelles (defects) created by the SAMs modifications on the surfaces. As the SAMs structure becomes disordered, weaker van der Waals interactions are observed between the tip and the surface and therefore, the tip is able to penetrate deeper into the monolayer accompanied by an increase in contact area.[124]

Electrochemical techniques like cyclic voltammetry (CV) and impedance measurements (EIS) are easy techniques for monitoring monolayer characteristics.[7, 56, 62, 63, 134, 135] EIS is an effective method of determining a film's protective properties by measuring the resistive and capacitive characteristics of the coating. It has been widely

used to evaluate the barrier properties of SAMs.[136, 137] Organic films confined to electrodes can affect charge transfer resistance (R_{ct}), interfacial capacitance, as transport of reactants to the electrode surface and, the apparent heterogeneous, rate constant for electron transfer (k°).[138] These electrochemical studies also provide useful information about the distribution of defects like pinholes, redox property of attached groups (ferrocene, and simple bipyridine molecules), kinetics and mechanism of monolayer formation, and quantitative estimate of coverage.[7, 56, 62, 137, 139] Similarly, impedance measurements can provide valuable information about the kinetics of monolayer formation, and a rough estimate of the dielectric constant of the film is also possible.[63, 139, 140] The impedance technique is especially well-suited for studies on thin films because the very small ac perturbation causes only minimal changes in the coverage or the structure of the film compared to cyclic voltammetry analysis in which can occur electrochemical reactions at the interface.[55, 63, 138, 141, 142]

EIS data can be graphed using a Nyquist diagrams which is plotted of $Z^{''}$ (imaginary part of the impedance) versus $Z^{'}$ (the real part of the impedance). Each point represents the values of the $Z^{'}$ and $Z^{''}$ at specific frequency. For a reversible reaction at a solid interface, these plots typically exhibit two important regions: a semicircle at high frequencies, which describes the faradaic electron transfer process and a straight region at lower frequencies, which depicts the diffusion limited transport of the redox species from the electrolyte to the electrode interface.[132, 133, 143] The R_{ct} is expected to increase due to the inhibition of the electron transfer by the organic film present on the electrode surface. In the Nyquist plot, the protection efficiency or the approximate film surface coverage can be calculated as well other useful electrochemical data using the reference of the

charge transfer resistance (R_{ct}). Further details of the charge transfer resistance are explained in more details in Chapter 5.

These techniques have been used to study corrosion inhibition systems which utilize thin films. For example, gold is the most common noble metal used to be modified with thiols SAMs and these systems are well-known for corrosion protection.[7, 55, 56, 62, 63, 142-145] However, noble metals are not used for engineering applications, and thiols are toxic and have a strong odor. Therefore, researchers have been trying to find other environmental friendly molecules which can have the same or even better corrosion protection than thiols such as long organic acids on metal oxide surfaces.[22, 29, 137, 146-149] One of the first metal oxide surfaces modified using thiols was copper.[150] The oxidation barrier by the SAMs was studied using XPS analysis.[150] In this report, it was demonstrated that the ability of SAMs to control the oxidation on the copper surface as the length of the molecules was increased and subsequently, the thiols also were oxidized in the process to sulfonates.[150] Phosphonates are anodic inhibitors which protect steel mostly in neutral and slightly alkaline solutions and also these compounds are less toxic.[146] Moreover, phosphonic films exhibit outstanding corrosion protection by EIS analysis which indicates a large charge transfer resistance (R_{ct}) from a blocking effect on the surface.[146] The blocking behavior attributed to SAMs is due to the densely packed structure of the alkyl chains which impede the approach of solution ions and molecules to the electrode surface.[55, 142] However, pinholes and other defects can be observed after long periods of time which permit a close approach of solution species and therefore the protection efficiency of the film decreases and SAMs can not behave as a pure capacitor.[139, 151]

1.2 Applications of SAMs

The control of surfaces impact systems such as biomaterials, electronic devices, chemical or biological sensors.[59, 152] SAM systems can be used as a protective coating for electronic applications, due to their ability to control the corrosion that can reduce performance and device lifetime on metal surfaces, such as copper, iron, and nickel.[29, 69, 137, 139, 147, 148, 153-156] Control of wetting properties is an advantage in the areas of biocompatibility, friction and lubrication. Moreover, mixed monolayers can be tailored on the nanometer scale by photopatterning, microprinting, and electrochemical treatments.[40, 59, 61, 80, 157-159] SAMs can also be easily functionalized with polymers, DNA and carbohydrates by reaction at the interface of the organic monolayers.[85, 86, 160, 161] The tail groups presented at the interface can be reactive and available to participate in organic reactions.

One potential application of SAMs is to mediate the interaction between a biomaterial and the human body. The science of biomaterials is defined as "the study and knowledge of the interactions between living and non-living materials," and a biomaterial as "a material intended to interface with biological systems to evaluate, treat, augment or replace any tissue, organ or function of the body".[162] Biomaterials are in contact with tissue fluid, blood and other body fluids for long periods of time.[163] Many different types of materials, including polymers,[92, 159, 164] ceramics,[165] and metals[74, 166-168] have been used for biomedical applications. These materials have to be physiologically useful, economically viable, and non-toxic to the human body. Prostheses, implants, and medical tools are some examples of biomaterials. Biomaterials are generally constructed of metals, ceramics, or plastics.[163] The two main factors that determine the

biocompatibility of a material are the host reaction induced by the material and the degradation of the material in the body. Certain physical, chemical, and mechanical properties render some materials more desirable than others for biomaterials. Some of the chemical properties are corrosion and fatigue resistance.[169] The corrosion resistance relies on the presence of a passive layer on the surface.[170] However, breakdown of the passive layer can occur both during surgery and in service life. When a biomaterial is implanted, electrochemical reactions also take place inside the body which may lead to structural and mechanical degradation of the device. Metal ions originating from these processes can cause problems in the human body that can be toxic for surrounding tissues and living cells.[166, 169, 171] Therefore, if the implant fails it has to be removed by revision surgery and replaced with a new implant.

Biomaterial development has focused on creating adhesion resistant interfaces as a solution of protein fouling, bacterial infection and physiologically reactions.[130, 169] First, if the adsorbed proteins are unable to maintain their native structures and in turn will cause adverse reactions such as the formation of fibrous capsules adjacent to soft tissue implants or blood clots inside synthetic vascular grafts.[130, 172] Also, protein fouling of biomaterials renders biomaterials susceptible to colonization and infection by bacteria.[130, 169, 173, 174] Therefore, a variety of alternatives have been developed to modify the tissue-implant interface.[128, 130, 152, 160, 164, 174-176] One approach to modify the biomaterial interface could be using SAMs at the interface and then react different functional groups with the tail group such as polymers, biological active molecules, therefore creating a boundary which can be controlled.[176]

1.3 Metal Oxide Surface

Nitinol (nickel–titanium alloy, NiTi) was first used for medical purposes in the early 1970s[177-183] In the early 1980s, nitinol was used for orthodontic devices. However, in the 1990s, the first commercial stent constructed of nitinol was sold.[178-180] After that, nitinol (NiTi) was commonly used in medical tools, orthopedic, and implants devices, because it has important properties that make it a desirable biomaterial.[166, 181, 182] The surface of untreated nitinol is composed of oxygen (in metal oxides), carbon, titanium and nickel.[179]

Thermal shape memory,[178, 182, 183] superelasticity,[178, 179, 183, 184] and good damping properties[183] are some of the material properties that make this alloy unique compared to ordinary implant metals.[8-10] Nitinol is a shape memory metal, meaning the crystal structure changes between martensite and austenite structures[166, 179] based on the temperature. When nitinol is at a low temperature(< 70°C), it has a martensite structure, and when heated, it changes to an austenite structure.[170, 185] An idealized sketch of the hysteresis loop is shown of Figure 1.4. The phase transformation is characterized by temperatures corresponding to the start and finish of the transformation into the austenite, A_s and A_f and by temperatures corresponding to the start and finish of the transformation into the martensite, M_s and M_f. The width of the hysteresis loop is typically 20-50°C. The martensite form of NiTi is soft and easily deformable, which makes it a valuable soft tissue implant, such as arterial stents. When heated to its higher temperature form, it is more rigid,[180, 186] which is useful during machining and fabrication of the implants. Thus, the thermal shape memory property, which makes the material able to convert to a preprogrammed shape, allows for optimal material properties during fabrication,

implantation, and use of the implant. (Figure 1.4) [178, 179, 186, 187] This physical property of nitinol is an advantage in the biomaterial field because it can be used in orthodontic archwires and orthopedic implants, where high compressive forces are often required as well high temperatures when they are manufactured.[167, 187]

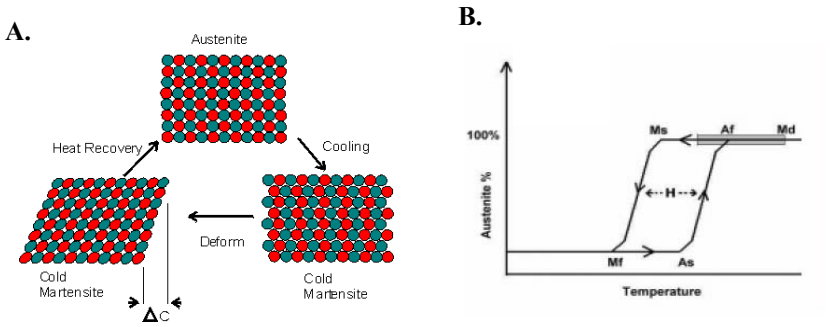

Figure 1.4 (a) The nickel-titanium ratio tunes the temperatures at which the high-temperature austenite phase, which has the CsCl structure, and the low-temperature martensite phase, which has a monoclinic structure, interconvert, (b) Hysteresis loop associated with the NiTi phase change. There are two sets of transition temperatures: A_s and A_f (the start and end of the transition into the austenite), and M_s and M_f (the start and end of the transformation into the martensite).[178, 188]

The term "superelasticity" refers to the ability of a material to undergo large elastic deformations in isothermal conditions through a mechanism involving some stress induced martensite.[178] Nitinol elasticity can be ten times more than the elasticity of the best stainless steel used in medicine today.[179, 186, 189] For example, the superelasticity of the NiTi material allows the stent to expand tightly against the vascular lumen upon deployment, and as a result, minimizes the vascular damage, which can lead to restenosis or other health problems.[126, 179, 190] The stress-strain behavior of nitinol is different from

conventional materials, such as stainless steel, as observed in Figure 1.5. Stainless steel has a elastic limit of < 0.5 %.[178, 179, 189] Further strain will achieve by plastic deformation that is not recovered after unloading. However, nitinol can be deformed up to 8-10 % and is still recoverable. [178, 179, 189] This is an important mechanical property of a biomaterial due to the possibility to use this alloy as self-expandable stents.[190, 191] Traditional stents must be expanded by inflating a balloon positioned within the stents and does not expand uniformly.[191] The superelasticity of nitinol is also advantageous with respect to wear resistance, which is of great importance to the functionality of an implant *in vivo*.[183, 191] Under abrasive conditions, if deformation does not exceed the elastic limit, damage will not general occur and therefore wear is not expected.[179, 191]

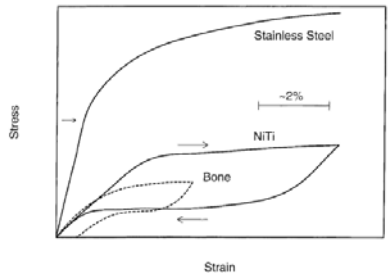

Figure 1.5 Stress-strain diagram (schematic), for living tissues, NiTi superelastic alloy and stainless steel (the left arrow indicates the elastic limit in stainless steel).[179]

A good example of how NiTi dynamic properties can positively impact implant performance is demonstrated by the self-expandable vascular stent and filters.[184, 190, 191] A traditionally used vascular stainless steel stent following balloon expansion does not expand uniformly.[179] A rigid, non-uniformly extended, plastically deformed stainless steel stent can cause significant arterial wall injury and vascular necrosis predisposing the patient for the development of a thrombosis. The different expansion mechanism of an

nitinol stent associated with a specific form of stress-strain diagram results in a more uniform expansion, and in gentle push outward against the vessel wall preventing undesirable changes in stent position despite the movements in the vessel.[192] Significantly lower vascular injury resulting from the mechanical action of nitinol stents on the vessel wall is associated with a tremendous reduction in their thrombogenic potential compared to stainless steel stents.[192]

Many of the reactions causing acute clotting and restenosis are thrombin-mediated.[173, 193] Heparin is the most frequently used agent for thrombin regulation. In order to prevent these reactions, the immobilization of heparin on the surface of the biomaterial has been used to prevent thrombus formation and improve hemocompatibility.[173, 193] However, the actual performance of immobilized heparin may vary significantly depending on many factors, including the method of immobilization, the amount and type of heparin and person's individual biology.[193]

The success of a biomaterial in the body depends on factors such as the material properties, design and biocompatibility of the material used. The material/ cellular interface is known to be an important attribute of biocompatibility with the wetting behavior of surface participating in the cellular adhesion mechanism.[182, 193-195] Therefore, the corrosion behavior of NiTi should correspond to that of titanium which has an excellent corrosion resistance.[170, 196] The corrosion resistance of a material is defined as excellent at rates of 0.02– 0.1 mm/year and good with rates of 0.1– 0.5 mm/year, respectively.[197] The corrosion resistance of nitinol *in vitro* has been previously evaluated, and it's resistance has been reported to range from excellent to poor with no visible rationale.[177-179, 184, 198, 199] *In vivo* studies of nitinol in rats have illustrated that the

inflammatory response was minimal after periods of few months.[178, 179, 181] The use of nitinol as an implant or medical devices requires it to be shape set by heat treating at approximately 500°C.[184, 191, 198] This is designed to improve the corrosion resistance, nickel ion release and biocompatibility of the alloy by increasing the oxide layer.[198] The toxicity of metal salts in cell cultures has shown decreasing toxicity in the order cobalt > vanadium > nickel > chromium > titanium > iron.[169] Therefore, if the passive oxide layer of nitinol is tightly bound and stable due to the presence of the stabilizing titanium dioxide or not damaged in the implant process, the human body would not be subject to unwanted effects such as toxicity, inflammation or cancer. However, this is very difficult to accomplish and therefore toxic effects are seen. [169]

1.4 Previous Work Performed on Nitinol Surface

Several attempts have been made to control and tailor the nitinol surface, and therefore avoid allergic and toxic reactions to the nickel ions released from surface.[163, 187, 200, 201] Nickel may dissolve more easily than titanium because its oxide is not as stable as titanium dioxide.[202, 198, 203] Surface pretreatment is the most common technique employed to alter the nitinol surface properties.[163, 187, 195, 198-202] A nitrogen coating was deposited using ion plasma onto the NiTi surface and the coating exhibited island morphology.[195, 200] Electropolished,[187] plasma[187, 199, 200] and chemical etching[187] surfaces were prepared to decrease the roughness and the nickel content on the surface. The electrochemical treatment of the surface led to improved corrosion resistance.[201] Moreover, the nitinol surface has been modified by plasma immersion to increase the corrosion resistance and decrease the nickel content on the surface.[199] Alternatively,

polysacharide multilayers have been formed to passivate the surface.[126] Finally, the nitinol surface has been modified by poly(ethylene oxide) PEO grafting onto a silanized surface and then irradiated with γ electrons.[163] This surface modification showed a substantial reduction of fibrogen and platelet adsorption.[163] Aside from these surface modifications, monolayer formation has not been achieved and few of the modifications were performed on the native metal oxide surface.

1.5 Hypothesis and Approach

Carboxylic, hydroxamic, sulfonic and phosphonic acids are to be used in this dissertation to form SAMs on nitinol, and its constituent metals nickel and titanium oxides. One key difference among these acids is the acid dissociation constant (Ka). Sulfonic acid is the strongest acid followed by phosphonic, hydroxamic, and carboxylic acids. We hypothesize that the strongest acid will form the most stable and well-ordered monolayer on the metal oxides. Further, the ability to form monolayers on nitinol oxide will closely map to monolayer formation on the most reactive metal oxide. Phosphonic acid monolayers were useful in reducing corrosion of the nitinol surface.

This hypothesis has been tested by controlling and analyzing the factors that affect the efficiency of SAM packing on the surface, such as chain length, organic head group, and functionalized tail group. These factors were tested on the three oxide surfaces: nitinol, nickel and titanium oxide surfaces. After the modification using and aerosol spray method with the thin organic films, the substrates were characterized by IR, AFM, MALDI, and contact angles to monitor the monolayer formation. Alkyl chain ordering, wettability, head-group substrate interactions, and film quality were

determined. This information was then utilized to understand the role of organic and surface factors, such as crystal structure, play in successful monolayer formation. The reactive tail groups were then utilized to increase corrosion resistance through surface-initiated polymerization.

Chapter 2

An Approach to Differentiating between Multi- and Monolayers Using MALDI-TOF MS

2.1 Introduction

Matrix-assisted laser desorption/ionization time-of-flight mass spectrometry (MALDI-TOF MS) is used to give fast and accurate determination of molar masses of the analyte by the fragmentation pattern and detection of the parent molecule, as an ion.[204] MALDI-TOF has been used to determine the sequencing of repeating units, recognition of polymer additives and impurities, large molecules and synthetic polymers of molar masses greater than 550,000 Daltons (Da) by ionization and vaporization without degradation.[205-207] MALDI-TOF provides a soft ionization method with very little fragmentation. It utilizes a pulsed laser beam to ionize the sample. The matrix separates and isolates the sample, absorbs energy and desorbs the analyte. The matrix molecules typically are aromatic acids or aromatic carbonyl compounds, selected on the basis of a

high absorption coefficient for the laser light and ability to convert the absorbed UV laser energy into heat and ionize the analyte molecules.[95, 204, 208] The laser beam is focused on the surface of the sample and ionizes the molecules, which can be directed to the detector. (Figure 2.1) [95, 209] The desorption and ionization mechanisms of the MALDI process are not well understood at the molecular level.[95, 208] However, several models have been proposed including proton transfer between electronically excited matrix molecules and neutral analyte molecules, or the ion-molecules reaction involving radical molecule ions.[95, 204, 208] The most widely accepted ion formation mechanism involves gas-phase proton transfer in the expanding plume with photoionized matrix molecules.[204]

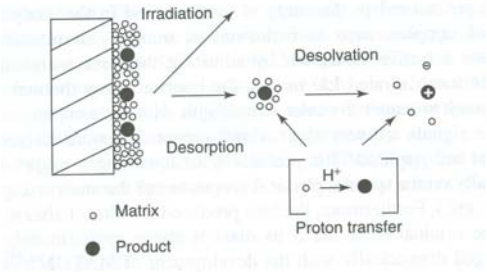

Figure 2.1 A schematic diagram of the mechanism of MALDI.[204]

MALDI-TOF achieves low mass detection limit in the attomole to nanomole range, and also it has a high sensitivity with an accuracy of 10^{-3}-10^{-4}.[95] MALDI-TOF has a large mass range that makes it ideal for biomaterials characterization of lipids, proteins, polymers and surface analysis.[205-207, 210] However, it has been difficult to use MALDI-TOF for the analysis of low-mass molecules and considerable efforts have been made to overcome this problem.[211] Recent advances in instrumentation have allowed for the detection of small molecules without a strong ionizing group present.[94-96, 205, 210, 212, 213] Small molecules can now be easily detected due to the high signal-to-noise ratio using

high resolution instruments without further sample preparation. Detector responses relate to the number of ions reaching the detector and ion velocities. Fast ions, with low *m/z*, produce stronger detector responses than slow ions; therefore, high resolution MALDI TOF usually provides more sensitive detection of small molecules.[214] Using the low mass detection limits, the composition of self-assembled monolayers has been identified using MALDI-TOF.[94, 96, 205] Here, we present the use of MALDI-TOF to differentiate between monolayer and multilayer formation on planar oxide surfaces.

A SAM is a single layer of molecules on a substrate formed spontaneously in which the molecules exhibit a high degree of orientation, molecular order and packing.[57, 168] SAMs provide one of the easiest ways to obtain efficiently close packed films. Also, SAMs are used as fundamental models in the studies of wettability and corrosion on surfaces.[76, 215] Surface properties such as the oxide layer thickness, hydroxyl content, and the roughness affect the formation of SAMs altering the efficiency of molecular packing on the surface. Another important advantage is that SAMs can be prepared in a laboratory using simple deposition methods with small concentrations of the organic molecules. Some common deposition methods used in SAM preparation are aerosol spraying, solution dipping, or vapor deposition.[8-10, 12-14, 16]

Characterization of the monolayer can be accomplished through a variety of techniques. IR is used to determine head-substrate binding and alkyl chain ordering.[17, 18, 106] This can be supported by X-ray photoelectron spectroscopy (XPS) or solid state NMR data.[46, 99, 104, 216, 217] AFM imaging and contact angle data is used to study monolayer uniformity. Height of the film can be inferred from AFM, surface plasma resonance (SPR) or ellipsometry data.[67, 212, 218, 219] The latter are limited by the

reflectance of the surface. While the analysis of the film height can be done using a new XPS charging technique, most people do not have access to this technique.[99, 220] Time-of-flight secondary ion mass spectrometry (TOF-SIMS) has received increased attention in the literature as a model to study thin organic layers.[24, 97, 98, 100, 221, 222] However, in monolayer samples, both monomers and dimers are seen in the TOF-SIMS spectra.[97, 222] As a result, TOF-SIMS can be used to identify species in the thin films, but establishing the height of the film may be difficult using this technique.[97] A previous report using EI mass spectrometry showed when thiols were exposed to laboratory ambient air for a long period of time dimerization of the molecules was detected due to the formation of disulfides (-S-S-).[212] Therefore, determining monolayer vs. multilayer formation in a film is still difficult especially on oxide surfaces, where island and micelle formation is common. We demonstrate the capability of MALDI-TOF to determine film formation on metal oxide surfaces.

MALDI-TOF has been used to characterize SAMs on gold using alkanethiolates.[96] Previously, mass spectrometric analysis using thiols showed the presence of monomers only without detecting dimers with dependence on the high concentration.[23, 33, 212] Mrksich et al. observed disulfides in the MALDI analysis of SAMs on gold, because thiols have a high thermal desorption and the molecules easily form disulfides after desorption due to spontaneous oxidation.[96, 208, 223] Moreover, MALDI-TOF can be used to analyze and screen interfacial reactions on the surface due to their rapid and efficient evaluation.[103, 224] As a result of the non-destructive nature of the technique, the bonding between molecules in the film is intact and the reproducibility between samples is good.[95, 96, 205, 206]

Octadecylphosphonic acid was used to form SAMs on titanium, iron and stainless steel. Furthermore, carboxyalkylphosphonic acid was used to form organic films on titanium as reported.[24, 49, 76] These thin films are known to be strongly attached to the surface.[8, 16, 26, 27, 42, 47, 71, 74, 75, 225-230] Variations in the deposition method for these SAMs can lead to multilayers or monolayers. The multilayers and monolayers formed were characterized by IR, AFM, contact angle measurements and MALDI-TOF. Using these well known systems demonstrates the new capacity of MALDI-TOF to distinguish between multi and monolayers on planar surfaces. Moreover, this is the first time using MALDI-TOF to characterize other molecules such as phosphonic acids as an alternative of the well develop model system of thiol SAMs on gold.

2.2 Experimental Section

2.2.1 Methods and Materials

Octadecylphosphonic acid (ODPA, 99.0% purity) was purchased from Alfa Aesar and used without further purification. 12-bromododecanoic acid (97%), acetyl chloride (>99%,), and triethyl phosphite (98%) were purchased from Aldrich and hydrochloric acid (Certified ACS Plus,) was purchased from Fisher Scientific. 12-(carboxydodecyl)phosphonic acid was synthesized according to literature.[24, 49, 76] Titanium (0.25 mm thickness), iron (0.125mm thickness) and stainless steel 316L (0.50mm thickness), > 99.0 % purity metal oxide foils were purchased from Goodfellow Inc.

2.2.2 Preparation of the Substrates

Substrates were cut into 1 x 1 cm squares and sanded using different grit (220, 320 and 400) sand paper and polished (Buehler Ecomet 4 mechanical polisher) using 400, 800, 1200 and 1μm diamond suspension. The substrates were rinsed with acetone or methanol and cleaned by ultrasonication in acetone for 1 hour. Then, the substrates were rinsed and stored in the oven at 90° C for 30 minutes - 1hour. The substrates were rinsed again and stored under vaccum (0.1 Torr) overnight.

2.2.3 Formation of Monolayers

Monolayers were formed by spraying the solutions of ODPA in dry tetrahydrofuran ((THF) distilled over Na and stored under argon) using an aerosol sprayer (TLC sprayer and N_2). 0.35mM and 0.75mM concentration of ODPA were used to spray the samples, allowed to dry at room temperature and then rinsed with THF. 0.50mM concentration of 12-(carboxydodecyl)phosphonic acid was used to spray the titanium samples. The samples were kept under vacuum overnight (0.1 Torr). Monolayers on iron and stainless steel 316L were formed using previously described methods.[8]

2.3 Characterization of the Multilayers and Monolayers

2.3.1 DRIFT

The monolayers were analyzed using a Diffuse Reflectance Infrared Fourier Transform Spectroscopy (DRIFT). DRIFT (Thermo Nicolet-NEXUS 470 FT-IR) was used to analyze the molecules' adhesion to the surface and the monolayer ordering using

the ν_{CH2} peaks as the reference, before and after rinsing. The spectra were recorded under nitrogen to eliminate the background signal due to CO_2 and H_2O absorption bands. Typically, 1024 scans were collected for each sample with a resolution of 4 cm^{-1}.

2.3.2 Contact Angle

The contact angle measurements (VCA Optima Gionometer Instrument) were used to analyze the hydrophobicity of the surface. 1 μL of deionized water (Millipore) was brought into contact with the surface and the contact angle was measured. Measurements of five different spots on five separate samples were taken and the average and standard deviation were calculated. The values were compared to the contact angle value of cleaned substrates.

2.3.3 AFM

Atomic force microscopy (AFM) was used to analyze the surface before and after the formation of the organic layers. AFM imaging (Molecular Imaging) of the samples was performed in non-contact mode at ambient conditions using silicon tips. The roughness analysis on the two-dimensional topography image was based on a calculation of the standard deviation of all height values within the given imaged area (root-mean-square-roughness (rms)).[8]

2.3.4 AP MALDI-TOF MS

MALDI-TOF was used to characterize the formation of monolayers or multilayers on the surface. A high resolution MALDI TOF (Agilent Tech.) with pulsed dynamic

focusing was used to characterize the molecules. MS analyses of the ions were detected in positive mode using a 337nm N_2 laser, pulse width of 20 ns, a capillary voltage of 3500 V, fragmentor voltage of 260V, skimmer voltage of 40V and drying temperature of 325º C. The spectra were externally calibrated using an ES-TOF tunning mix of 10 masses for the range of 100-2300 m/z. Three-to-five areas of each sample were characterized using the MALDI-TOF. The spectra were collected by uniformly moving the laser in a circular pattern across the sample for one minute. The spectra were reproducible using different samples. The matrix fragmentation can be observed in each of the spectra with their background. The matrix, α-cyano-4-hydroxycinnamic acid (CHCA) (Sigma-Aldrich, >99.0% purity), was used without further purification and added in THF (10mg/mL).

2.3.4.1 Sample Preparation

MALDI-TOF preparation was done by dried-drop method in which a 1μL aliquot of the matrix solution was dropped onto each of the metal surfaces previously modified with thin organic films and then dried at room temperature.[95] The matrix solution was added after thorough rinsing of the sample to remove loosely bound material and as a result the molecules detected by MALDI-TOF are covalently bound on the surface. This method yields a uniform layer of matrix crystals on the samples. The samples were then placed directly onto a MALDI sample plate using double sided tape and loaded onto the MALDI-TOF. Analyte ionization was achieved by focusing a pulse of laser light onto the sample/matrix preparation.

2.4 Results and Discussion

2.4.1 Multilayers

Titanium, iron, and stainless steel were cleaned and modified with organic molecules of octadecylphosphonic acid. The samples were initially characterized by DRIFT (Figure 2.2).

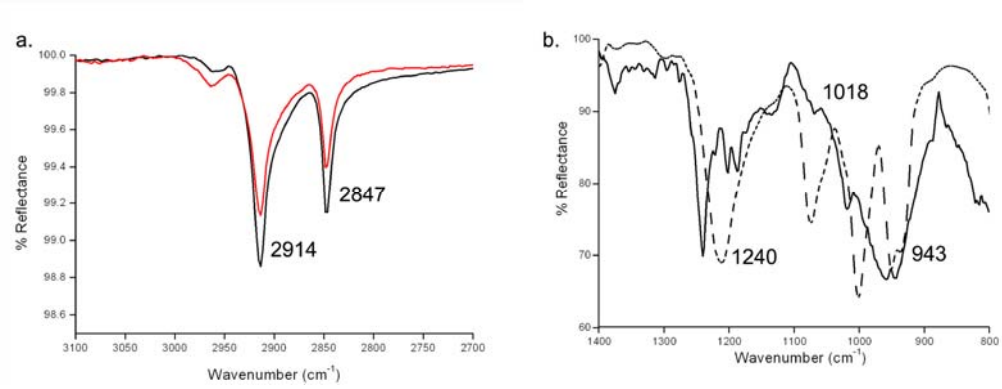

Figure 2.2 (a) IR spectra of ODPA on titanium surface before (black spectrum) and after the rinse test (grey spectrum) ($\nu_{CH2\ asym}$ 2914 cm^{-1} and $\nu_{CH2\ sym}$ 2847 cm^{-1}) and (b) PO region giving $\nu_{P=O}$ 1240 cm^{-1}, and the ν_{P-O} 1018 cm^{-1} and ν_{POH} at 943 cm^{-1} (continuous line spectrum). The PO region of ODPA solid (dash line spectrum) is shown overlapping the PO region on titanium surface $\nu_{P=O}$ =1211 cm^{-1}, ν_{P-O} =1075cm^{-1}, and ν_{POH} = 947 and 931 cm^{-1}. This PO region of the ODPA on the titanium surface spectrum corresponds to a multilayer since the region is consistent with solid ODPA indicating no change (on average) in the bonding region.

The position of the peaks corresponding to ν_{CH2} after rinsing were $\nu_{CH2\ asym}$ 2914 cm^{-1} and $\nu_{CH2\ sym}$ 2847 cm^{-1} shown in (Figure 2.2a). The C-H stretches of the methylene group are used as the reference peaks for SAM organization.[17, 106] The ν_{CH2} is consistent

with *all-trans* alkyl chains forming an ordered film. The PO region of the ODPA solid (dash line spectra) shows $\nu_{P=O}$ =1211 cm^{-1}, ν_{P-O} =1075cm^{-1}, and ν_{POH} = 947 and 931 cm^{-1}. The PO region of the ODPA on the titanium oxide surface from Figure 2.2b (continuous line spectrum) includes $\nu_{P=O}$ =1240 cm^{-1}, ν_{P-O} =1018 cm^{-1}, and ν_{POH} = 943 cm^{-1} (Figure 2.2b). This spectra is consistent with that of the solid indicating multilayer formation.[26] The results of the deposition on iron and stainless steel 316L were collected and the data are presented in Table 2.1. Ordered and stable multilayers were formed on all surfaces.

Table 2.1 Summary of IR results before and after rinsing on surfaces with multilayers.

Metal Oxide	**Deposition (cm^{-1})**	**Rinse Test (cm^{-1})**	**Intensity (%)**
Titanium	2914 / 2847	2914 / 2847	0.8-5
Iron	2915 / 2848	2915 / 2848	0.9-2.5
Stainless steel 316L	2913 / 2847	2914 / 2848	1-5

AFM imaging of the modified surfaces clearly illustrates multilayer formation. Figure 2.3 shows AFM images of titanium surface before modification and after multilayer formation. The control sample has an average rms roughness of 11Å (left image). In multilayer films the molecules are not uniformly distributed and the rms roughness is higher (rms=29Å, right image). Additionally, the image shows island agglomerates in particular areas.

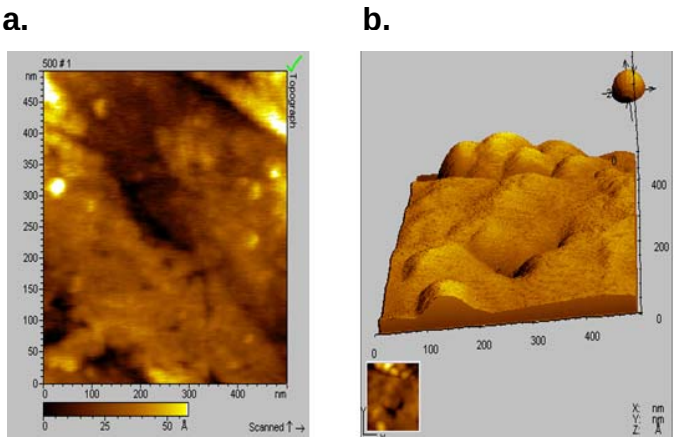

Figure 2.3 AFM image of titanium (a) before modification (rms roughness = 11Å) and (b) after multilayer formation with ODPA (rms roughness = 29Å).

Contact angle measurements were collected on each metal oxide surface (control) and on the modified surfaces (Table 2.2). The contact angle measurement is used to demonstrate the wettability of the surface compared with the control before modification.[111] Contact angle literature values of methyl-terminated SAMs using alkenethiolates on gold are close to 110° for hydrophobic and 40° for hydrophilic surfaces.[33, 113, 168, 231] These angles are indicative of densely packed methyl-terminated self-assembled monolayers and smooth surfaces after modification.

Table 2.2 Contact angle values of the control, multilayer and monolayer modification on titanium, iron and stainless steel 316L.

Metal Oxide	**Control**	**ODPA-Multilayers**	**ODPA-Monolayer**
Titanium	35º ± 1 º	97 º± 6 º	96º ± 5 º
Iron	58º ± 2 º	105 º ± 9 º	94 º ± 6 º
Stainless steel 316L	64º ± 4 º	106º ± 4 º	111 º ± 4º

Multilayer formation was well characterized using IR, contact angles and AFM imaging. Further analysis of the multilayer by MALDI-TOF (Figure 2.4) reveals peaks at *m/z* 335.276 and 669.556 corresponding to the ODPA monomer and dimer peak respectively on the titanium surface. Numerous small peaks can be seen due to the low-mass matrix related ion signal and matrix background.

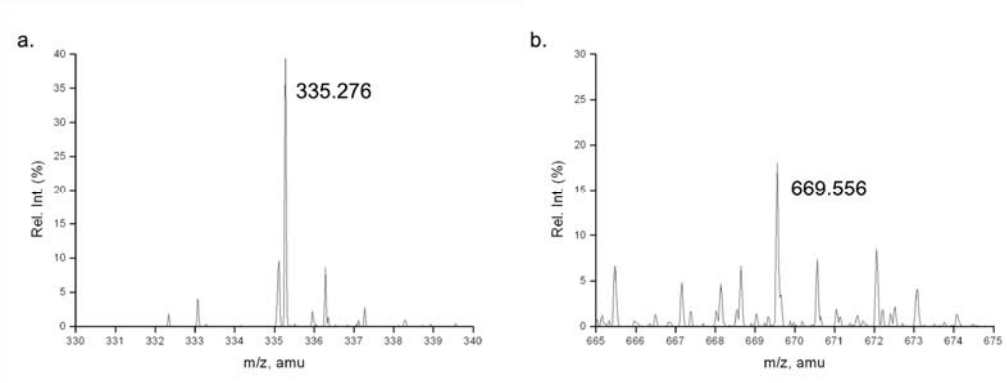

Figure 2.4 MALDI-TOF spectra of the ODPA multilayer on titanium surface shows mass peaks at *m/z* 335.276 and 669.556 resulting from the monomer and dimeric peak respectively.

Since multilayer formation requires layers of organic molecules which are bound to each other on the surface, MALDI-TOF detects this particular modification by the presence of the dimeric peak from two molecules which are bound to each other.[208] Mass spectrometer analysis using the electrospray was performed on control ODPA (MW 334.28g/mol) and is shown in Figure 2.5a illustrating the monomer (335.287 m/z + H^+) and dimeric (2 x 334.28 = 669.549 m/z + H^+) peaks. The cleaned but unmodified oxide surfaces were analyzed and only the matrix ions from CHCA were observed (Figure 2.5b).

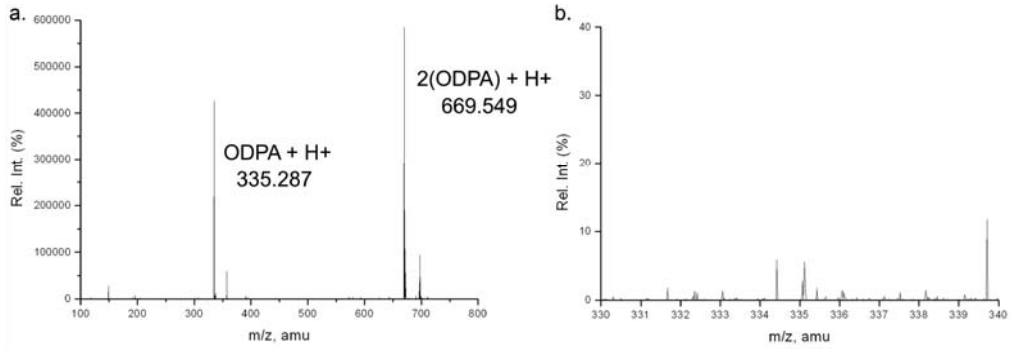

Figure 2.5 (a) ESI spectra of ODPA control showing mass peaks at *m/z* 335.287 and 669.549 resulting from the monomer and dimeric peak respectively. (b) MALDI-TOF spectra of the unmodified titanium surface in which the matrix ion can only be observed at *m/z* 335.106. Note the relative intensity (y-axis) are different in (a) and (b).

MALDI-TOF analysis on titanium, stainless steel 316L and iron surfaces showed the same pattern when modified with multilayers. In each case monomer and dimer peaks were seen in the spectra.[15]

2.4.2 Monolayers

Titanium, iron, and stainless steel were cleaned and modified with self-assembled monolayers of octadecylphosphonic acid. The samples were initially characterized by DRIFT (Figure 2.6).

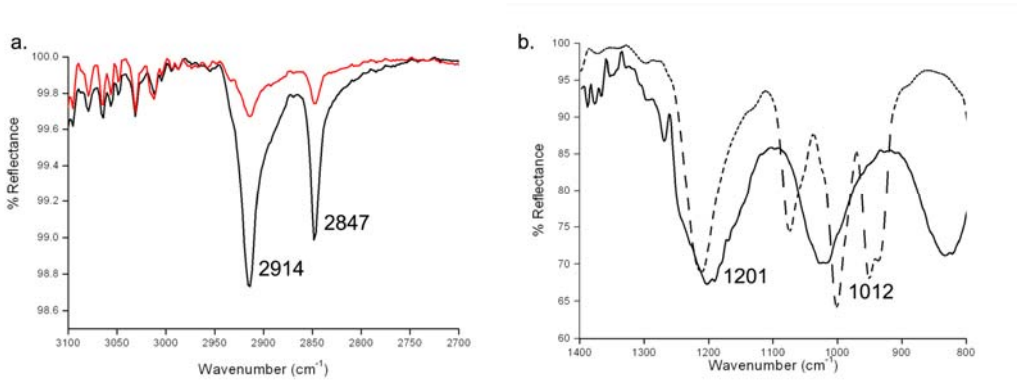

Figure 2.6 (a) IR spectra of ODPA on titanium surface before (black spectra) and after the rinse test (grey spectra) ($\nu_{CH2\ asym}$ 2914 cm^{-1} and $\nu_{CH2\ sym}$ 2847 cm^{-1}) and (b)PO region giving $\nu_{P=O}$ at 1201cm^{-1}, and the ν_{P-O} at 1012 cm^{-1}(black spectra). (b) The PO region of ODPA control is shown overlapping the PO region on titanium surface giving $\nu_{P=O}$ =1211 cm^{-1}, ν_{P-O} =1075cm^{-1}, and ν_{POH} = 947 and 931 cm^{-1} (continuous line spectra). The PO region of ODPA solid (dash line spectrum) is shown overlapping the PO region on titanium surface $\nu_{P=O}$ =1211 cm^{-1}, ν_{P-O} =1075cm^{-1}, and ν_{POH} = 947 and 931 cm^{-1}.

Rinsing and sonication was done using THF to remove any physisorbed material or multilayers. The CH_2 values are characteristic of ordered alkyl chain in monolayers based on the IR spectra $\nu_{CH2\ asym}$ 2914 cm^{-1} and $\nu_{CH2\ sym}$ 2847 cm^{-1}.[18, 106] The PO region of the monolayer on the titanium surface from Figure 2.6 b (continuous line spectra) shows the $\nu_{P=O}$= 1201 cm^{-1} and ν_{P-O}= 1012 cm^{-1}. This indicates covalent bonding between ODPA and the surface in a bidentate manner. A substantial difference is seen between multilayer and monolayer spectra, for a multilayer sample the monomer and dimer peak are detected by MALDI-TOF. In contrast, for a monolayer sample that just the monomer peak is detected.[26] The results from iron and stainless steel 316L were collected and the data is presented in the Table 2.3. All three systems were characterized (titanium, iron and stainless steel 316L) and ordered and strongly chemisorbed monolayers were formed on the substrates.

Table 2.3 Summary of results from iron and stainless steel surfaces before and after modification with self-assembled monolayers.

Metal oxide	Deposition (cm^{-1})	Rinse test (cm^{-1})	Intensity (%)
Titanium	2914 / 2847	2914 / 2847	0.3
Iron	2912 / 2847	2912 / 2847	0.2
Stainless steel 316L	2913 / 2847	2914 / 2848	0.3

Figure 2.7 shows AFM images of the titanium surface before and after the monolayer formation with ODPA. The control sample has an average rms roughness of 11Å (left image). Samples with monolayers had an rms roughness of 12Å. This indicates that a single layer of molecules covered the surface unlike in multilayer samples (Figure 2.3, rms 29Å) where there was not uniform coverage.

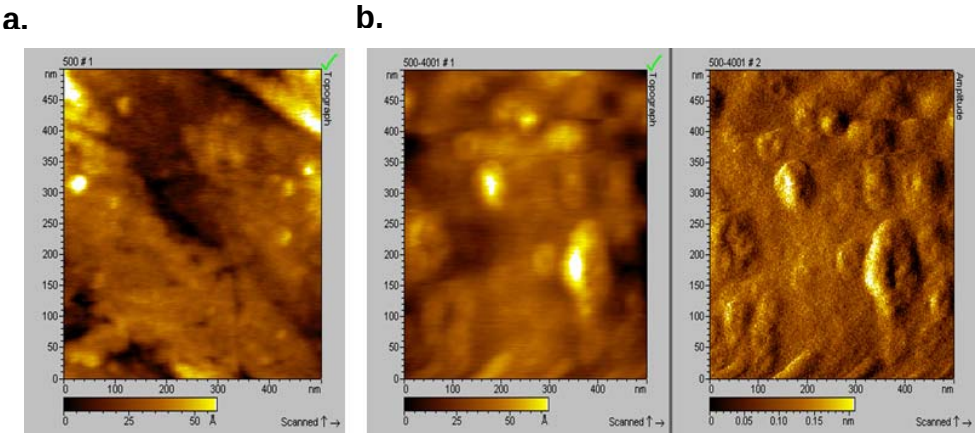

Figure 2.7 (a) AFM image of titanium before (rms roughness =11Å) and (b) after modified with ODPA (rms roughness = 12Å) in topography and amplitude. This imaging of the titanium surface can be considered monolayer.

The MALDI-TOF of monolayers considerably differs from that of multilayers. Analysis of the SAMs using MALDI-TOF (Figure 2.8) reveals peaks at *m/z* 335.276, 335.281, and 335.280 corresponding to ODPA on titanium, stainless steel 316L and iron surfaces respectively. The dimeric peak seen in multilayer spectra were not detected when the monolayers were analyzed although matrix background can be seen (Figure 2.8d, e). This indicates that surface monomers do not aggregate in the process of obtaining the mass spectrum. Therefore, the dimerization seen in the multilayer spectrum comes from the sample and not the technique. As a result, MALDI-TOF can be used to differentiate between multi and monolayers.

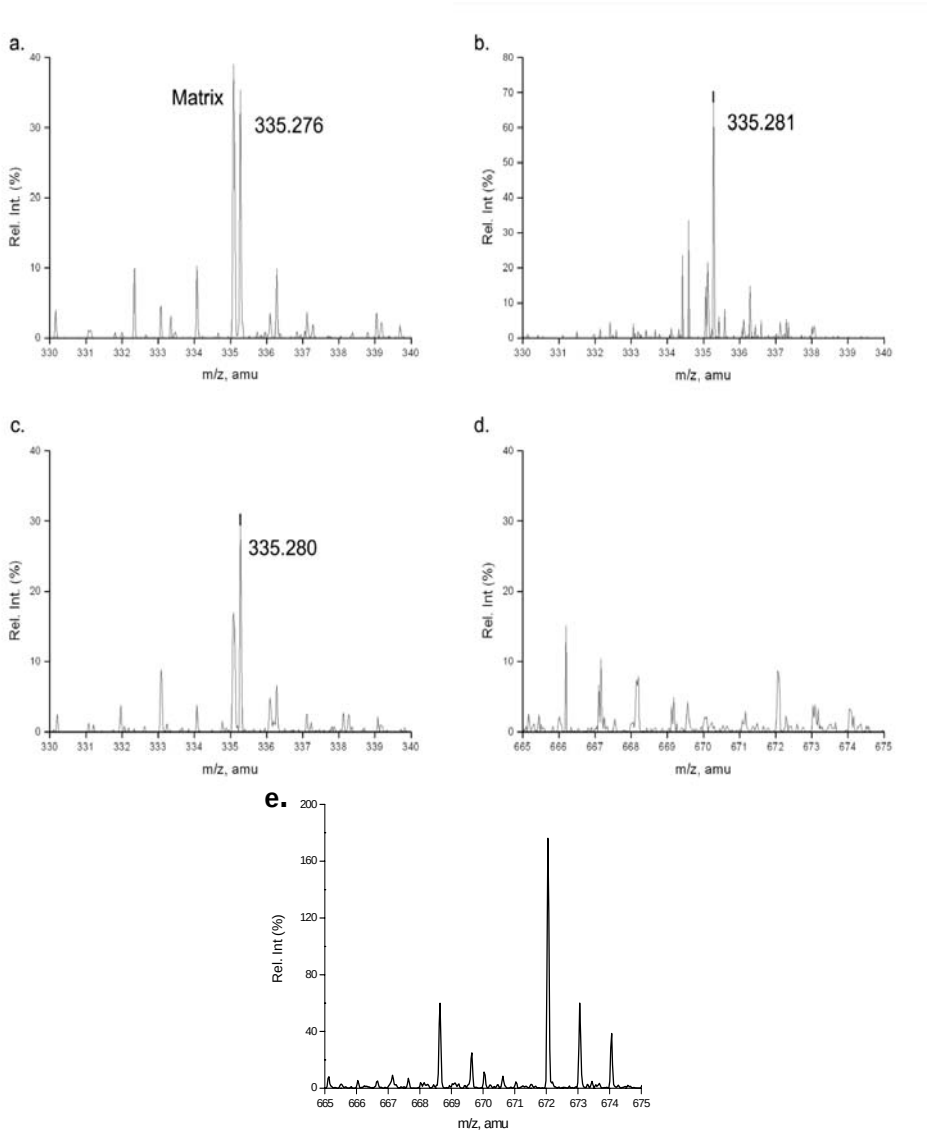

Figure 2.8 MALDI-TOF spectra of the monomer region of ODPA SAMs on (a) titanium (*m/z* 335.276), (b) stainless steel 316L (*m/z* 335.281), and (c) iron (*m/z* 335.280); (d) dimeric region of ODPA on stainless steel; (e) dimeric region of ODPA on titanium.

Octylphosphonic acid was used to form SAMs and in order to corroborate our MALDI analysis. The samples were initially characterized by DRIFT. The ν_{CH2} values

are characteristic of ordered alkyl chain monolayers on the titanium surface based on the IR spectra $\nu_{CH2asym}$ = 2913 cm^{-1} and ν_{CH2sym} = 2846 cm^{-1} after deposition and $\nu_{CH2asym}$ = 2915 cm^{-1} and ν_{CH2sym} = 2847 cm^{-1} after rinsing with THF. (Figure 2.9a) Analysis of the SAMs using MALDI-TOF (Figure 2.9b) reveals peaks at *m/z* 195.120 corresponding to octylphosphonic acid monomer protonated on titanium surface. The dimeric peak was not detected when the monolayers were analyzed. (Figure 2.9c) Mass spectrometer analysis using the electrospray was performed on the octylphosphonic acid control (MW 194.11 g/mol) and exhibits the monomer protonated (195.137 m/z + H^+), and dimeric protonated (2 x 194.137 = 389.224 m/z + H^+) peaks. Therefore, this method also is useful to characterize also molecules (< 200 amu) with short chain length on the metal oxide surfaces.

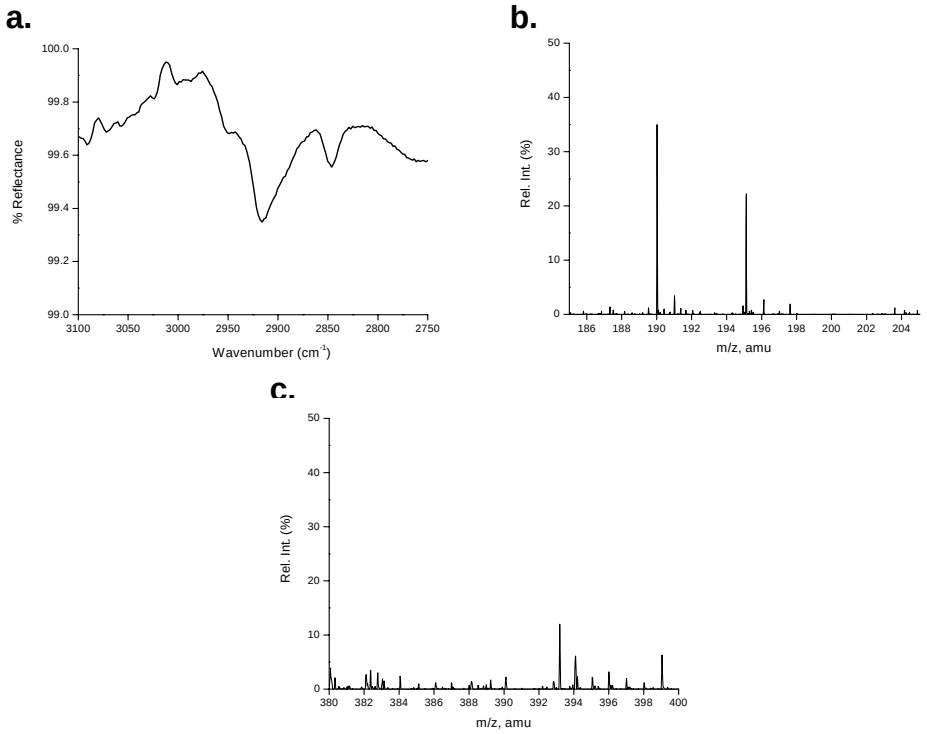

Figure 2.9 (a) IR spectra of octylphosphonic acid on titanium surface after the rinse test (black spectrum) ($\nu_{CH2\ asym}$ 2915 cm^{-1} and $\nu_{CH2\ sym}$ 2846 cm^{-1}), MALDI-TOF spectra of the (a) monomer region of octylphosphonic acid SAMs on titanium (*m/z* 195.120); (b) dimeric region.

12-(carboxydodecyl)phosphonic acid was used to form organic films on the titanium surface. This hydrophilic molecule has been demonstrated to bond strongly on the metal oxide binding preferentially by the phosphonic group.[24, 49, 76] Therefore, carboxyalkylphosphonic acid was used to corroborate our MALDI-TOF analysis. The samples were initially characterized by DRIFT. The ν_{CH2} values are characteristic of ordered alkyl chain in monolayers based on the IR spectra $\nu_{CH2asym}$ = 2912 cm^{-1} and ν_{CH2sym} = 2846 cm^{-1} after deposition and $\nu_{CH2asym}$ = 2912 cm^{-1} and ν_{CH2sym} = 2847 cm^{-1} after rinsing with THF. (Figure 2.10a) The PO region of the monolayer on the titanium

surface shows the $\nu_{P=O}$= 1264 cm^{-1} and ν_{P-O}= 1109 cm^{-1}. (Figure 2.10b) There was no evidence in the IR of bridging by the carboxylic acid tail group. To understand the reactivity of the carboxylic acid moiety, octadecylcarboxylic acid was deposited under the same conditions, and no evidence of film formation was seen in the IR spectrum. Moreover, the wettability of the modified surface was analyzed by contact angle having a 58º ± 7 º. This value means the water spread in general all the way through the surface compared to the methyl terminated phosphonic acid monolayers. (Table 2.2)

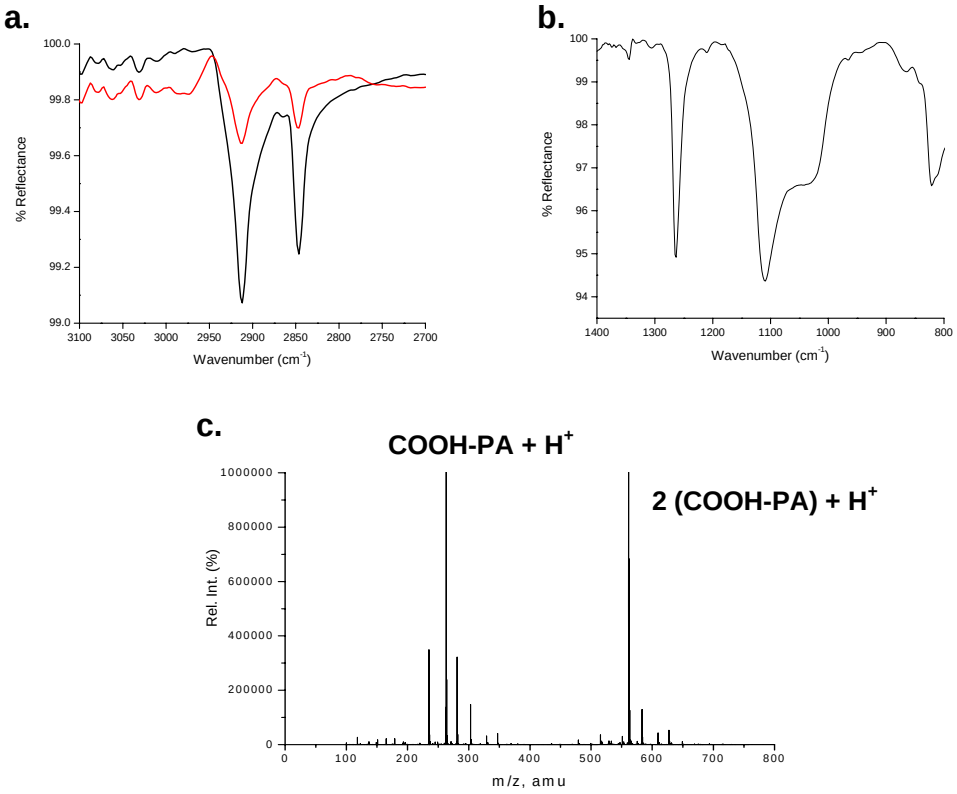

Figure 2.10 (a) IR spectra of 12-(carboxydodecyl)phosphonic acid on titanium surface before (black spectrum) and after the rinse test (red spectrum) ($\nu_{CH2\ asym}$ 2912 cm^{-1} and $\nu_{CH2\ sym}$ 2846 cm^{-1}), (b) PO region giving $\nu_{P=O}$ at 1264cm^{-1}, and the ν_{P-O} at 1109cm^{-1} , (c) ESI spectra of 12-(carboxydodecyl)phosphonic acid control showing mass peaks at *m/z* 281.156, 303.138, 561.310 and 669.549 resulting from the monomer, monomer sodiated and dimeric peaks respectively.

Analysis of the SAMs using MALDI-TOF (Figure 2.11) reveals peaks at *m/z* 303.134 corresponding to the sodiated 12-(carboxydodecyl)phosphonic acid monomer. The dimeric peak was not detected when the monolayers were analyzed (Figure 2.11b). Mass spectrometer analysis using the electrospray was performed on 12-(carboxydodecyl)phosphonic acid control (MW 280.30 g/mol) and exhibits the monomer protonated (281.156 m/z + H^+), monomer sodiated (303.138 m/z + Na^+), dimeric (2 x 281.156 =561.310 m/z + H^+), and dimer sodiated (2 x 281.156 + Na^+= 583.303) peaks (Figure 2.10c). Therefore, this method can also be used to characterize functionalized molecules on the metal oxide surfaces.

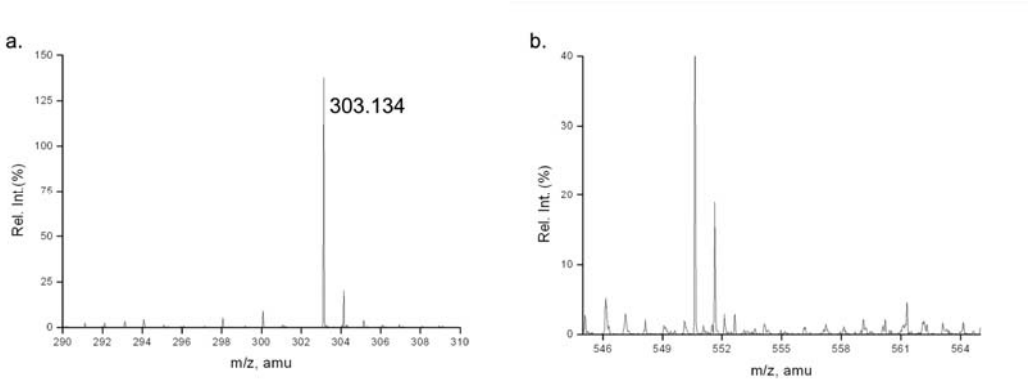

Figure 2.11 MALDI-TOF spectra of the (a) monomer region of 12-(carboxydodecyl)phosphonic acid SAMs on titanium (*m/z* 303.134); (b) dimeric region.

2.5 Conclusion

Strong and ordered films (mono and multilayers) were formed on titanium, iron and stainless steel 316L. IR, contact angle, AFM and MALDI-TOF were used to characterize the unmodified and modified surfaces. Infrared analyses have demonstrated the alkyl chain ordering and binding between the organic and the surface through peak

shifting. AFM images were used to characterize the surfaces before and after modification with alkylphosphonic acid in order to infer film height. The established monolayer systems of iron, titanium and stainless steel and IR and AFM techniques were used to prove substrate characterization and to demonstrate that MALDI-TOF can be used to distinguish between multi and monolayer formation in thin films on surfaces. The monomer and dimer peak of ODPA was used to indicate the formation of mono or multilayer. If the dimer peak of the molecule is seen by MALDI-TOF, then the modification is considered to be a multilayer on the surface, and the presence of only a monomer indicates the presence of a monolayer. The analyte does not dimerize in the gas phase at low concentration of the analyte. The instrument has been able to quantify analyte as low as 2 picomol for detection of limit.[232] Therefore, the monolayer samples have been analyzed to differentiate between high concentration and multilayer modification. This easy and effective method is useful in characterizing thin films on different substrates.

Chapter 3

Study of the Formation of Self- Assembled Monolayers on Nitinol and its Constituents Nickel and Titanium Oxide Surfaces

3.1 Introduction

The surface of nitinol (NiTi) is composed of 50% titanium oxide (TiO_2) and 50% nickel compounds (both nickel oxides (NiO and Ni_2O_3) and metallic nickel), while nickel-titanium constitutes the inner layers.[186, 191] The biocompatibility of nitinol has been studied with special attention because of the high nickel content.[233] Nickel may dissolve in the human body more easily than titanium leading to toxicity and infection. Titanium, however, has been extensively used for implants, and has very good biocompatibility.[187, 234] Nitinol is an alternative to titanium due to the shape memory and superelasticity properties.[178, 179, 182, 184] These properties facilitate minimally invasive

keyhole surgical procedures that minimize trauma and accelerate recovery.[178, 179] It has been found to be noncarcinogenic in humans and does not corrode *in vivo*.[187] To reduce the immune response, researchers are trying build a protective interface between the biomaterial and the human body using organic, coatings, or other surface treatments.[126, 172, 199, 200] Self-assembled monolayers (SAMs), an organic coating, may form an effective interface between the human body and the biomaterial surface. The self-assembly technique represents a cost-effective way of modifying and controlling the surface properties of metal oxide surfaces through the simple processes of dipping, spraying or vapor deposition.[8, 13, 16] This self-assembly process is cost effective because the solution concentration is small, the chemicals used are normally easy to find and synthesize, and film formation can take place in seconds.

SAMs can be arranged as condensed (ordered) or dilute (disordered) monolayers. Condensed monolayers contain rigid molecules due to greater van der Waals forces between alkyl chains of each molecule resulting in a closely packed monolayer.[17] Alkyl chains in condensed films have an all-trans conformation. Additionally, inter-tail interactions of the molecules such as hydrogen bonding can be strong and aid in aligning the molecules. These hydrogen bonding interactions can form between the tail groups as well as with the head groups of the molecules used in the SAM formation. In dilute monolayers, the alkyl chains contain gauche conformations resulting in gaps between the molecules and thus, low density monolayers are formed.[57, 168, 215]

The most widely researched class of SAMs is alkanethiols on noble metals, particularly gold.[19, 33, 221] Alkanethiols on gold have been utilized as model systems for various purposes, including corrosion resistance[48, 55, 56], adhesion enhancement,[57, 58] and

biosensors.[59-61] Alkyl thiols on gold have been studied extensively,[19, 21, 33, 63, 235] and it is known that, when adsorbed, the molecules are oriented at an angle of 30°relative to the surface normal.[236] The nature of S-Au bond has been discussed extensively, and it has been established that the adsorbed molecules are highly mobile. [236] However, the formation of well-ordered and strong alkanethiol monolayers has been extremely limited on metal oxides.[68] For example, thiols were used to modify the nickel oxide surface. [21, 57] However, in order to form the SAMs on the surface, the oxide layer was removed by electrochemical methods to expose a clean metallic surface to which thiols can bond to through at S-Ni bond.[153, 237] Thiols generally do not adhere to metal oxides or are easily removed by rinsing. Therefore, a different type of molecule must be utilized to form SAMs on NiTi oxide. Researchers have used long chain organic acids (carboxylic, sulfonic, hydroxamic, phosphonic) on a variety of metal oxides but these acids have been studied far less than alkanethiols on gold.[16, 18, 25, 27, 28, 42, 45, 68-72, 76, 238] Some examples of monolayers on metal oxides are those formed by carboxylic acids on copper,[23, 72] aluminum oxide,[17, 68, 70, 73] and stainless steel.[8, 9, 74, 75] Previously, phosphonic acids have been used to form robust and ordered films on relatively inert oxide surfaces such as titanium and stainless steel.[8, 16, 24, 26, 27, 42, 68, 71, 76, 239] The reason for the increased reactivity of phosphonic acids over other organic acids may be due to the phosphonic acid's low pKa and thus, its ability to participate in acid-base reactions with surface hydroxyl groups and μ-oxo groups or others were speculated that the monolayer may be physisorbed onto the surface in the form of salts.[8, 16, 239] Here, SAMs were formed and characterized on the native oxide surface of nitinol using phosphonic acid head groups for the first time. Moreover, one of the main and potentially toxic, components of the

nitinol surface is nickel oxide which also was modified using phosphonic acids to understand the reactivity and effect of different oxides on the surface. Titanium oxide which also is a component of the nitinol surface was previously modified and analyzed using alkylphosphonic acid.[15, 16, 24, 26, 42, 47] Therefore, we confirmed monolayer formation on the titanium oxide surface using the phosphonic acid head group and varied the alkyl chain length and the tail groups at the interface.

3.2 Experimental Section

3.2.1 Methods and Materials

Butylphosphonic acid (BPA, 98% purity), Octylphosphonic acid (OPA, 98% purity), undecylphosphonic acid (UPA, 98% purity) and octadecylphosphonic acid (ODPA, 99.0% purity) were purchased from Alfa Aesar and used as received without further purification. 12-bromododecanoic acid (97%), 11-bromoundecanol (98%), 1, 12-dibromododecane (98%), acetyl chloride (>99%), and triethyl phosphite (98%) were purchased from Aldrich and hydrochloric acid (Certified ACS Plus,) was purchased from Fisher Scientific. (11-hydroxyundecyl)phosphonic (12-carboxydodecyl)phosphonic and 1,12 dodecyldiphosphonic acids were synthesized as previously described.[24, 49, 76, 240, 241] Nitinol foils (51% nickel: 49 % titanium; 0.008" thickness, >99.0 % purity) were purchased from Johnson Matthey, Inc. Nickel and titanium foils (0.25mm thickness, > 99.0 % purity) were purchased from Goodfellow Inc.

3.2.2 Preparation of the Substrates

Substrates were cut into 1 x 1 cm squares, sanded (220, 320 and 400 grit sandpaper) and then polished (Buehler Ecomet 4 mechanical polisher) using sandpaper of 400, 800, 1200 grits and 1μm diamond suspension. The substrates were rinsed with acetone and methanol and cleaned by ultrasonication in acetone for 1 hour. The substrates were then rinsed with acetone and stored in the oven at 90° C for 30 minutes – 1 hour. The substrates were rinsed again and stored under vacuum overnight (0.1 Torr).

3.2.3 Formation of Monolayers

Monolayers were formed by spraying the solutions of phosphonic acid in dry tetrahydrofuran ((THF) distilled over Na and stored under argon) using an aerosol sprayer (TLC sprayer, Sigma Aldrich and N_2). A 0.35mM solution of ODPA was used to spray the samples. The substrates were allowed to dry at room temperature and then rinsed with THF for 15 minutes. Solutions of undecylphosphonic (0.50mM), (12-carboxydodecyl)phosphonic (0.50mM), octylphosphonic (0.75mM), (11-ydroxyundecyl)phosphonic (0.75mM) and 1,12 dodecyldiphosphonic acids (0.50mM) respectively. The resulting samples were stored under vacuum overnight (0.1 Torr).

3.2.4 Characterization of the Monolayers

3.2.4.1 DRIFT

The substrates were studied using a Diffuse Reflectance Infrared Fourier Transform Spectroscopy (DRIFT; Thermo Nicolet-NEXUS 470 FT-IR). DRIFT was used to analyze the alkyl chain ordering and bonding mode of the molecules to the surface. The spectra were recorded under nitrogen to eliminate the background signal due to CO_2

and H_2O absorption bands. The unmodified NiTi, Ni or Ti substrates, respectively, were used as the background spectra for analysis purposes. Typically, 1024 scans were collected for each sample for the measurements on the monolayer samples. A total of nine samples were analyzed by IR.

3.2.4.2 Contact Angle

The contact angle measurements (VCA Optima Goniometer Instrument) were used to analyze the hydrophobicity of the surface. One μL of deionized water (Millipore) was brought into contact with the sample to analyze the wettability of the SAMs formed on nitinol. Measurements on five different places on five samples were taken and the average and standard deviations were calculated. The values were compared to the contact angle value of cleaned but unmodified nitinol substrates.

3.2.4.3 AFM

Atomic force microscopy (AFM) was used to characterize the surface topography before and after the formation of the organic films. AFM imaging (Molecular Imaging, Pico SPM) of the nitinol oxide samples was performed in non-contact mode at ambient conditions using silicon tips. The samples were scanned over 500 x 500 nm region. Imaging of the nickel oxide samples were performed in non-contact mode under ambient conditions using MAC-lever silicon tips (Veeco Inc.). MAC mode was used to image the nickel oxide substrates due to the fact that nickel oxide surface is ferromagnetic and the images were superior to those obtained in AC mode. Imaging of 1,12-dodecyldiphosphonic acid modification on the NiTi surface was performed in contact mode at ambient conditions using silicon nitride tips. The roughness analysis on the two-dimensional topography image was based on a calculation of the standard deviation of all

height values within the given imaged area (root-mean-square-roughness (rms)).[8]

3.2.4.4 AP MALDI-TOF MS

Atmospheric pressure matrix-assisted laser desorption/ionization time-of-flight mass spectrometry (AP MALDI-TOF MS) was used to differentiate between monolayer and multilayer formation as explained previously in Chapter 2.

3.2.4.5 Electrochemical Characterization

Electrochemical measurements were carried out in a Bioanalytical Systems (BAS) model CV-50W. Voltammograms were recorded with a standard three-electrode system consisting of nitinol and nickel oxide as the working electrodes with a 0.8 cm^2 exposed area, a saturated calomel electrode (SCE) as the reference electrode and a Pt-wire auxiliary electrode. The cyclic voltammetry analysis was performed in a 0.1M NaOH aqueous solution after soaking the samples for 30 minutes in the solution. Potential was scanned -0.3 to +0.6 V for the nickel oxide and -0.3 to +0.7 V for the nitinol substrates at 50 mV s^{-1}. Using the same three-electrode system, the current density was measured using an EG&G Princeton Applied Research scanning potentiostat Model 362 and was plotted using an EG&G Princeton Applied Research (Houston Model RE0074) X-Y recorder and a 169 Keithley multimeter with y scale 2.5 mA, a current at 10mA at 10 mV s^{-1}scan rate.

The Electrochemical Impedance Spectroscopy (EIS) measurements were performed in the frequency range from 0.1 Hz to 300 kHz with 5 points per decade. The sinusoidal perturbation signal's amplitude was 10 mV at corrosion potential. The

impedance data were analyzed with Gamry Framework v5.30 software using a Gamry Instruments FAS2 Femtostat potentiostat.

3.3 Results and Discussion

3.3.1 Nitinol Surface

Nitinol (NiTi) samples were cleaned and octadecylphosphonic acid (ODPA) was deposited by a simple procedure of aerosol spraying (0.35mM solution in THF). This leads to the spontaneous formation of a film on the NiTi surface. After deposition, rinsing and sonication, to remove loosely bound material, the samples were characterized by DRIFT (Figure 3.1). The spectra of the unmodified NiTi substrates contained no peaks attributable to organic deposition. In the spectra of the modified substrates, the C-H stretches of the methylene group are used as the reference peaks for SAM organization.[17, 66, 106] The symmetric and asymmetric C-H stretches are shifted to higher or lower frequencies depending on the alkyl chain conformation. Thus, this indicates weather the alkyl chains are ordered (trans conformation) or disordered (gauche conformation).[14, 106] The position of the peaks corresponding to ν_{CH2} after sonication were $\nu_{CH2\ asym}$= 2913 cm^{-1} and $\nu_{CH2\ symm}$= 2846 cm^{-1}, respectively, showing a strongly bound and ordered film is present (Figure 3.1a). The contact angle measurements of the modified surface are consistent with that of a well-ordered monolayer with complete coverage of the surface. A water contact angle of 107° is observed, compared to the bare nitinol oxide surface contact angle of 46°.

The spectra acquired following sonication indicate that the molecules are bound

to the surface in a monodentate manner. Sonication removes weakly bound or physisorbed material, therefore the remaining material is bound strongly to the surface. The nature of the interaction between the molecules and the surface can be can be determined from the shifts and broadening of $\nu_{P=O}$, ν_{P-O} and ν_{POH}, indicating a change in head group bonding.[16, 136] Specifically, the PO region of the ODPA solid shows $\nu_{P=O}$= 1211 cm^{-1}, ν_{P-O}= 1075 cm^{-1}, and ν_{POH}= 947 cm^{-1} and 931 cm^{-1} (Figure 3.1b-black spectra). In contrast, the PO region of the bound ODPA contained broad PO group stretches at $\nu_{P=O}$ = 1239 cm^{-1}, ν_{P-O} = 1055 cm^{-1} and ν_{POH} = 897 cm^{-1} (Figure 3.1b-red spectra). The broad peak at 1055 cm^{-1} is characteristic of P-O-surface species in other phosphonic acid-metal oxide systems where the molecule is bound to the surface.[25, 49, 76] The peak at 1239 cm^{-1} is consistent with the continued presence of P=O groups. Therefore, the bonding is not tridentate as seen in some phosphonate-oxide systems, such as silicon dioxide.[230, 242] Furthermore, we have attributed the peak at 897 cm^{-1} to the continuing presence of a P-O-H group. This peak is shifted from that seen in the solid spectra to lower wavenumber values and most likely due to hydrogen bonding between the remaining P-O-H group and the surface (Figure 3.1c). Therefore, the bonding is monodentate (Figure 3.1d). This result varies from that reported on TiO_2 which is reported as bi or tridentate.[15, 16, 71, 230] This may be due to the difference between the TiO_2 structure which is rutile and the alloy structure which is martensite -austenite. This is explained in more detail in Chapter 4.

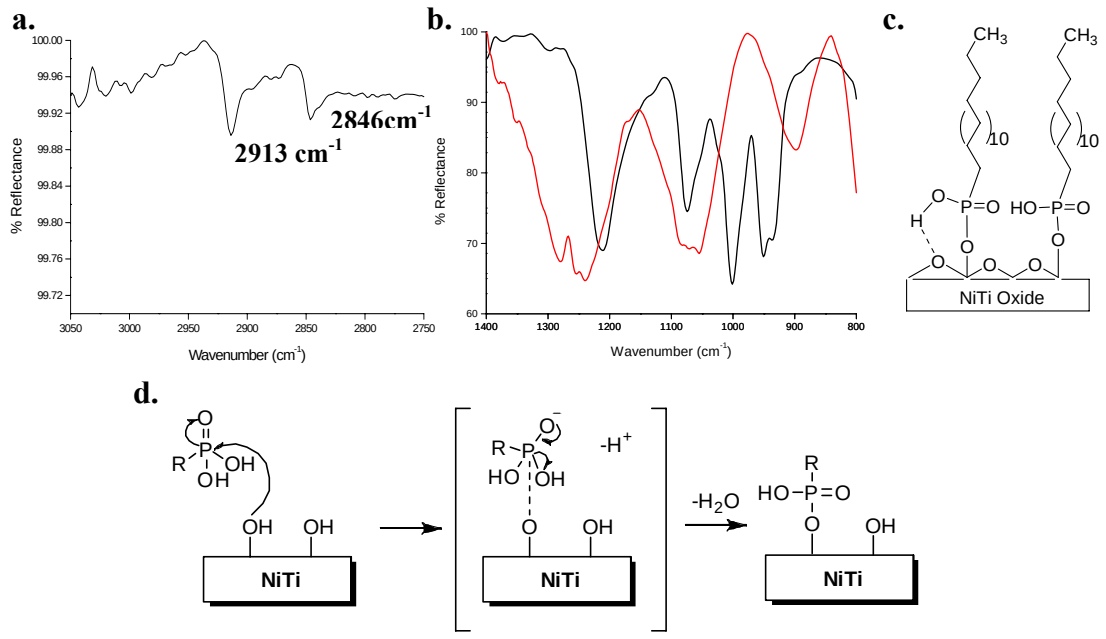

Figure 3.1 IR spectra of ODPA on nitinol surface (a) CH region after sonication (b) PO region after deposition, (red spectra) and the PO region of ODPA solid (black spectra). (c) The PO region of the IR spectra indicates a monodentate orientation of the acid with some hydrogen bonding to the nitinol oxide surface as shown. (d) Proposed mechanism of monodentate binding of ODPA on nitinol surface.

While IR can be used to characterize alkyl chain ordering and binding of the molecules to the surface, it cannot determine film height or integrity. Therefore, AFM imaging was used in this study to further characterize monolayer formation. The root mean square (rms) roughness parameter is a measure of the deviations in the surface from the mean plane within the sampling area, which gives insight into height and uniformity.[243] The analysis is carried out by comparing the rms roughness of the unmodified and modified substrates. Modified surfaces with a similar rms roughness to the control surface are considered to be films of monolayer height that follow the contour of the surface, while modified surfaces that have much larger rms roughnesses than the

control are multilayer or nonuniform films.[15, 244] The nitinol control sample had an average rms roughness of 8Å (Figure 3.2a). Modified samples with monolayers, after sonication, had an rms roughness of 10Å (Figure 3.2c). Therefore, it is concluded that the molecules followed the contour of the sample with a single layer of molecules with no aggregates. An illustration of the NiTi surface modified with multilayers with an rms roughness of 29Å can be seen in Figure 2b. Multilayer films were imaged before sonication in THF. In a multilayer sample, as expected, islands of agglomerate layers can be observed and the surface is not homogeneously covered.

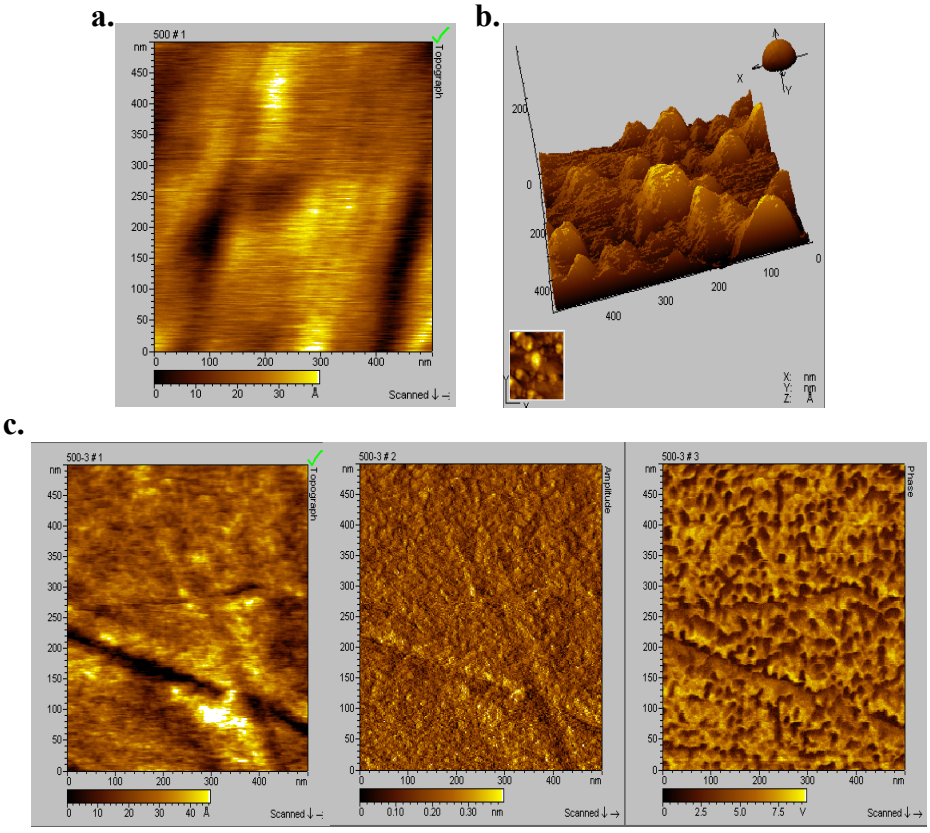

Figure 3.2 (a) AFM image of clean NiTi (rms roughness=8 Å) (b) Multilayer formation of ODPA on NiTi surface in 3D image (rms roughness = 29 Å) and (c) NiTi surface after modification with ODPA and sonication in THF (rms roughness=10Å) in amplitude, topography, and phase.

MALDI-TOF MS analysis was used to confirm the height of the films on the surface. Using this technique we are able to differentiate between mono- and multilayers in these systems.(Chapter 2)[15] Multilayer formation is a common problem which is traditionally difficult to analyze, but analysis by MALDI-TOF MS has proven to provide reliable and easy-to-acquire data about the number of layers in an organic thin film. Here MALDI-TOF analysis was performed in positive mode on the modified samples. To obtain statistically significant results three to five spots per sample and three samples were analyzed. In each sample, the matrix background (CHCA) can be seen. ODPA was detected in the MALDI-TOF at *m/z* 335.282, corresponding to an ODPA molecule plus H+. In the mass spectra of monolayer samples, only the monomer peak can be seen.[15] This data is consistent with mass spectra from other well-characterized phosphonate-metal oxide systems. Mass spectra of phosphonate monolayers on titanium, iron, or stainless steel oxide substrates contain a peak at ODPA+ H^+.[15] This result is independent of bonding motif. In contrast, in the mass spectra of multilayer samples (as determined by AFM), peaks corresponding to monomer at *m/z* 335.282 and dimer at *m/z* 669.560 aggregates can be seen (Figure 3.3c and Figure 3.3d respectively). This data is consistent with the AFM data and confirms the formation of uniform monolayers on the NiTi surface.

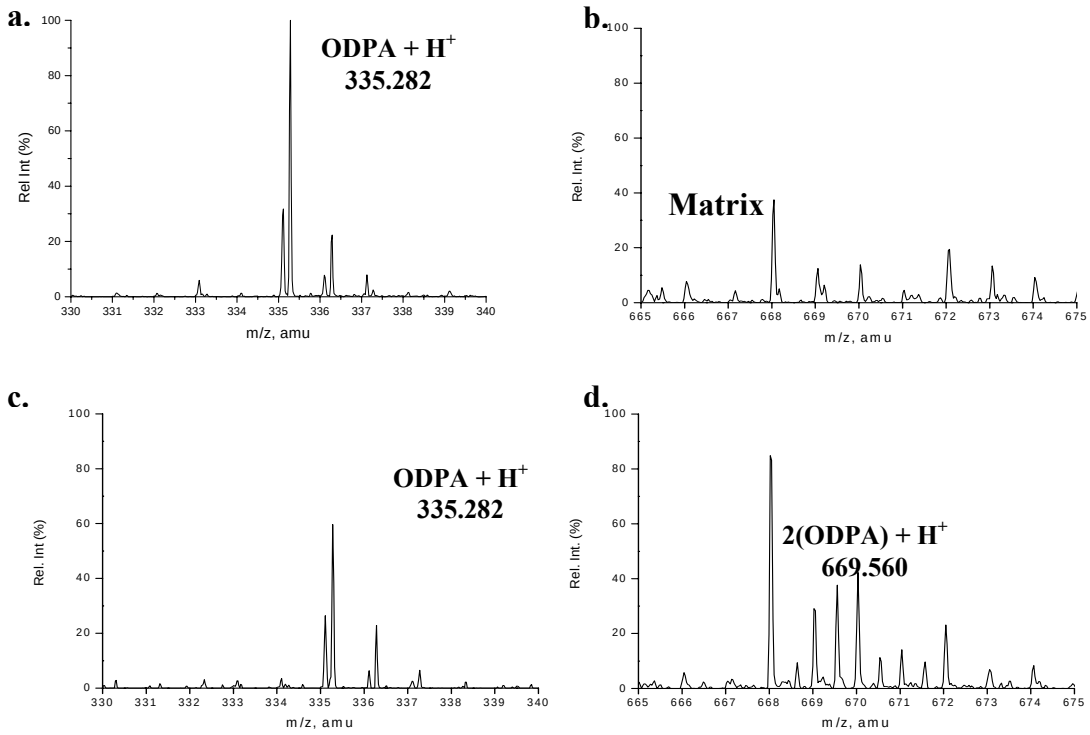

Figure 3.3 (a) Representative MALDI-TOF spectra of the ODPA monolayer on nitinol surface shows mass peak at *m/z* 335.282 resulting from the monomer peak; (b) Dimeric region of ODPA on NiTi surface; (c) Monomer region of ODPA multilayer modification shows mass peak at *m/z* 335.282 on NiTi surface; (d) Dimeric region of ODPA multilayer modification on NiTi surface shows a mass peak at *m/z* 669.560.

Stability of the monolayers was analyzed under several different conditions. The samples were first left under atmospheric conditions and analyzed once per week for over a year. The monolayers remained ordered and bound to the surface as indicated by the lack of change in the DRIFT spectra. In this study, the position of the peaks corresponding to ν_{CH2} after the monolayers were being formed over one year and five months were $\nu_{CH2\ asym}$= 2908 cm^{-1} and $\nu_{CH2\ symm}$= 2842 cm^{-1}, respectively, showing a strongly bound and ordered film is present (Figure 3.4a).

The modified samples were then rinsed using 1M and 6M HCl and NaOH. DRIFT spectra after the acid and base immersion remained unchanged. When the ODPA samples were rinsed with 6M HCl the peaks corresponding to ν_{CH2} were $\nu_{CH2\ asym}$= 2907 cm^{-1} and $\nu_{CH2\ symm}$= 2840 cm^{-1}, respectively (Figure 3.4b). Moreover, the modified samples were rinsed with 1M HCl and showed the PO region of the bound ODPA contained broad PO group stretches at $\nu_{P=O}$ = 1260 cm^{-1}, ν_{P-O} = 1046 cm^{-1} and ν_{POH} = 945 cm^{-1}. When the modified samples were rinsed with 6M NaOH, the peaks corresponding to ν_{CH2} were $\nu_{CH2\ asym}$= 2913 cm^{-1} and $\nu_{CH2\ symm}$= 2847 cm^{-1}, respectively. (Figure 3.4c) Rinsing the sample with protic solvents (water and ethanol) also had no effect on the stability of the films.

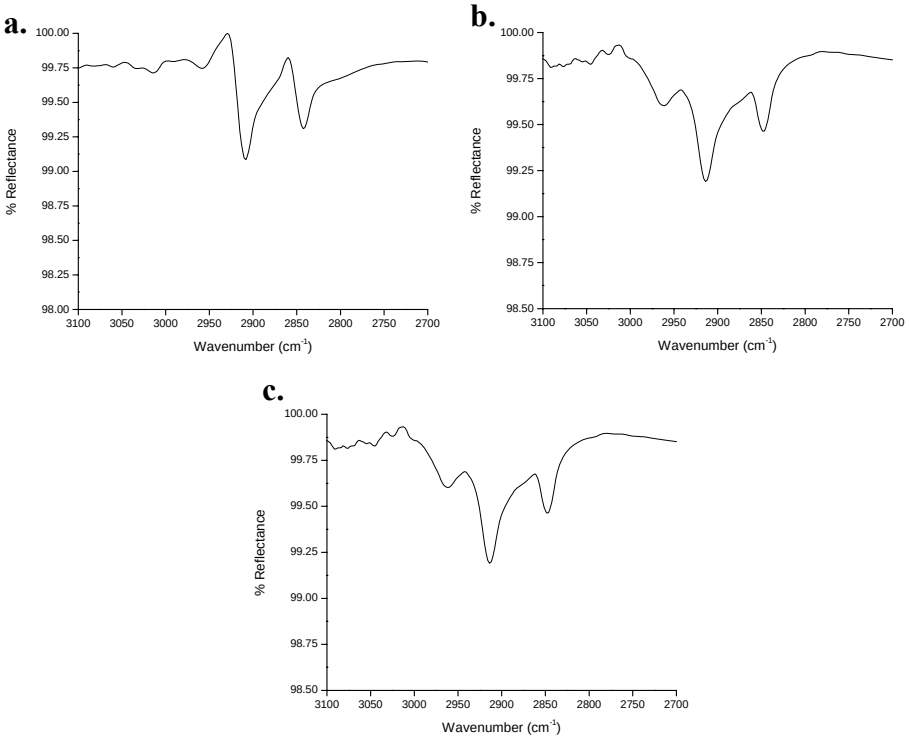

Figure 3.4 (a) IR spectra of ODPA on nitinol surface after one year of being formed on the NiTi surface; (b) IR spectra of ODPA on nitinol surface after been rinsed with 6M HCl. (c) IR spectra of ODPA on nitinol surface after been rinsed with 6M NaOH.

3.3.1.1 Chain Lengths

An important stabilizing factor in organic monolayers films is the attractive van der Waals interaction between chains, which play an essential role in the packing and self-organization of the molecules.[106] This stability and chain ordering increases as the chain length of the alkyl-headgroup backbone increases.[12, 18, 245] A long alkyl chain, >12 carbons, is commonly used in the formation of SAMs because longer chain lengths tend to form all trans conformations in the alkyl chain instead of gauche conformation on the surface due to the high number of van der Waals interactions.[17, 18, 246, 247] Substantial disorder is generally found in films formed by short chain molecules.

Here, short chain alkylphosphonic acids (eleven, eight, and four carbons) were used to form films on the NiTi oxide surface. As the chain length decreased, it was necessary to use different deposition conditions to form monolayers on the NiTi surface.

Undecylphosphonic acid was used to form monolayers by aerosol spraying the substrates twice (0.50mM in THF solution) and drying the substrates at room temperature in between sprays. The DRIFT spectra of the samples contained peaks at 2913 cm^{-1} ($\nu_{CH2\ asym}$) and 2845 cm^{-1} ($\nu_{CH2\ sym}$) in the IR after deposition, which shifted to 2914 cm^{-1} and 2847 cm^{-1}, respectively after rinsing in THF (Figure 3.5a). MALDI-TOF analysis was performed on NiTi after modification with undecylphosphonic acid, and a peak at *m/z* 237.162 (UPA + H^+) corresponding to the monomer was seen and the dimer peak was not observed concluding a monolayer formation (Figure 3.5b). Undecylphosphonic acid samples have a contact angle= 109° caused by the hydrophobic tail group as seen in ODPA samples. These results are consistent with alkyl-chain ordered monolayers.

Previous reports of odd chain length organic acid monolayers indicate that the molecules are not as well organized on the surface as even chain molecules with organic acid head groups,[72, 248, 249] however, this disorder was not observed here.

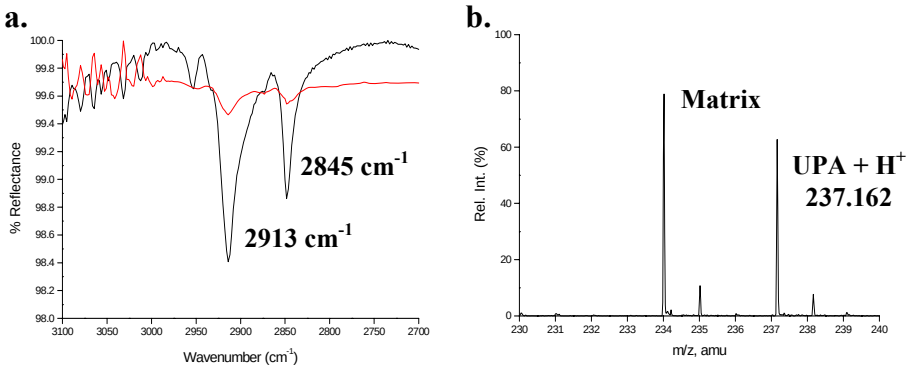

Figure 3.5 (a) IR spectra of undecylphosphonic acid on nitinol surface after deposition (black spectra) and after the rinse test (red spectra). (b) MALDI-TOF spectra of the monomer region of undecylphosphonic acid SAMs on NiTi at *m/z* 237.162.

To form monolayers with octylphosphonic acid, an increase in concentration and temperature was required. The samples were aerosol sprayed twice (0.75mM concentration) and heated to 120°C after each deposition. The IR peaks attributed to $\nu_{CH2\ asym}$ = 2915 cm^{-1} and $\nu_{CH2\ sym}$ = 2847 cm^{-1} after deposition, shift slightly to 2914 cm^{-1} and 2848 cm^{-1} after rinsing with THF (Figure 3.6a). Octylphosphonic acid samples have a contact angle of 105° caused by the hydrophobic tail group as seen in ODPA samples. MALDI-TOF analysis gave at *m/z* 195.118 (OPA + H$^+$) corresponds to the monomer peak with no dimer peak present; confirming monolayer film formation (Figure 3.6b).

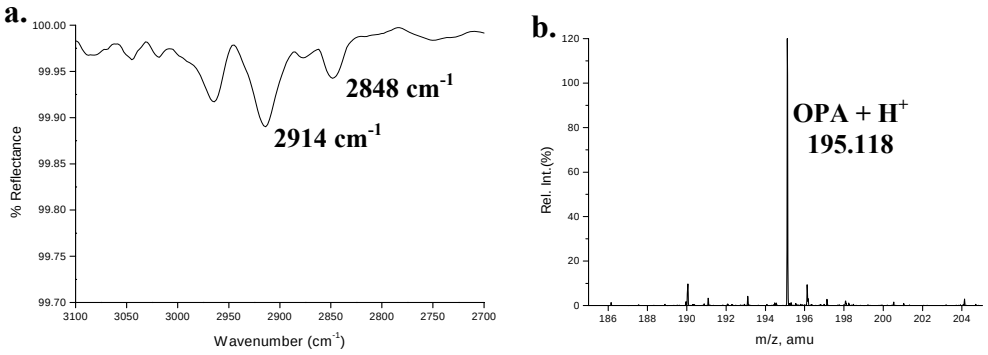

Figure 3.6 (a) IR spectra of octylphosphonic acid on nitinol surface after rinsing. (b) MALDI-TOF spectra of the monomer region of octylphosphonic acid SAMs on NiTi at *m/z* 195.118.

Butylphosphonic acid did not form monolayers on the NiTi surface. This is due to limited van der Waals interactions in the short chains. Our results are consistent with other reports that a limited degree of orientation for short chains is observed.[8, 16, 18, 110, 250]

3.4.1.2 Tail Groups

Tail group functionality can affect SAM formation and stability and can be used to change the surface from hydrophobic (methyl terminated) to hydrophilic (carboxylic acid and hydroxyl terminated).[35, 42, 44, 47] Hydrogen bonding between terminal groups in SAMs is thought to contribute to the stabilization of monolayers in hydroxyl- and carboxylic acid-terminated monolayers.[49] Thus, a hydrophilic interface was prepared using carboxylic acid (-COOH) hydroxyl (-OH) and phosphonic acid ($-PO_3H_2$) terminated alkylphosphonic acid SAMs on the NiTi surface.

A DRIFT spectrum of 12-carboxydodecanephosophonic acid is shown in Figure 3.7a. The peaks corresponding to $\nu_{CH2\ asym}$ (2910 cm^{-1}) and $\nu_{CH2\ sym}$ (2846 cm^{-1}) after

deposition and rinsing with THF indicate that a strongly bound and ordered monolayer is present (Figure 3.7a). There was no evidence in the IR of bridging by the carboxylic acid tail group. To understand the reactivity of the carboxylic acid moiety, octadecylcarboxylic acid was deposited under the same conditions, and no evidence of film formation was seen in the IR spectrum. The carbonyl stretching was analyzed by IR showing a peak at 1691 cm^{-1} corresponding to the carbonyl peak (C=O) of the carboxylic acid tail group. This peak is attributed to hydrogen bonding between the surface and free carboxylic acid peak , because the carboxylate asymmetric and symmetric peaks are not observed.[104, 251] (Figure 3.7b- red spectra) The carbonyl peak of the solid compound is seen at 1684 cm^{-1}. (Figure 3.7b-black spectra) Furthermore, MALDI-TOF was used to characterize this functionalized surface. Analysis of the SAMs using MALDI-TOF (Figure 3.7c) reveals a peak at *m/z* 303.137 corresponding to a (12-carboxydodecyl)phosphonic acid monomer sodiated on the NiTi surface. The dimeric peak was not detected when the monolayers were analyzed, however, matrix background can be seen (Figure 3.7d).

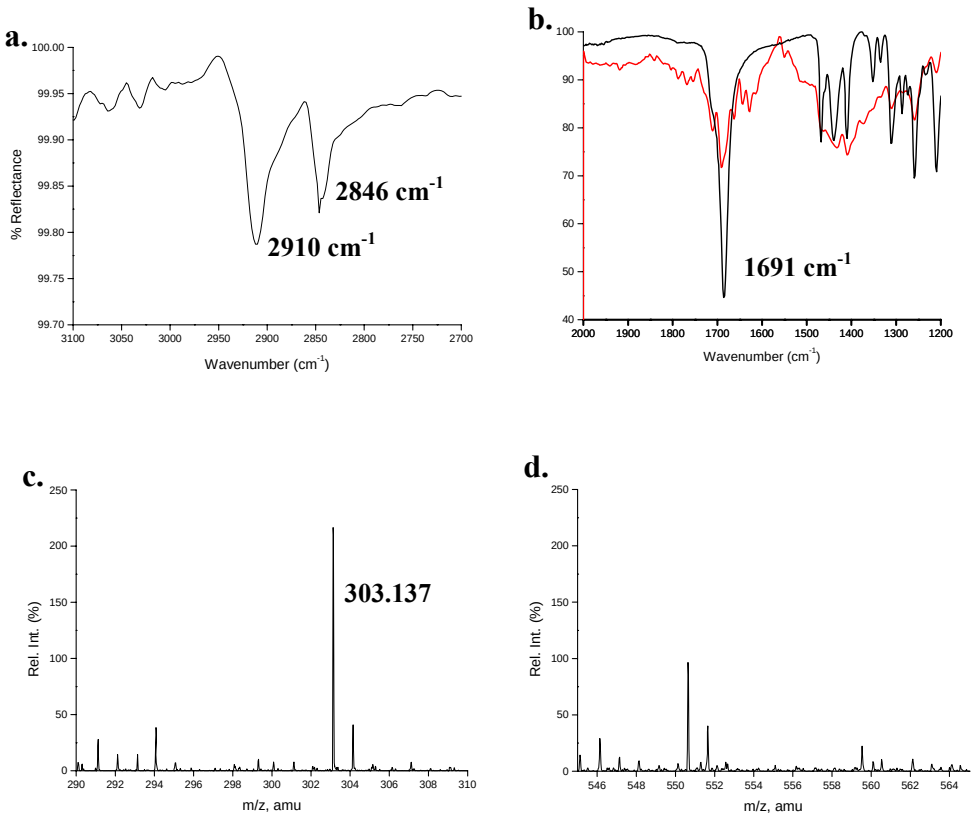

Figure 3.7 (a) IR spectra of (12-carboxydodecyl)phosphonic acid on nitinol surface after rinsing; (b) IR of carboxylic acid region of the modified sample (red spectra) and the solid control (black spectra) (c) MALDI-TOF spectra of the monomer region of (12-carboxydodecyl)phosphonic acid SAMs on NiTi at *m/z* 303.137 and (d) dimeric region which shows no evidence of dimer formation from the surface.

Hydroxyl tail groups have been shown to have a stabilizing effect on SAMs formed from alkanethiols on gold.[19, 42] The stabilization of the well-ordered structure is accomplished via hydrogen-bonding. 12-hydroxyl (-OH) terminated phosphonic acid was synthesized and used to form ordered monolayers.[24, 240, 241, 252] The position of CH_2 peaks after deposition were $\nu_{CH2\ asym}$ =2914 cm^{-1} and $\nu_{CH2\ sym}$ =2848 cm^{-1} and at 2913 cm^{-1} and 2848 cm^{-1}, respectively, after rinsing with THF. The PO region of the IR spectra indicates a monodentate orientation of the acid on the surface. (Figure 3.8a) This is

supported by the presence of the PO group stretches at $\nu_{P=O}$ = 1162 cm^{-1}, ν_{P-O} = 1016 cm^{-1} and ν_{POH} = 935 cm^{-1} and is consistent with the bonding seen earlier. (Figure 3.8b) Further, unbound -OH was detected at 3737 cm^{-1},[253] indicating that the –OH tail group was not bound to the surface and therefore, is free to react at the interface (Figure 3.7). Since the hydroxyl groups are not hydrogen bound to each other, the molecules do not act as a stabilizing influence here on the monolayer as in other systems.[42] This is illustrated by the fact that the monolayers are stable to rinse but not sonication. The alkyl chain of the hydroxyl monomers is seven carbons shorter than that of the methyl terminated chain. This chain length effect may play a role in the instability of the film. Previously, a lower degree of order was reported for (shorter)hydroxyl terminated-thiols on gold than longer methyl counterparts.[42] To better understand the bonding affinity of the hydroxyl group, octadecanol was deposited on the NiTi surface. However, there was no evidence of organic moities on the surface after deposition. This supports the supposition that bridging of the molecules is not seen in this system. Mass spectrometer analysis using the electrospray was performed on (11-hydroxyundecyl)phosphonic acid solid control (MW 252.29 g/mol) and exhibits the monomer peak protonated and sodiated at 253.29 *m/z* and 275.28 *m/z* respectively. The modified samples were characterized using MALDI-TOF showing a peak at 275.093 *m/z*.

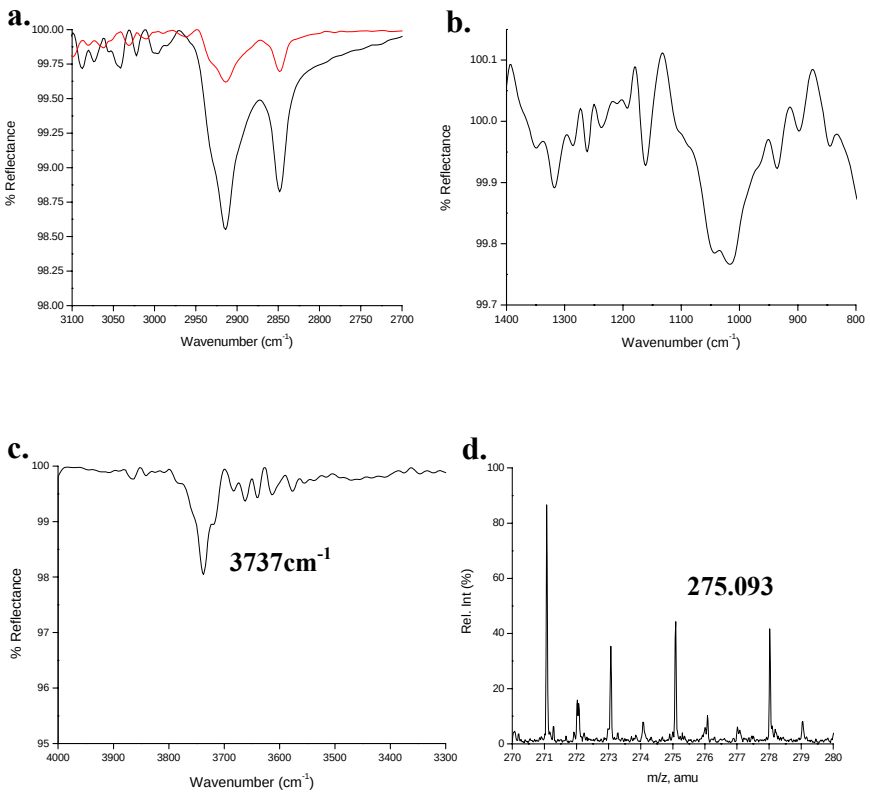

Figure 3.8 (a) IR spectra of (11-hydroxyundecyl)phosphonic acid on nitinol surface after deposition (black spectra) and rinsing with THF (red spectra); (b) IR of PO region of the modified sample (c) OH region of (11-hydroxyundecyl)phosphonic acid on nitinol surface after the deposition showing a -OH unbounded peak at 3737 cm^{-1}; (d) MALDI-TOF spectra of the monomer region of (11-hydroxyundecyl)phosphonic acid SAMs on NiTi at *m/z* 275.093.

3.4.1.3 Multilayer Formation using Diphosphonic Acid Functionalized SAMs

The phosphonic acid head group has been used to modify the titanium oxide surface previously.[254] Researchers have reported the formation of self-assembled monolayers of phosphonic acid can be strongly bonded onto the titanium oxide or titanium alloy surfaces via reaction of phosphonic acids with their native oxides.[16, 24, 42, 47] However, attempts to control film formation when the molecules contain two phosphonic

acids have not been successful.[2, 254] Here, 1,12 dodecyldiphosphonic acid was synthesized according to literature.[240] A solution of 0.50mM was used to modify the bare NiTi surface. The samples were sprayed once with the organic acid solution, dried at room temperature and rinsed with THF. The position of CH_2 peaks after deposition were $\nu_{CH2\ asym}$ =2915 cm^{-1} and $\nu_{CH2\ sym}$ =2848 cm^{-1} after rinsing with THF. The PO region of the IR spectra of the acid on the surface was analyzed. Moreover, the presence of the PO group stretches at $\nu_{P=O}$ = 1227 cm^{-1}, ν_{P-O} = 1023 cm^{-1} and ν_{POH} = 935 cm^{-1} were seen. (Figure 3.9b) The PO region of the 1,12 dodecyldiphosphonic acid solid shown peaks in the IR at $\nu_{P=O}$ = 1133 cm^{-1}, ν_{P-O} = 1001 cm^{-1} and ν_{POH} = 946 and 935 cm^{-1}. Mass spectrometer analysis using the electrospray was performed on (1,12 dodecyldiphosphonic acid solid control (MW 330.29 g/mol) and exhibits the monomer peak protonated and sodiated at 331.14 *m/z* and 353.13 *m/z* respectively. The modified samples were characterized using MALDI-TOF showing a peak at 331.146 *m/z* indicating monolayer formation. (Figure 3.9c)

The modified samples were imaged by contact mode AFM. Tightly packed molecules can be seen in the AFM image with no aggregates. (Figure 3.9e) These images were taken in the repulsive or contact mode where the probe is dragged across the surface of the sample.[131] The unmodified, silicon nitride tip is brought close enough to the surface to detect the repulsive force between the atoms of the tip material and the sample and this interatomic forces will induce bending of the cantilever.[131] Given that a phosphonic acid interface should theoretically be hydrophilic and that a silicon nitride tip was used, the interatomic interactions between the moisture on the tip and the modified sample should have prevented the image from being taken.[120, 130] For example, a relative

humidity between 20-40%, can cause discontinuities in the force measurements as a result of the formation of a capillary meniscus.[255, 256] Because capillary forces can critically affect the measurements, the relative humidity was recorded for each experiment and found to be around 30%. Therefore, it appears that the tip was hydrophilic and could not image a hydrophilic surface in contact more. This led to the supposition that the diphosphonic acid was in a bridging orientation on the surface (Figure 3.9d).

This inference from the AFM data was supported by other pieces of data. First, acetyl chloride could not be reacted with the "terminus" phosphonic acid indicating the phosphonic acid tail groups were inaccessible for reaction, either due to hydrogen bonding or covalent bonding with each other or the surface. Further, the contact angle was only 80°. This value is higher than expected and previously reported.[254] The contact angle value is not as hydrophobic as if there were a close-packed, methyl terminated film, however the tilt angle and orientation of the monolayer on the surface effects in the wettability.[68, 239, 257, 258] In the case of this bridging system, the water is interacting with the methylene region. The IR indicates the formation of an ordered film but cannot rule out bridging interactions. Therefore, it is clear that the diphosphonic acid is bound to the surface through a bridging motif where both phosphonic acid groups are bound to the surface.

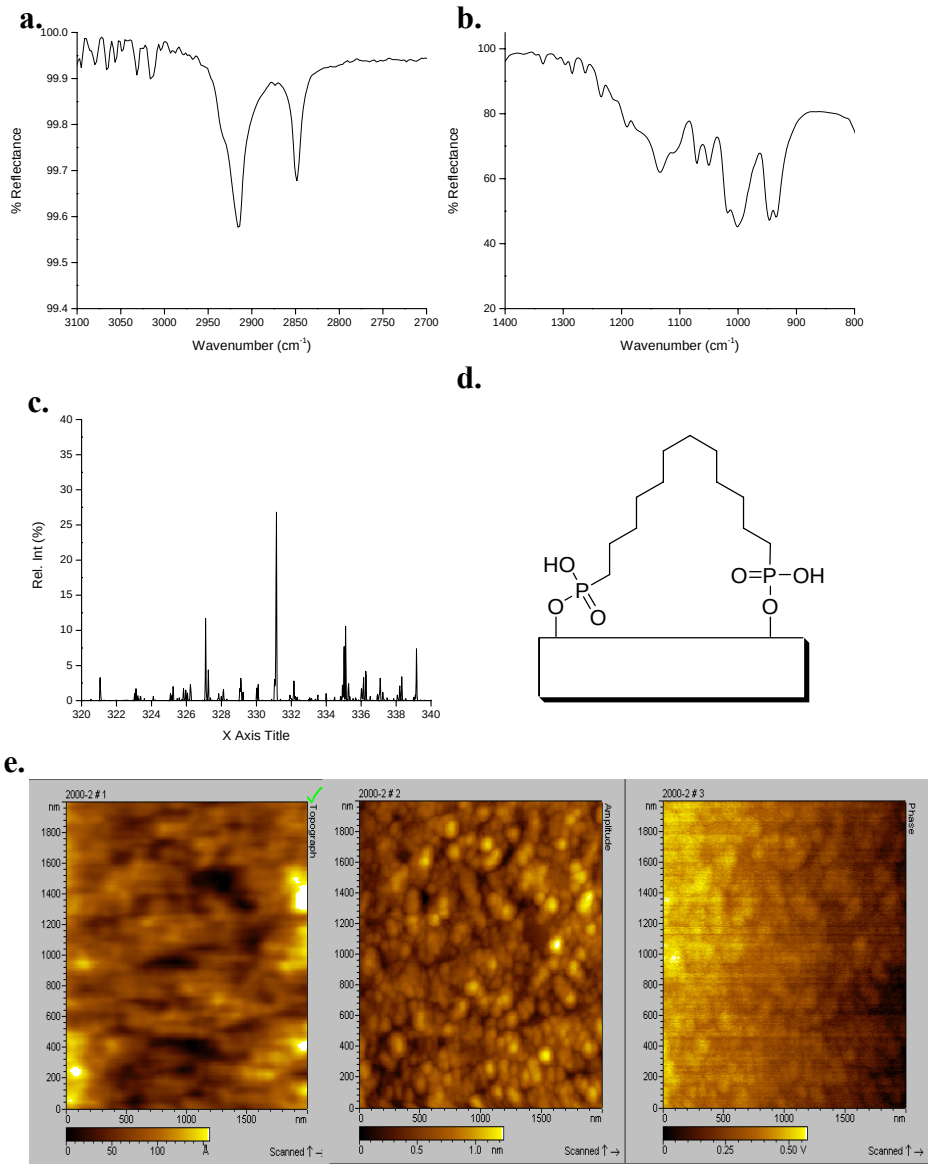

Figure 3.9 (a) IR spectra of 1,12 dodecyldiphosphonic acid on nitinol surface after rinsing with THF, (b) IR of PO region of the solid 1,12 dodecyldiphosphonic acid, (c) MALDI-TOF spectra of the monomer region of 1,12 dodecyldiphosphonic acid SAMs on NiTi at *m/z* 331.146, (d) Structure proposed of 1,12 dodecyldiphosphonic acid on the nitinol surface in a bridging binding with the oxide layer, (e) AFM image in contact mode of 1,12 dodecyldiphosphonic acid 3μm range.

Table 3.1 Summary of results of modifications of the nitinol oxide surface.

Organic Acids	**Deposition (cm^{-1})**	**Rinsed (cm^{-1})**	**Sonication (cm^{-1})**	**Contact angles (degrees)**	**MALDI (m/z)**
Butylphosphonic	Not formed				
Octadecylphosphonic (ODPA)	2915 / 2847	2913 / 2846	2913 / 2846	107 ± 3	335.282
Undecylphosphonic (UPA)	2913 / 2845	2914 / 2847	2915/ 2848	109 ± 7	237.162
Octylphosphonic (OPA)	2915 / 2847	2914 / 2848	removed	105 ± 5	195.118
(12-carboxydodecyl)phosphonic	2910 / 2846	2910 / 2846	2913/ 2847	42 ± 4	303.137
(11-hydroxyundecyl)phosphonic	2916 / 2848	2917 / 2848	removed	64 ± 3	275.093
1,12 dodecyldiphosphonic	2914/ 2848	2915/ 2848	2913/ 2847	80 ± 9	331.154

The surface hydrophobicity of the modified substrates was determined by contact angle measurements. By convention, contact angles were evaluated using water. Larger contact angles indicate a more hydrophobic surface due to the rounding of the water on the surface and smaller angles are seen on hydrophilic surfaces.[111, 259] As expected, the methyl terminated SAMs had the largest contact angle of 107°, compared to 46º for the native surface. This is comparable to methyl terminated SAMs on gold, carboxylic acid on stainless steel 316L, and phosphonic acid on titanium surface and stainless steel 316L.[8, 9, 16, 19] The hydroxyl terminated SAMs were more hydrophilic with a contact angle of 64º, as were the carboxylic acid terminated SAMs with a contact angle of 42º. Moreover, the total surface energy increases with the hydrophilicity of the surfaces. [255]

Therefore, we can control the interfacial properties of the surface using the bifunctional molecules, additionally, the tail groups are presented in a reactive manner. These polar terminal groups are expected to increase the degree of order in the monolayer[240] and stability of the monolayer. The carboxylic acid terminated monolayers remained after both rinse and sonication, as predicted; however, the hydroxyl terminated monolayers were bound to the surface after rinse but not after sonication.

3.4.1.4 Electrochemical Stability

The stability of the organic monolayers and their ability to reduce electrochemical activity on the surface was analyzed. The samples were placed in a 0.1M NaOH solution and the potential was scanned from -300 to 700 mV at a scan rate of $50mVs^{-1}$ in solution, which are typical conditions for these studies.[199, 201] For comparison, the cyclic voltammogram of a cleaned but atmospherically oxidized nitinol oxide surface (Figure 3.10a, black line) is superimposed on the modified surface (Figure 3.10a. red line). During the anodic potential sweep, the clean nitinol surface shows a peak at 0.418V assigned to the oxidation of the metal and the formation a passive layer of nickel oxide.[153, 154, 237] The samples were scanned 5 times with no change in the size of the oxidation peak indicating that the monolayers are stable to electrochemical oxidation. Based on the cyclic voltammograms collected, and calculated on current-potential intensity relations, in which mean values of the potential and current intensity obtained at the beginning and the end of the current step were presented. The bare oxide surface has a charge density of 0.25 mA/cm^2 and the modified NiTi surface with ODPA has charge density of 0.15 mA/cm^2 overall through the electrochemical analysis. (Figure 3.10b) Therefore, the monolayer reduced the electrochemical activity on the surface by 40% at

a potential of 700mV which is the highest current measured and is the potential at which the nickel component oxidizes.[155, 237] As a result, the oxidation of the nitinol oxide specially the nickel species has decreased compared to the unmodified substrates.

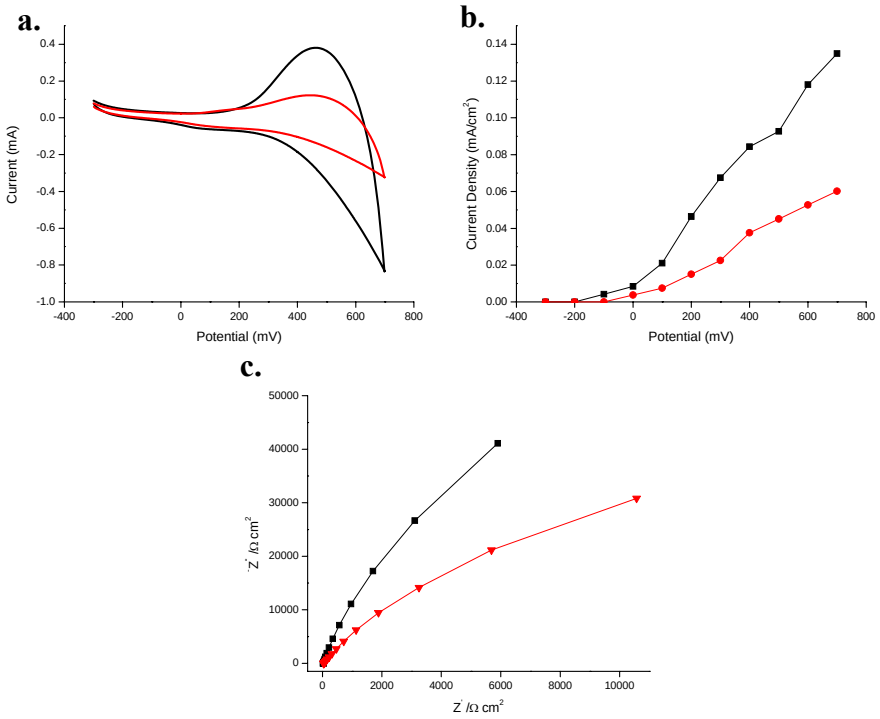

Figure 3.10 (a) Cyclic voltammograms for the bare nitinol electrode (black line) and modified by ODPA monolayers (red line), (b) Current density measurements for the bare nitinol electrode (black line) and modified by ODPA monolayers (red line), (c) Nyquist plot of bare nitinol surface (black line) and ODPA modification (red line**).**

Electrochemical impedance spectroscopy (EIS) provides an effective method for measuring the film's resistance to the ionic attack of the underlying the surface and has been widely used to evaluate the barrier properties of SAMs.[136, 137] The Nyquist impedance plots of bare nitinol and nitinol modified with ODPA SAMs in 0.1 M NaOH

solution is shown in Figure 3.10c. The capacitive loop is attributed to the relaxation time constant of the charge-transfer resistance (R_t) whose value is approximately equal to the diameter of the capacitive loop.[136, 151, 260] Here, the value of R_t of the bare nitinol oxide surface was 5.9 x 10^3 Ω cm^2 (Figure 3.10c black line). Comparing the Nyquist impedance plot of the bare nickel oxide surface with the SAM coated substrate, the size of the capacitive loop has increased. This indicates that SAM coated surface has the better corrosion protection than nitinol oxide surface since larger semicircles (capacitive loop) in impedance plots represented better corrosion resistance with a R_{SAM} of 1.1 x 10^4 Ω cm^2 (Figure 3.10c-red line). The R_t was expected to increase due to the inhibition of the electron transfer by the monolayer present on the electrode surface.

The protection efficiency (PE) of a film can be calculated comparing the R_{CT} of the bare surface and the R_{SAM} of the modified surface in corrosive solution. Using 0.1 mM NaOH as the aqueous solution,[136, 260] a PE value of 46% was calculated by the following equation:

$$PE\ (\%) = \frac{(R_{SAM} - R_{CT})}{R_{SAM}} \times 100\ \% \qquad (1)$$

3.4.2 Nickel Oxide Surface

Nickel oxide which is 50% of the NiTi composition was modified with 0.35mM aerosol spraying of ODPA. The position of the peaks in the IR spectrum, after aerosol spraying, rinsing and sonication were $\nu_{CH2asym}$= 2915 cm^{-1} and ν_{CH2sym}= 2848 cm^{-1} (Figure 3.11a). The IR spectrum of the PO region of the modified substrates shows that ODPA was bound to the nickel oxide surface in a bidentate manner, as evidenced by the shift

and broadening of $\nu_{P=O}$, ν_{P-O} and disappearance of ν_{POH} peak.[8, 16] (Figure 3.11d) The PO region of the bound ODPA (Figure 3.11b-black spectra) contained PO group stretches at $\nu_{P=O}$ = 1203 cm^{-1}, and ν_{P-O} = 1013 cm^{-1}, while the solid ODPA (Figure 3.11b-gray spectra) showed peaks for $\nu_{P=O}$ = 1211 cm^{-1}, ν_{P-O} = 1075 cm^{-1}, and ν_{POH} = 947 and 931 cm^{-1}.

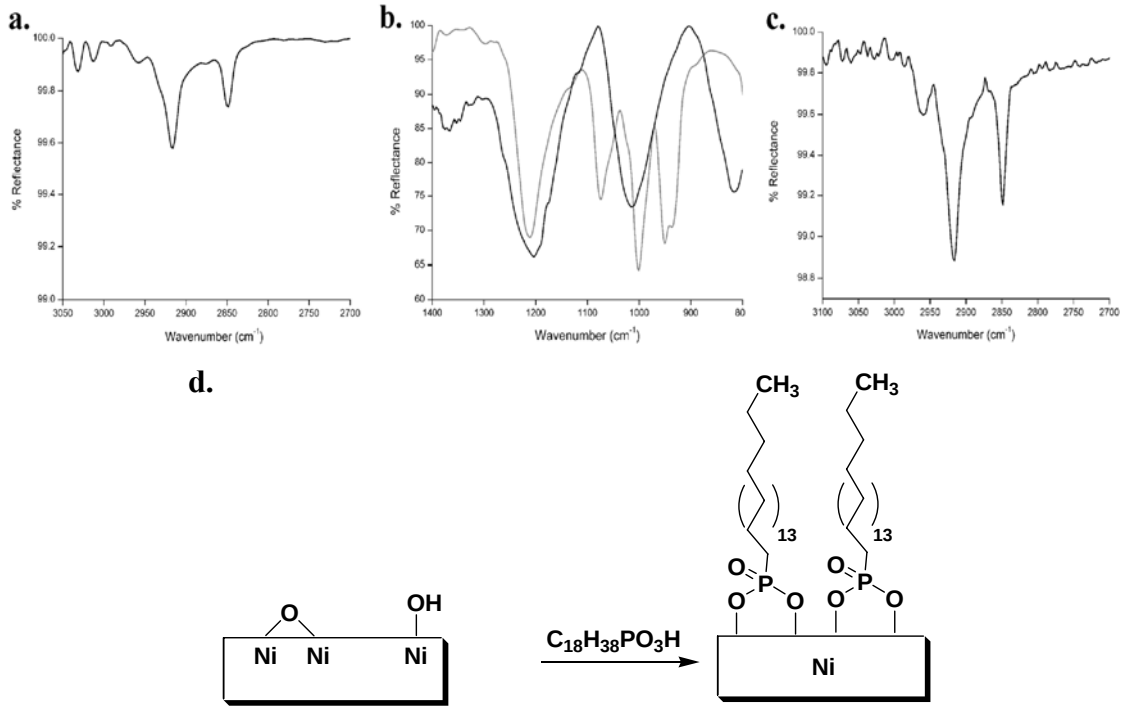

Figure 3.11 (a) IR spectra of ODPA modified nickel oxide formed by aerosol spraying method (0.35mM) after sonication ($\nu_{CH2asym}$ 2915 cm^{-1} and ν_{CH2sym} 2848 cm^{-1}), (b) PO region of same with $\nu_{P=O}$ 1203 cm^{-1}, and the ν_{P-O} 1013 cm^{-1} (black spectra). The PO region of ODPA solid (grey spectra) is shown overlapping the PO region of the nickel oxide modified surface, (c) IR spectra of 0.35mM ODPA formed by aerosol spraying method on nickel oxide one year after being formed ($\nu_{CH2asym}$ 2916 cm^{-1} and ν_{CH2sym} 2848 cm^{-1}), (d) Structure proposed of ODPA on the nickel oxide surface in a bidentate binding with the oxide layer.

Contact angle measurements were consistent with the formation of an ordered, methyl- terminated film on the surface. Modified substrates had a contact angle of 109º ±

5 º with water, while control samples had a contact angle of 68° ± 7.

AFM imaging was performed on substrates modified by the 0.35mM solution aerosol spraying method. The nickel oxide control sample had a rms roughness of 25Å (Figure 3.12a). Modified samples had a rms roughness of 26Å (Figure 3.12b). A tightly packed, smooth and uniform film can be seen in the AFM image of the modified sample. Therefore it is concluded from the AFM results that the adsorbed molecules followed the topography of the substrate.

a.

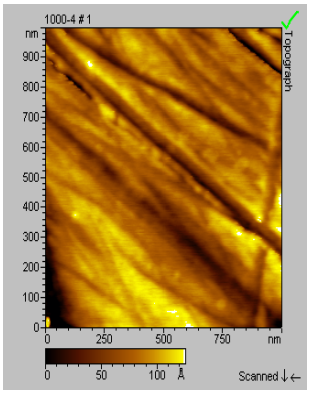

b.

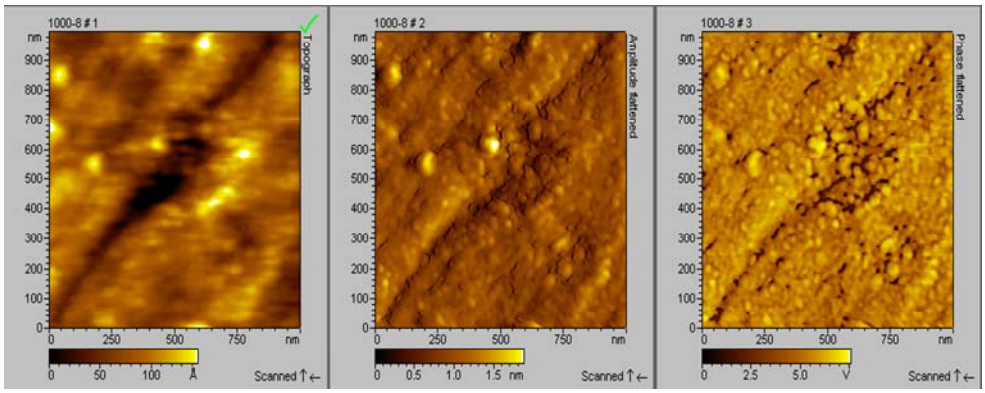

Figure 3.12 (a) AFM image of clean nickel oxide (rms roughness=25 Å), (b) AFM images of the nickel oxide surface after modification with 0.35mM ODPA using aerosol spraying method (rms roughness=26 Å; Topography, amplitude and phase shown L to R).

MALDI-TOF spectrum of the substrates after modification contained a peak at *m/z* 335.276 corresponding to an ODPA molecule plus H+. No dimer peak was detected. This data confirms that the film is a monolayer and not a multilayer when deposited by aerosol spraying deposition using a 0.35mM solution (Figure 3.13).

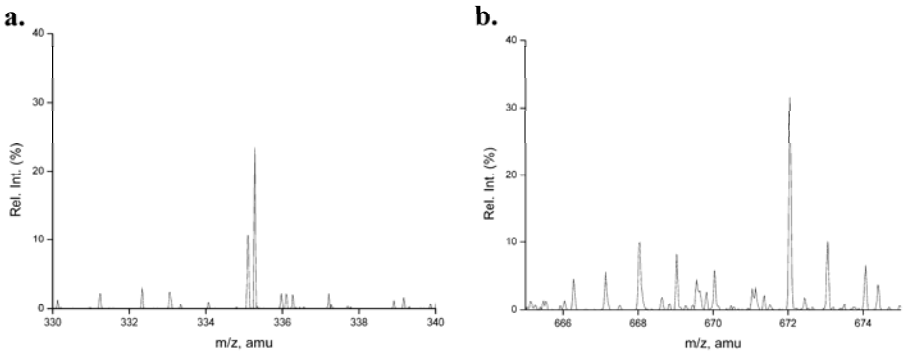

Figure 3.13 (a) Representative MALDI-TOF spectra of the 0.35mM ODPA monolayer on nickel surface formed by aerosol spraying method shows mass peaks at *m/z* 335.276 amu resulting from the monomer peak, (b) dimeric region which shows no evidence of dimer formation from the surface. Matrix peaks can be seen in the spectra at *m/z* 672 amu.

The monolayers formed were analyzed for stability. After rinsing and sonication in THF, the samples were left under atmospheric conditions and analyzed once per week for more than a year. The monolayers remained ordered and bound to the surface as indicated by the lack of change in the DRIFT spectra over the course of one year (Figure 3.11c). Stability to acid and base exposure was tested by rinsing modified substrates in 1M and 6M HCl or NaOH. DRIFT spectra taken after these treatments indicate that the films remain unchanged. Similarly, modified samples were rinsed with water and ethanol, with no change observed in the monolayer by DRIFT.

3.4.2.1 Chain Lengths

Film stability and chain ordering can be dependent on alkyl chain length. In general, stability and order increase as the chain length increases.[18, 98, 245, 247, 261] Monolayer formation utilizing shorter chain phosphonic acids was successful on nickel oxide but the rigor of the deposition conditions increased with decreasing chain length. For example, ordered, stable, monolayers were successfully formed using undecylphosphonic acid by aerosol spraying the substrates twice with a solution concentration of 0.50mM and drying the substrates at room temperature between aerosol exposures.

However, in order to form monolayers with octylphosphonic acid, an increase in concentration and temperature was required. The samples were aerosol sprayed twice with a solution concentration of 0.75mM and heated to 120°C after each spraying. The position of the peaks corresponding to ν_{CH2} of octylphosphonic and after rinsing the substrates with THF were $\nu_{CH2asym}$= 2917 cm^{-1} and ν_{CH2sym}= 2848 cm^{-1} (Figure 3.14a). In both cases, the infrared spectra were consistent with the formation of an alkyl-chain ordered monolayer bound to the substrate through a bidentate interaction between the phosphonic acid and the nickel oxide surface (Figure 3.11b). The films remained intact after solvent rinsing and sonication.

Decreasing the chain length to four carbons led to the formation of a disordered but strongly bound film. The substrates were exposed to the aerosol five times (2mM solution concentration) and heated at 120ºC for 20 minutes after each exposure. The position of the peaks corresponding to ν_{CH2} after deposition of butylphosphonic and rinsing the substrates with THF were $\nu_{CH2asym}$= 2922 cm^{-1} and ν_{CH2sym}= 2851 cm^{-1} (Figure

3.14b). The aerosol deposition conditions to achieve this disordered monolayer were more rigorous than for the other alkyl chains. The need for the increasing rigor of deposition conditions to achieve quality monolayer formation is due to the fact that the shorter chains have less van der Waals interactions to help overcome the energetic penalties of film formation and therefore, more energy is required to form these short chain films.

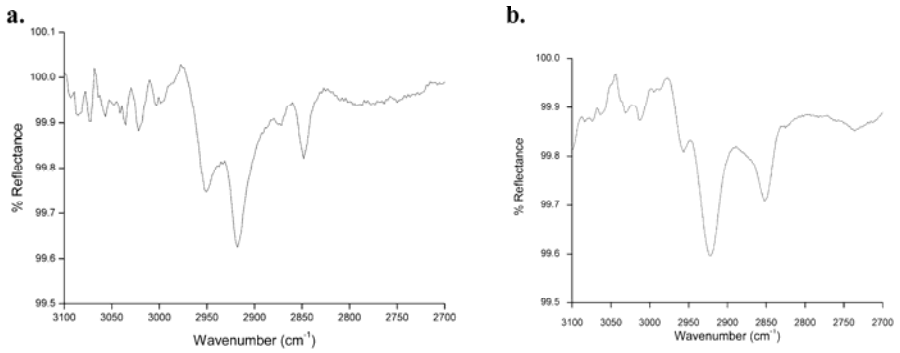

Figure 3.14 (a) IR spectra of Octylphosphonic acid monolayer formed by aerosol deposition method on nickel oxide after rinsing ($\nu_{CH2asym}$ 2917 cm^{-1} and ν_{CH2sym} 2848 cm^{-1}) (b) IR spectra of Butylphosphonic acid film formed by aerosol method on nickel oxide after rinsing ($\nu_{CH2asym}$ 2922 cm^{-1} and ν_{CH2sym} 2851 cm^{-1}).

Functionalized monolayers were formed on the nickel oxide surface using hydroxyl and carboxylic acid terminated monolayers. All the modifications performed on the nickel oxide are shown in a summary chart. (Table 3.2) The modifications were analyzed after deposition, rinsing and sonication in THF solvent, MALDI-TOF analysis and contact angles measurements.

Table 3.2 Summary results modifications performed on the nickel oxide surface using phosphonic acid head group.

Organic Acids	**Deposition (cm^{-1})**	**Rinsed (cm^{-1})**	**Sonication (cm^{-1})**	**Contact angles (degrees)**	**MALDI (m/z)**
Butylphosphonic	2918/ 2849	2922/ 2851	Removed	100 ± 7	138.048
Octylphosphonic (OPA)	2918/ 2848	2917/ 2848	2920/ 2849	110 ± 5	195.189
Undecylphosphonic (UPA)	2914/ 2848	2915/ 2848	2919/ 2848	105 ± 5	237.154
Octadecylphosphonic (ODPA)	2914/ 2847	2914/ 2847	2915 / 2848	109 ± 5	335.276
(11-hydroxyundecyl)phosphonic	2913/ 2848	2913/2848	Removed	69 ± 4	275.087
(12-carboxydodecyl)phosphonic	2912/ 2847	2912/ 2847	2913/ 2847	59 ± 8	303.137
1,12 dodecyldiphosphonic	2916/ 2848	2914/ 2849	2918/ 2849	84 ± 6	331.163

3.4.2.2 Electrochemical Stability

The stability of the organic monolayers and their ability to reduce electrochemical activity on the surface was analyzed. The samples were placed in a 0.1M NaOH solution and the potential was scanned from -300 to +600 mV at a scan rate of $50mVs^{-1}$ in solution, which are typical conditions for these studies.[154, 237] For comparison, the cyclic voltammogram of a cleaned but atmospherically oxidized nickel surface (Figure 3.15a, black line) is superimposed on the modified surface (Figure 3.15a, grey line). During the anodic potential sweep, the clean nickel surface shows a peak at 0.418V assigned to the oxidation of the metal and the formation a passive layer of nickel oxide. The samples

were scanned 5 times with no change in the size of the oxidation peak indicating that the monolayers are stable to electrochemical oxidation. Based on the cyclic voltammograms collected, and calculated o current-potential intensity relations, in which mean values of the potential and current intensity obtained at the beginning and the end of the current step were presented. (Figure 3.15b) The bare oxide surface has a charge density of 0.25 mA/cm^2 and the modified nickel surface with ODPA has charge density of 0.15 mA/cm^2 overall through the electrochemical analysis (Figure 3.15b). Therefore, the monolayer reduced the electrochemical activity on the surface by 40% at 600mV potential in which is the highest current measured due to the oxygen evolution.[155, 237]

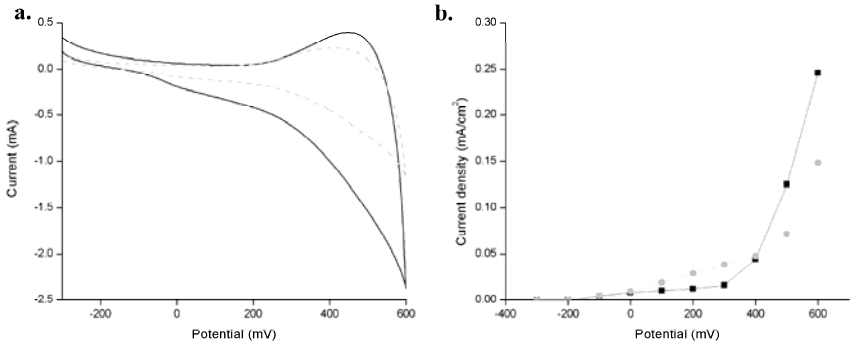

Figure 3.15 (a) Cyclic voltammograms for the bare nickel oxide electrode (black line) and modified by ODPA monolayers (gray line), (b) Current density measurements for the bare nickel oxide electrode (black line) and modified by ODPA monolayers (gray line).

The Nyquist impedance plots of bare nickel oxide and nickel oxide modified with ODPA SAMs in 0.1 M NaOH solution is shown in Figure 3.16. The capacitive loop is attributed to the relaxation time constant of the charge-transfer resistance (R_t) whose value is approximately equal to the diameter of the capacitive loop.[136, 151, 260] Here, the value of R_t of the bare nickel oxide surface was 1.4×10^4 Ω cm^2 (Figure 3.16 grey line).

Comparing the Nyquist impedance plot of the bare nickel oxide surface with the SAM coated substrate, the size of the capacitive loop has increased, indicating SAM has better corrosion protection for the nickel oxide surface since larger semicircles (capacitive loop) in impedance plots represented better corrosion resistance with a R_{SAM} of 2.5 x 10^4 Ω cm^2 (Figure 3.16-black line).[136] The R_t is expected to increase due to the inhibition of the electron transfer by the monolayer present on the electrode surface.

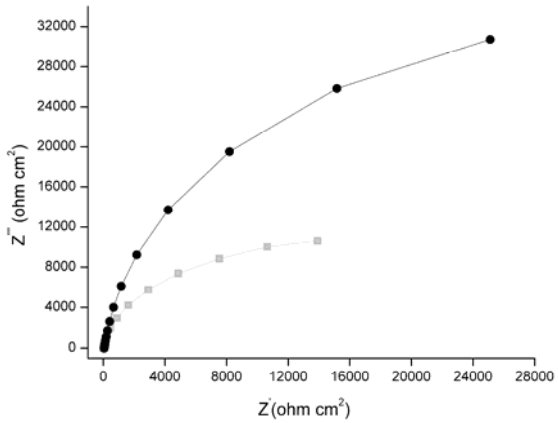

Figure 3.16 Nyquist plot of bare nickel oxide surface (grey line) and ODPA modification (black line).

The protection efficiency (PE) of ODPA on nickel oxide has a value of 45%.[10] Previous reports, show that phosphonic acid on iron monolayers surface had a PE of 52%, however they used diphosphonic acid molecules which can increase the corrosion barrier due to formation of a multimolecular layer on the iron surface.[137, 262] The impedance parameters obtained for nitinol and nickel oxide surfaces are summarized in Table 3.3.

Table 3.3 Summary of impedance parameters obtained by nitinol and nickel oxide modified with ODPA.

	R_t (Ω cm^2)	PE (%)
Bare Nickel Oxide	1.4×10^4	__
ODPA on Nickel Oxide	2.5×10^4	45
Bare Nitinol	5.9×10^3	__
ODPA on Nitinol	1.1×10^4	46

3.4.3 Titanium Oxide Surface

Titanium oxide samples were cleaned and ODPA was deposited by a simple procedure of aerosol spraying (0.35mM solution in THF). This leads to the spontaneous formation of a film on the titanium oxide surface. After deposition, rinsing and sonication in THF solvent, to remove loosely bound material, the samples were characterized by DRIFT. (Chapter 2; Figure 2.7) Then, AFM imaging was performed on substrates modified by the 0.35mM solution aerosol spraying method. The titanium oxide control sample had an rms roughness of 11 Å. Modified samples had an rms roughness of 12Å.(Chapter 2; Figure 2.8) A tightly packed, smooth and uniform film can be seen in the AFM image of the modified sample.[15] A hydrophilic interface was prepared using carboxylic acid (-COOH) and hydroxyl (-OH) terminated alkylphosphonic acid SAMs on the titanium oxide surface. These hydrophilic molecules have been demonstrated to bond strongly on the metal oxide binding preferentially by the phosphonic group.[24, 49, 76]

3.4.3.1 Chain Lengths

Undecylphosphonic acid was used to form monolayers by aerosol spraying the substrates twice (0.50mM in THF solution) and drying the substrates at room temperature

in between sprays. The DRIFT spectra of the samples contained peaks at 2917 cm^{-1} ($\nu_{CH2\ asym}$) and 2848 cm^{-1} ($\nu_{CH2\ sym}$) in the IR after deposition (Figure 3.17a- black spectra) and shifted to 2915 cm^{-1} ($\nu_{CH2\ asym}$) and 2847 cm^{-1} ($\nu_{CH2\ sym}$) after rinsing in THF (Figure 3.17a-red spectra). The PO region of the bound undecylphosphonic acid (Figure 3.17b-red spectra) contained PO group stretches at $\nu_{P=O}$ = 1187 cm^{-1} and ν_{P-O} = 1016 cm^{-1}, while the solid undecylphosphonic acid (Figure 3.17b- black spectra) showed peaks for $\nu_{P=O}$ = 1223 cm^{-1}, ν_{P-O} = 1106 cm^{-1}, and ν_{POH} = 966 and 939 cm^{-1}. The IR spectrum of the PO region of the modified substrates shows that UPA was bound to the titanium oxide surface in a bidentate manner, as evidenced by the shift and broadening of $\nu_{P=O}$, ν_{P-O} and disappearance of ν_{POH} peak as previously observed using ODPA.[15, 16, 57, 263]

MALDI-TOF analysis was completed and a peak at *m/z* 237.148 (UPA + H^+) corresponding to the monomer was seen in the spectrum (Figure 3.17c). Undecylphosphonic acid samples have a contact angle= 105° caused by the hydrophobic tail group as seen in ODPA samples.[15, 16] These results are consistent with alkyl-chain ordered monolayers. This is the first time reported that an odd chain length phosphonic acid monolayer is used to modify the titanium oxide surface. All the modifications successfully achieved on titanium oxide surface were summarized in Table 3.4. A comparison of the data obtained for nitinol, nickel and titanium oxide surfaces is explained in Chapter 4.

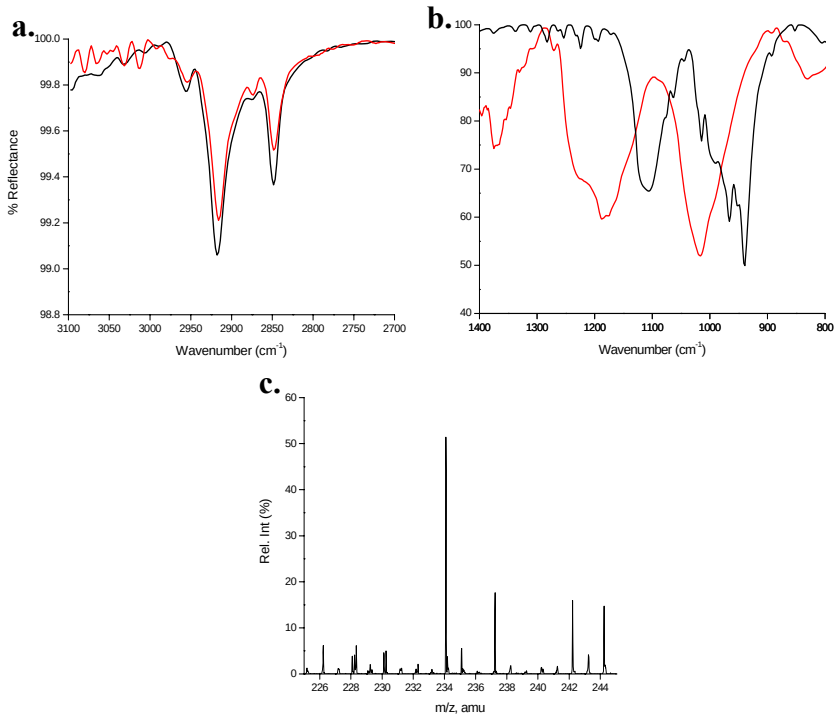

Figure 3.17 (a) IR spectra of CH region of undecylphosphonic acid (UPA) on titanium oxide surface after deposition (black spectra) and after rinsing with THF (red spectra), (b) PO region after rinsed, (red spectra) and the PO region of UPA solid (black spectra), (c) (a) Representative MALDI-TOF spectra of the 0.35mM UPA monolayer on titanium oxide surface shows mass peaks at *m/z* 237.148 amu resulting from the monomer peak.

Table 3.4 Summary results of modifications performed on the titanium oxide surface using phosphonic acid head group.

Organic Acids	**Deposition (cm^{-1})**	**Rinsed (cm^{-1})**	**Sonication (cm^{-1})**	**Contact angles (degrees)**	**MALDI (m/z)**
Butylphosphonic	Not formed	___	___	___	___
Octylphosphonic (OPA)	2915/ 2847	2916/ 2848	removed	108 ± 5	195.121
Undecylphosphonic (UPA)	2915/ 2848	2916/ 2848	2917/ 2849	105 ± 2	237.148
Octadecylphosphonic (ODPA)	2913/ 2847	2913/2847	2913/ 2847	96 ± 5	335.276
(11-hydroxyundecyl)phosphonic	2914/ 2847	2915/ 2847	removed	69 ± 9	275.087
(12-carboxydodecyl)phosphonic	2912/ 2847	2912/ 2847	2913/ 2847	51 ± 7	303.132
1,12 dodecyldiphosphonic	2915/ 2847	2913/ 2848	2913/ 2848	85 ± 5	331.159

3.4 Conclusion

For the first time, well-ordered SAMs using short and long chain phosphonic acids were formed on the native oxide of the nitinol and nickel. In addition, the titanium oxide surface was also modified with phosphonic acid SAMs. SAMs remained intact after rinsing and sonication and were analyzed by IR. The SAMs formed were found to be robust and ordered films over long time periods and able to withstand a range of pH, solvent, and temperature conditions. These strongly bound monolayers were found to interact with the nitinol surface in a monodentate manner. However, the phosphonic acid

monolayers interact with the nickel and titanium oxide surfaces in a bidentate manner.

The hydrophilicity of the surfaces was controlled using hydroxyl (OH), carboxylic acid (COOH) and methyl (CH_3) tail groups. DRIFT, contact angle, AFM and MALDI-TOF were used to characterize the unmodified and modified surfaces. Additionally, these monolayers are stable over the course of at least one year. The organic monolayers were tested by electrochemical analysis and the results of this study show that phosphonic acid monolayers adsorbed on the nitinol and nickel oxide surfaces can reduce electrochemical activity on the surface, often the first step in corrosion. Monolayer formation on the native oxide surface of nitinol and nickel oxide is a significant advance in surface modification of the surfaces and can be used as a building block for future applications in corrosion barriers, biomaterials and electronics.

Chapter 4

Characterization of a Variety of Metal Oxides Using Organic Acid Monolayers

4.1 Introduction

In formation of self-assembled monolayers (SAMs), no preassembly of the adsorbate molecules is carried out, the substrates are exposed directly to the adsorbate in the liquid or gas phase and self-assembly takes place naturally.[17, 264] These organic films form spontaneously on the active sites of solid surfaces such as hydroxyl or μ-oxo groups.[17, 23, 101] SAMs consist of a head group that reacts with the substrate, a tail group that interacts at the outer surface of the film, and a backbone alkyl chain group that connects the head and the tail groups.[264-266] Interactions between backbone groups of the molecules in a film, such as van der Waals and/ or hydrogen bonding can increase the ease of SAM formation and contribute to its stability.[17, 168, 266] Long chain aliphatic molecules with head groups such as silanes,[102, 158, 247, 266] thiols,[20, 21, 23, 33, 48, 155, 267] carboxylic,[9, 17, 46, 66, 70, 73, 251] phosphonic,[8, 14, 16, 24, 25, 27] sulfonic, [25, 27] and hydroxamic acids[22, 28, 29, 147, 148] have been utilized on a variety of substrates. The choice of head

group is critical for the stability of SAMs. For oxide substrates, chemisorption of the molecules is thought to occur via acid-base reactions of the organic acid head group with the –OH and μ-oxo groups on the oxide surfaces.[268] Alternatively, the interaction between the headgroup and the surface may involve proton transfer or salt formation between the organic acid and the metal or the molecules may be physically adsorbed to the surface on the metal.[17, 46] Despite a significant number of reports of SAMs on metal oxides, it is difficult to predict which head groups will result in successful monolayer formation on a given surface. This has been proven to be even more difficult on alloy oxides, where little work has been done. In this study, a variety of organic acids were used to modify oxide surfaces.

In this study several factors will be explored and analyzed in the formation of SAMs using carboxylic, hydroxamic, and sulfonic acids on nickel oxide, titanium oxide and nitinol oxide surfaces. The main difference among these organic acids is the head group acidity; sulfonic is more acidic than hydroxamic or carboxylic acid. However, additional factors such as the chain lengths, isoelectric points, bond lengths, and head group sizes were analyzed. Furthermore, the reactivity of the metal oxide surfaces was evaluated and compared. The modifications on the surfaces were characterized by infrared (IR), matrix assisted laser desorption ionization spectrometry (MALDI), atomic force microscope (AFM) and contact angle measurements.

The adsorption and organization of carboxylic acid monolayers on metal oxide surfaces has been studied.[9, 17, 46, 70, 73, 75] One advantage of carboxylic acid monolayers over other systems is the ability to directly monitor the nature of the interaction between the head group and the oxide surface via the CO stretches in the infrared spectrum. There

are two different surface pKa values reported for the carboxylic acid deprotonation: a pKa value ~ 5 corresponds COOH groups hydrogen-bonded to the interfacial water only, while a pKa around 9 corresponds to COOH headgroups that are hydrogen-bonded to each other as seen in organic solvent solutions.[31] Phosphonic acids, which have a pKa of 4.5,[269, 270] should bind more strongly to metal oxides than carboxylic acids through an acid-base mechanism.[46, 49, 76, 240, 271]

Hydroxamic acids are commonly used in agricultural applications such as pesticides or plant growth promoters.[121, 272-274] Hydroxamic acid or its salts are weak acids that are used as flotation agents due to its strong and selective formation of metal ion complexes such as iron.[273, 275-277] Additionally, hydroxamic acid are used as inhibitors for copper corrosion and as therapeutic agents.[29, 121, 147, 148, 274, 278] This organic acid is not well studied compared to phosphonic and carboxylic acids in monolayers. According to Folkers et al, alkanehydroxamic acid monolayers are more stable than carboxylic or phosphonic acid on metal oxides such as copper, aluminum and iron.[28] These films have been shown to have good corrosion inhibition efficiency due to their well-ordered formation and chain length.[22, 29, 148] The acidity of hydroxamic acids, which have a pKa around 9[28, 279-281], is due to the resonance between the carbonyl and the hydroxyl group and therefore, hydroxamic acids are more acidic than carboxylic acids.[280] Folkers et al. studied the modification of titanium oxide using alkanehydroxamic acids and their results suggested that phosphonic acids form more stable monolayers than hydroxamic or carboxylic acid on TiO_2.[28]

Sulfonic acid has been mainly used as a tail group in monolayer systems of thiols on gold and silver surfaces.[25, 175, 282, 283] Sulfonic acid is known to form hydrogen

bonding interactions, which can increase the acidity and thus, increase the ability to participate in the acid-surface interaction.[284, 285] The pKa of sulfonic acid is approximately 2,[286] which makes it a stronger acid than hydroxamic, phosphonic and carboxylic acids. The interaction of sulfonic acid with surfaces is not well studied. However, the sulfonic acid head group is more acidic than phosphonic acid but the sulfonic acid monolayers are not stable under high temperatures.[25, 27]

4.2 Experimental Section

4.2.1 Methods and Materials

Octadecanehydroxamic acid was synthesized as previously reported.[28] Octanoic acid **(**99.5% purity), tetradecanoic acid (99% purity), pentadecanoic acid (99% purity), hexadecanoic acid (99% purity), octadecanoic acid (95% purity), 12-bromododecanoic acid (97% purity), 12-aminododecanoic acid (95% purity), 12-hydrododecanoic acid (97% purity), 16-hydrohexadecanoic acid (98% purity), tetradecanedioic acid (99% purity), octanohydroxamic acid, potassium salt, octadecanoyl chloride (97% purity), and O-benzylhydroxylamine hydrochloride (99% purity) were obtained from Sigma Aldrich and used without further purification. Heptadecanoic acid (98% purity), perfluorooctadecanoic acid (97% purity), 1-octanesulfonic acid sodium salt monohydrate (99% purity), and sodium 1-undecanesulfonate (98% purity) were obtained from Alfa Aesar and used without further purification. Sodium 1-octadecanesulfonate (97% purity) was obtained from Fluka and nonadecanoic acid (99% purity) was obtained form TCI. Sulfonic acid compounds were acidified using hydrochloric acid and sodium hydroxide.

Hydrochloric acid (Certified ACS Plus,) was purchased from Fisher Scientific without further purification. Nitinol foils (51% nickel: 49 % titanium; 0.008" thickness, >99.0 % purity) were purchased from Johnson Matthey, Inc. Nickel and titanium foils (0.25mm thickness, > 99.0 % purity) were purchased from Goodfellow Inc.

4.2.2 Preparation of the Substrates

Substrates were cut into 1 x 1 cm squares, sanded (220, 320 and 400 grit sandpaper) and then polished (Buehler Ecomet 4 mechanical polisher) using sandpaper of 400, 800, 1200 grits and 1μm diamond suspension. The substrates were rinsed with acetone and methanol and cleaned by ultrasonication in acetone for 1 hour. The substrates were then rinsed with acetone and stored in the oven at 90° C for 30 minutes – 1 hour. The substrates were rinsed again in acetone and stored under vacuum overnight (0.1 Torr).

4.2.3 Formation of Monolayers

Monolayers were formed by spraying the solutions of organic acid in dry tetrahydrofuran (THF) distilled over Na and stored under argon using an aerosol sprayer onto the metal substrates. (TLC sprayer, Sigma Aldrich and N_2) (Figure 4.1) A 0.75mM solution of octadecanesulfonic acid was used to spray the substrates twice. The samples were allowed to dry at room temperature. A 1.5mM solution of octadecanehydroxamic acid was used to spray the substrates 3 times which were dried between sprays in the oven at 120°C for 20 minutes each time. A 1mM solution of perfluorooctadenoic acid was used to spray the substrates twice and dried between sprays at room temperature. A 0.75mM solution of octadecanesulfonic acid was used to spray the samples twice and

dried between sprays at room temperature. A 2 mM solution of octanoic, octadecanoic 12-aminododecanoic, tetradecanoic, pentadecanoic, hexadecanoic, heptadecanoic, 12-hydrododecanoic, octanesulfonic, undecanesulfonic and octanehydroxamic acids were sprayed 5 times and dried between sprays in the oven at 120°C. A 1.5 mM solution of tetradecanedioic and octadecanehydroxamic acids were sprayed 3 times and dried between sprays at room temperature. 1.5 mM solutions of 16-hydrohexadecanoic and 12-bromododecanoic acids were sprayed 4 times and then dried between sprays in the oven. A 0.75mM solution of octadecanesulfonic acid was sprayed 2 times and the substrates were allowed to dry between sprays at room temperature. After modification, all samples were rinsed with THF for 15 minutes and then stored under vacuum overnight (0.1 Torr). The samples that survived the rinsed test were sonicated in THF for 10 minutes or tape tested using Scotch tape #234, which has an adhesion to steel strength of 37oz/in.

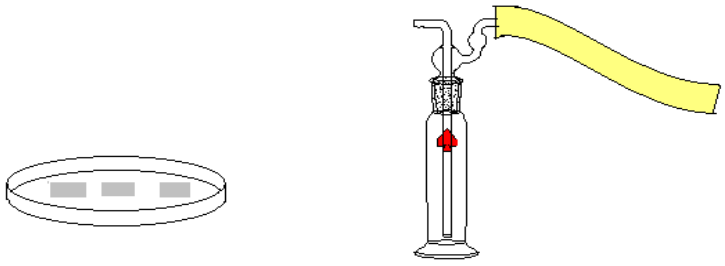

Figure 4.1 Diagram of the aerosol sprayer using for all surface modifications.

4.2.4 Characterization of the Monolayers

Monolayer formation was analyzed using Diffuse Reflectance Infrared Fourier Transform Spectroscopy (DRIFT; Thermo Nicolet-NEXUS 470 FT-IR). The contact

angle measurements (VCA Optima Goniometer Instrument) were used to analyze the hydrophobicity of the surface. Atomic force microscopy (AFM) was used to characterize the surface topography before and after the formation of the organic films. AFM imaging (Molecular Imaging, Pico SPM) of the samples was performed in non-contact mode at ambient conditions using silicon tips.

Atmospheric pressure matrix-assisted laser desorption/ionization time-of-flight mass spectrometry (AP MALDI-TOF MS) was used to analyze the monolayer formation. A high resolution AP MALDI TOF MS (Agilent Tech.) with pulsed dynamic focusing was used. MS analyses of the ions were detected in positive mode using a 337 nm N_2 laser, pulse width of 20 ns, a capillary voltage of 3500 V, fragmentor voltage of 260 V, skimmer voltage of 40 V and drying temperature of 325º C. MALDI preparation was done by the dried-drop method as explained in Chapter 2.

4.3 Results and Discussion

4.3.1 Hydroxamic Acid

4.3.1.1 Nitinol Surface

Modification of nitinol was attempted with an octanohydroxamic acid, however the monolayers were not observed. This could be a result of the weak van der Waals forces between the eight carbon alkyl chains in the monolayers. As a result, octadecanehydroxamic acid (ODHA) was synthesized to see if the stronger van der Waals interactions would increase the adhesion to and stability on the surface.[28] A solution of 1.5 mM ODHA was deposited by aerosol spraying. After deposition, rinsing and sonication, to remove loosely bound material, the samples were characterized by

DRIFT. In the spectra of the modified substrates, the C-H stretches of the methylene group are used as the reference peaks for SAM organization.[17, 66, 106] In this study, the position of the peaks corresponding to ν_{CH2} after rinsing with THF were $\nu_{CH2\ asym}$= 2915 cm^{-1} and $\nu_{CH2\ symm}$= 2848 cm^{-1}, showing that a strongly bound and ordered film is present (Figure 4.2a). The modification was removed from the surface after sonication. The contact angle measurements of the modified surface is consistent with the formation of a hydrophobic interface, with a water contact angle of 103° ± 3, when compared to the control sample's contact angle with water (46°). After sonication in THF, the molecules were removed from the surface.

The nature of the interaction between the molecules and the surface can be can be determined from the shifts and broadening of $\nu_{C=O}$, ν_{N-O}, and ν_{N-H}, indicating a change in head group bonding.[16, 136] Specifically, the CO and NH region of the ODHA solid shows ν_{N-H}= 3252 and 1565 cm^{-1}, $\nu_{C=O}$= 1660 cm^{-1}, and ν_{N-O}= 1080 cm^{-1}. (Figure 4.2b-black spectra) In contrast, the CO and NH region of the bound ODHA contained stretches at ν_{N-H}= 1556 cm^{-1}, and ν_{N-O}= 1067 cm^{-1} and a peak at 1167 cm^{-1} appeared attributed to ν_{C-O}. (Figure 4.2b-red spectra) The IR spectrum of the CO and NH region of the modified substrates shows that ODHA was bound to the nitinol surface in a bidentate manner, as evidenced by the shift to lower frequency of ν_{N-H}, ν_{N-O}, the appearance of ν_{C-O} and absence of $\nu_{C=O}$ peak (Figure 4.2c). Alternatively, the molecules could be bonding to each other in a multilayer/micelle fashion leading to a multiple binding motifs seen in the IR shifts.

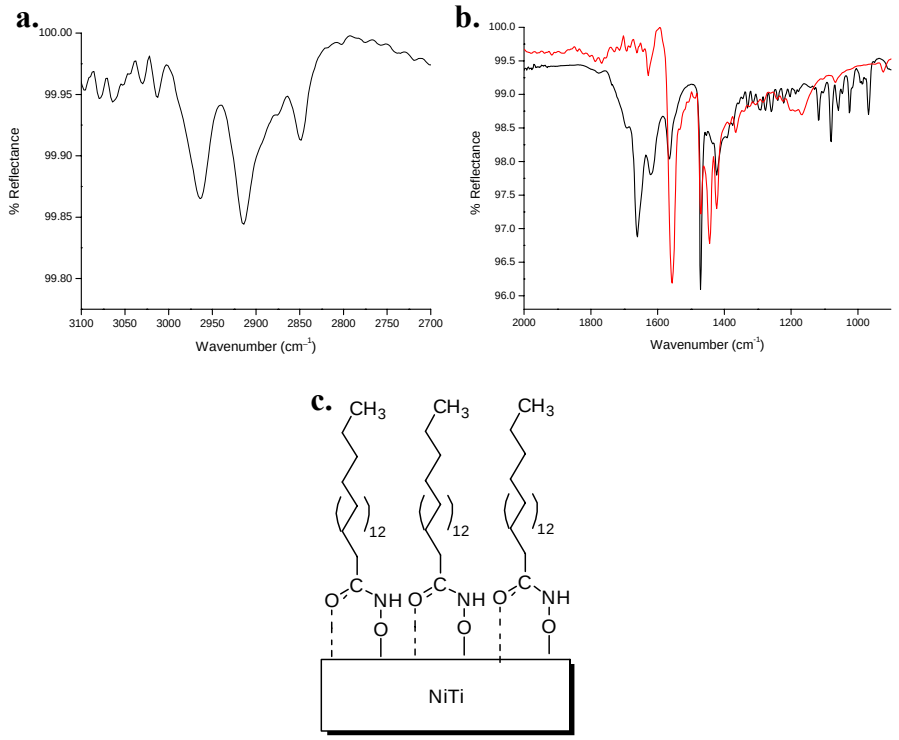

Figure 4.2 IR spectra of ODHA on nitinol surface (a) CH region after rinsed (b) CO region after deposition, (red spectra) and the PO region of ODHA solid (black spectra). (c) The CO and NH region of the IR spectra indicates a bidentate orientation of the acid on the nitinol oxide surface as shown.

AFM images of the surface were obtained before and after the formation of ODHA monolayer and after rinsing with THF. The rms roughness of the control and modified substrates were compared. Modified surfaces with a similar rms roughness to the control surface are considered to be films of monolayer height that follow the contour of the surface, while modified surfaces that have a much larger rms roughness than the control are multilayer or nonuniform films.[15, 244] The samples were scanned over a 1μm^2 region. AFM analysis showed that films formed but that the molecules are not covering

the surface. The rms roughness of the control and modified substrate were 14 Å and 75 Å, respectively (Figure 4.3a and 3b). These values and the images clearly indicate that the surface has non-uniform or multilayer coverage. In a multilayer sample, islands of agglomerate layers can be observed and the surface is not homogeneously covered. These images are correlated to the contact angle values obtained of ODHA on nitinol which are lower than those expected for a hydrophobic surface. It was concluded that ODHA is weakly bound or not covering the nitinol surface uniformly by forming surfactants or micelles.

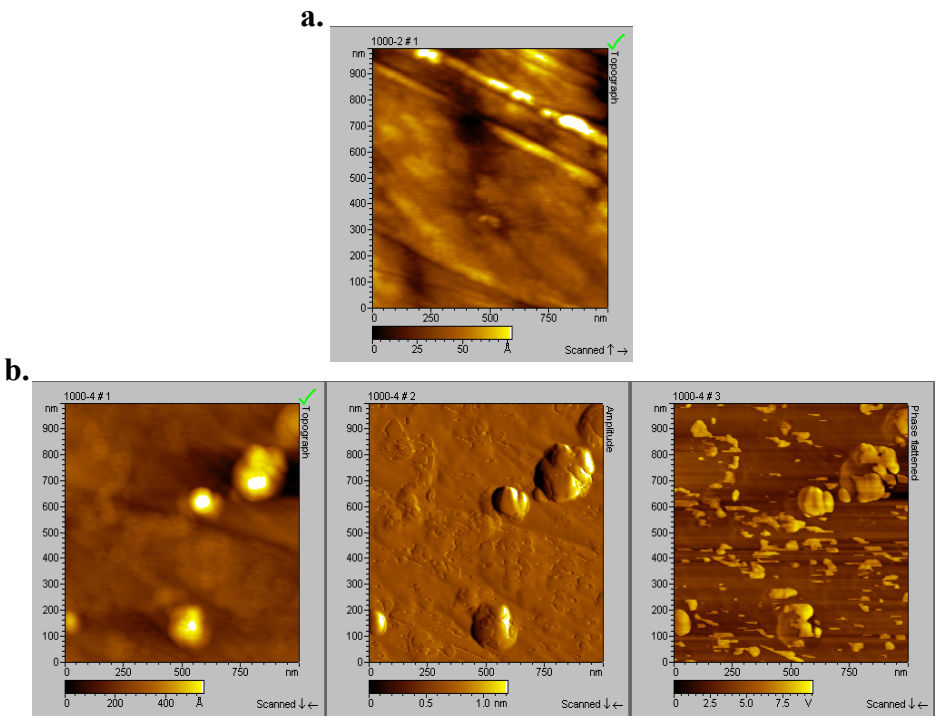

Figure 4.3 (a) AFM image of clean NiTi (rms roughness=14 Å), (b) NiTi surface after modification with ODHA and rinsed with THF (rms roughness=75Å) in amplitude, topography, and phase.

Analysis of the SAMs using MALDI-TOF reveals peaks at *m/z* 322.262 corresponding to a sodiated ODHA acid monomer on the nitinol surface. (Figure 4. 4)

Mass spectrometer analysis using the electrospray was performed on the ODHA solid (MW 299.28 g/mol) and the spectrum contains the sodiated monomer (322.272 + Na^+).

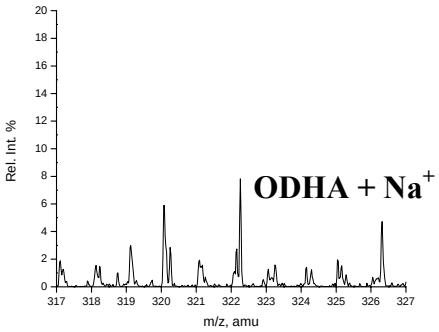

Figure 4.4 MALDI-TOF spectra of the monomer region of octadecanehydroxamic acid SAMs on NiTi at *m/z* 322.262.

4.3.1.2 Nickel Oxide Surface

Nickel oxide samples were cleaned and octadecanehydroxamic acid (ODHA) was deposited by aerosol spraying (1.5 mM solution in THF). The position of the peaks corresponding to ν_{CH2} after rinsed with THF were $\nu_{CH2\ asym}$= 2916 cm^{-1} and $\nu_{CH2\ symm}$= 2848 cm^{-1}, indicating that an ordered film is present. (Figure 4.5a) The modification was removed from the surface after sonication. The contact angle measurement of the modified surface is consistent with that of a hydrophobic surface, with a water contact angle of 100° ± 4, when compared to the control sample's contact angle with water (46°). The CO and NH region of the ODHA solid shows ν_{N-H}= 3252 and 1565 cm^{-1}, $\nu_{C=O}$= 1660 cm^{-1}, and ν_{N-O}= 1080 cm^{-1}. (Figure 4.5b-black spectra) In contrast, the CO and NH region of the bound ODHA contained stretches at ν_{N-H}= 1557 cm^{-1}, and ν_{N-O}= 1046 cm^{-1}. (Figure 4.5b-red spectra) A new peak appeared at 1184 cm^{-1}which corresponds to ν_{C-O} frequency. The IR spectrum of the CO and NH region of the modified substrates shows

that ODHA was bound to the nitinol surface in a bidentate manner, as evidenced by the shift to lower frequency of ν_{N-H}, ν_{N-O}, the appearance of ν_{C-O} frequency and disappearance of $\nu_{C=O}$ peak. (Figure 4.2c)

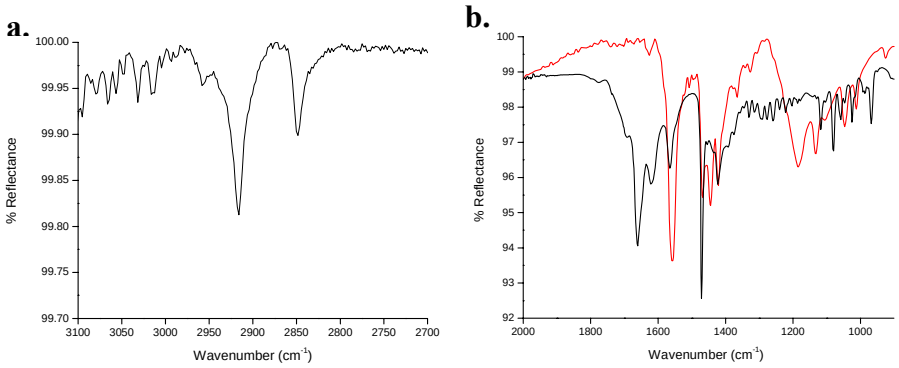

Figure 4.5 IR spectra of ODHA on nickel oxide surface (a) CH region after rinsed, (b) CO region after deposition, (red spectra) and the CO region of ODHA solid (black spectra).

4.3.1.3 Titanium Oxide Surface

Titanium oxide samples were modified using a 1.5 mM solution of ODHA and then rinsed with THF. The positions of the peaks corresponding to ν_{CH2} after rinsing with THF were $\nu_{CH2\ asym}$= 2915 cm^{-1} and $\nu_{CH2\ symm}$= 2848 cm^{-1}, showing an ordered film is present. (Figure 4.5a) The modification was removed from the surface after sonication. The contact angle measurements of the modified and rinsed surface is consistent with that of an ordered surface and indicates complete coverage of the surface, with a water contact angle of 101° ± 3, when compared to the control sample's contact angle with water (46°). The CO and NH region of the ODHA solid shows ν_{N-H}= 3252 and 1565 cm^{-1}, $\nu_{C=O}$= 1660 cm^{-1}, and ν_{N-O}= 1080 cm^{-1}. (Figure 4.6b-black line) In contrast, the CO and NH region of the bound ODHA contained stretches at ν_{N-H}= 1564 cm^{-1}, $\nu_{C=O}$= 1707 cm^{-1},

and ν_{N-O}= 1105cm^{-1}. (Figure 4.6b-red line) The IR data shows an upshift of the N-O peak that is characteristic of the adsorption of protonated hydroxamic acid on titanium oxide surface.[287]

The titanium oxide surface was previously modified by the Whitesides group.[28] Using XPS analysis, they confirmed that hydroxamic acid was bound on the titanium oxide surface on a protonated hydroxamic acid with hydrogen bonding interactions. (Figure 4.6c) Infrared analysis of the alkyl chain ordering was not clear although Whitesides group concluded that hydroxamic acid was in a trans conformation with some disordered chains.[28] Our results are consistent with their IR work concerning ordering and binding of the film. Our film was removed by sonication which they did not attempt.

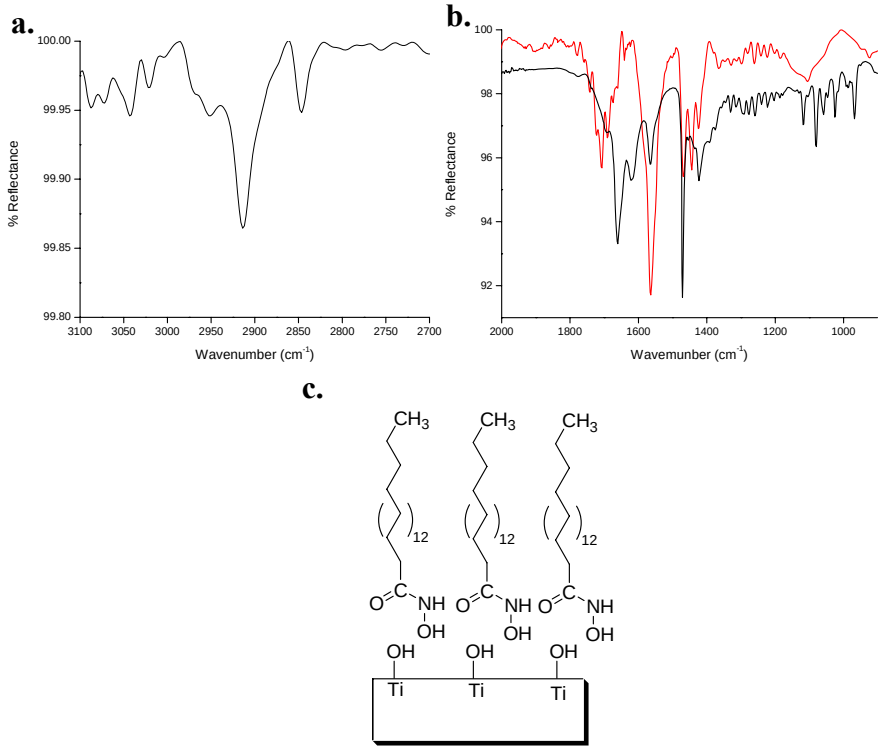

Figure 4.6 IR spectra of ODHA on titanium oxide surface (a) CH region after rinsed, (b) CO region after deposition, (red spectra) and the CO region of ODHA solid (black spectra), (c) the IR spectra indicates a hydrogen bonding of the acid on the titanium oxide surface.

Table 4.1 Hydroxamic acid head group modifications on metal oxide surfaces. Infrared data is shown after rinsing with THF.

Oxide Surfaces	**Octanehydroxamic**	**Octadecanehydroxamic**	
		Rinse	***Contact angles(°)***
Nitinol	No deposition	2916/ 2848	103 ± 3
Nickel	2914/ 2848 Removed after rinse	2916/ 2848	100 ± 4
Titanium	No deposition	2915/ 2848	101 ± 3

4.3.2 Sulfonic Acid

4.3.2.1 Nitinol Oxide Surface

NiTi samples were cleaned and exposed to octanosulfonic acid. Deposition was not successful and monolayers of octanosulfonic acid did not form. The alkyl chain length was increased to 11 carbons (undecanosulfonic acid) and after deposition and THF rinse, the IR spectrum indicated the presence of ordered films. (Table 4.2) NiTi was also modified with octadecanesulfonic acid (ODSA) by aerosol spraying using a 0.75mM solution in THF. After deposition and rinsing, the samples were characterized by DRIFT. (Figure 4.7) The position of the peaks corresponding to ν_{CH2} after rinsing were $\nu_{CH2\ asym}$= 2915 cm^{-1} and $\nu_{CH2symm}$= 2849 cm^{-1}, showing that an ordered film is present (Figure 4.7a). However, the modifications were removed upon sonication in THF for 5- 10 minutes. The contact angle measurement of the modified surface with water was 89 ± 8°, compared to the control sample's contact angle with water (46°). This value was lower than expected due; methyl terminated surfaces are expected to have contact angles >

100°.[8, 14, 16, 28, 110, 113]

To analyze the bonding between sulfonic acid and the nitinol surface, infrared data was collected and analyzed focusing on the O=S=O vibrations (1600-800 cm^{-1}). (Figure 4.7b) The SO region of the ODSA solid shows ν_{SOasym}= 1178 cm^{-1}, ν_{SOsym} = 1059 cm^{-1}, ν_{SOH}= 946 cm^{-1} and ν_{C-S}= 794 cm^{-1}. (Figure 4.7b-black spectra) In contrast, the SO region of the ODSA bound on the nitinol surface shows ν_{SOasym}= 1171 cm^{-1}, ν_{SOsym} = 1066 cm^{-1}, and ν_{C-S}= 803 cm^{-1}. (Figure 4.7b- red spectra) The IR spectrum of the SO region of the modified substrates shows that ODSA was bound to the nitinol surface by an acid-base reaction between the hydroxyl of the surface and the sulfonic groups forming a sulfonate group. This is evidenced by the shift of ν_{SOasym} to a lower frequency, which was assigned to the presence of "hydronium sulfonate salts" and the disappearance of the ν_{SOH} peak.[25, 283] Two structures are proposed for sulfonic acid on the nitinol surface, one sulfonate is a monodentate motif on the surface, and the other structure is bidentate with a partial double bond between sulfur and oxygen. The latter is favored due to the shifting of ν_{SOsym} to higher frequency values and ν_{SOasym} to a lower frequency value. This would also stabilize the bonding equilibrium on the surface (Figure 4.7c). Moreover, the ν_{SOsym} peak of the modified substrates is wider than the solid indicating multiple S-O bonds strengths, therefore supporting the proposal of the bidentate structure.

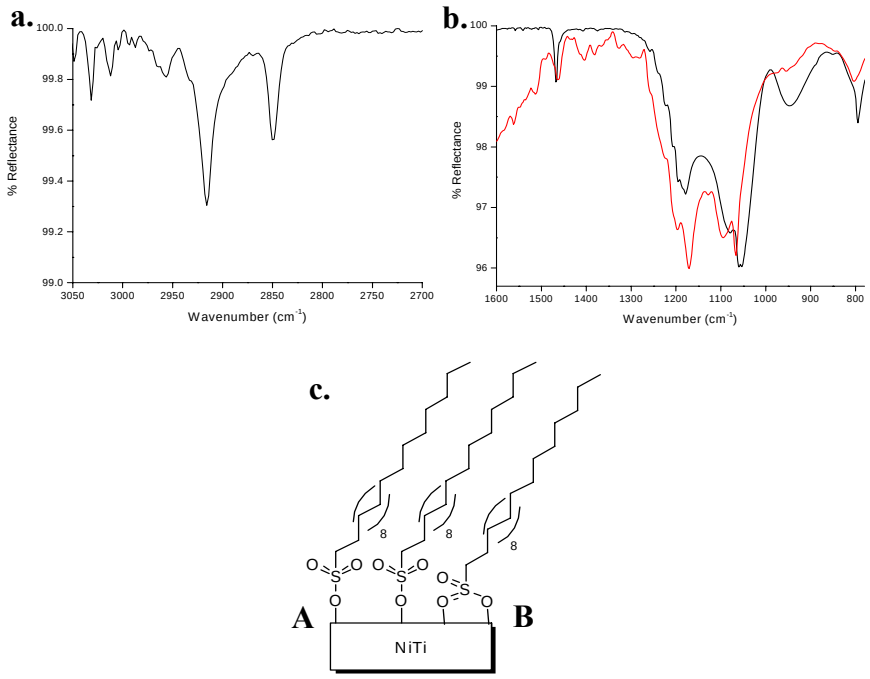

Figure 4.7 IR spectra of ODSA on nitinol surface (a) CH region after rinsed, (b) SO region after deposition, (red spectra) and the SO region of ODSA solid (black spectra), (c) the IR spectra indicates monodentate binding (structure A)or bidentate of the sulfonate (structure B).

Analysis of the SAMs using MALDI-TOF (Figure 4.8) reveals peaks at *m/z* 379.224 corresponding to the ODSA acid monomer with two sodium atoms on the nitinol surface. Mass spectrometer analysis using the electrospray was performed on the ODSA control (MW 334.25 g/mol) and the spectrum contains the monomer peak with two sodium atoms (379.238 *m/z* +2 Na^{+}).

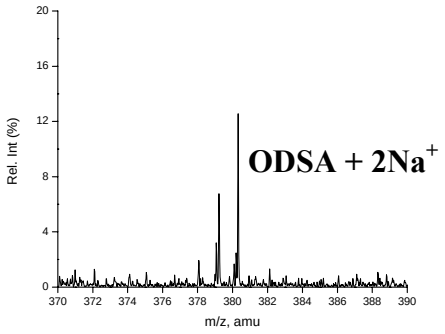

Figure 4.8 MALDI-TOF spectra of the monomer region of octadecanesulfonic acid SAMs on NiTi at *m/z* 379.224.

AFM imaging was used to further characterize monolayer formation. The nitinol control sample had an average rms roughness of 14Å. (Figure 4.3a) Modified samples with monolayers, after rinsing with THF, had an rms roughness of 15Å. (Figure 4.9) Tightly packed SAMs can be seen in the AFM image of the modified sample with no aggregates, pinholes or island formation. Therefore it is concluded that the film followed the homogeneously contour of the sample with a single layer of molecules.

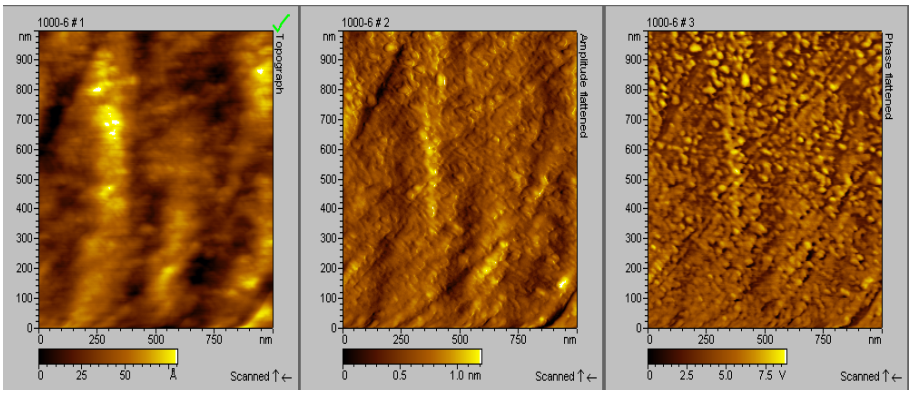

Figure 4.9 NiTi surface after modification with ODSA and rinsed in THF (rms roughness=15Å) in amplitude, topography, and phase images.

4.3.2.2 Nickel Oxide Surface

Nickel oxide samples were modified with octadecanesulfonic acid (ODSA) using a 0.75mM solution in THF. After deposition and rinsing, the samples were characterized by DRIFT. The position of the peaks corresponding to ν_{CH2} after rinsing were $\nu_{CH2\ asym}$= 2918 cm^{-1} and $\nu_{CH2\ symm}$= 2848 cm^{-1}, indicating that an ordered film is present. The modifications were removed upon sonication in THF for 5- 10 minutes. The contact angle measurement of the modified surface with water is 93± 8°, when compared to the control sample's contact angle with water of 46°. This value is not as high as expected for methyl terminated SAMs, which are usually higher than 100°.[8, 14, 16, 28, 110, 113]

To analyze the bonding between sulfonic acid and the nickel oxide surface, the SO region of the IR spectra was analyzed. The SO region of the ODSA solid shows ν_{SOasym}= 1178 cm^{-1}, ν_{SOsym} = 1059 cm^{-1}, ν_{SOH}= 946 cm^{-1} and ν_{C-S}= 794 cm^{-1}. In contrast, the SO region of the ODSA bound on the nickel oxide surface shows ν_{SOasym}= 1174 cm^{-1}, ν_{SOsym} = 1066 cm^{-1}, ν_{C-S}= 798 cm^{-1}. The IR frequency values of the SO region of the modified substrates shows that ODSA was bound to the nickel oxide surface by the formation of mostly hydrogen bonds.

4.3.2.3 Titanium Oxide Surface

A solution of 0.75mM octadecanesulfonic acid (ODSA) was used to modify the titanium oxide surface. After deposition and rinsing, the samples were characterized by DRIFT. The position of the peaks corresponding to ν_{CH2} after rinsing were $\nu_{CH2\ asym}$= 2916 cm^{-1} and $\nu_{CH2\ symm}$= 2845 cm^{-1}, showing an ordered film is present. The

modifications were removed upon sonication in THF for 5- 10 minutes. The contact angle measurement of the modified surface is 82± 18°. The standard deviation is higher than for the nickel and nitinol oxide modified surfaces and can be concluded that there was nonuniform monolayer formation of ODSA on titanium oxide surface.

The SO region of the IR spectrum was analyzed to propose the bonding between sulfonic acid and the titanium oxide surface. The SO region of the ODSA solid shows ν_{SOasym}= 1178 cm^{-1}, ν_{SOsym} = 1059 cm^{-1}, ν_{SOH}= 946 cm^{-1} and ν_{C-S}= 794 cm^{-1}. In contrast, the SO region of the ODSA bound on the nickel oxide surface shows ν_{SOasym}= 1226 cm^{-1}, ν_{SOsym} = 1061 cm^{-1}, ν_{SOH}= 885 cm^{-1} and ν_{C-S}= 799 cm^{-1}. (Figure 4.10a) The IR frequency values of the SO region of the modified substrates indicates that ODSA was hydrogen bonded to the nickel oxide surface because the peak assigned to ν_{SOH} is still observed. (Figure 4.10b)

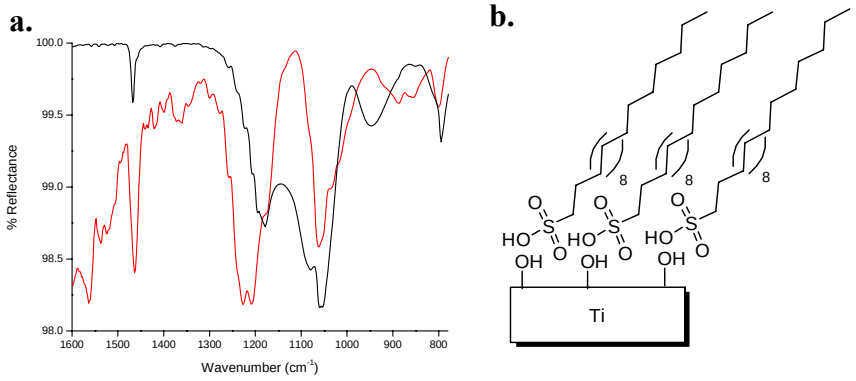

Figure 4.10 IR spectra of ODSA on the titanium oxide surface (a) SO region after deposition, (red spectra) and the SO region of ODSA solid (black spectra), (b) the IR spectra indicates bidentate of the sulfonate or hydrogen bonding.

Table 4.2 Sulfonic acid head group modifications on metal oxide surfaces. Infrared data is shown after rinsing with THF.

Oxide Surfaces	Octanesulfonic	Undecanesulfonic	Octadecanesulfonic		
			DRIFT after Rinsing (cm^{-1})	***Contact angles(°)***	***MALDI (m/z)***
Nitinol	__	2915/ 2850	2915/ 2849	89 ± 8	379.224
Nickel	__	__	2918/ 2848	93 ± 8	379.224
Titanium	__	__	2916/ 2845	82 ± 18	379.207

4.3.3 Carboxylic Acid

4.3.3.1 Chain Lengths

Chain ordering increases as the chain length of the alkyl-headgroup backbone increases.[12, 18, 245] Therefore, long alkyl chains, >12 carbons, are commonly used in the formation of SAMs.[17, 18, 246, 247] Disorder, or lack of formation, is generally found in films utilizing short chain molecules. Here, the alkyl chain length of the carboxylic acid was varied from C_8, C_{14}, C_{15}, C_{16}, C_{17}, C_{18}, C_{19} and then used to form films on the metal oxide surfaces. All the acids were sprayed onto the metal oxide surfaces using 2mM solutions and then rinsed to eliminate any weakly physisorbed molecules. Table 4.3 summarizes the results obtained using a carboxylic acid head group. The carboxylic acids with chain lengths of 8, 14 and 15 carbons were not able to form films on the surfaces.

4.3.3.2 Nitinol Surface

NiTi samples were cleaned and modified with heptadecanoic acid (17 carbons) (HDCA) by aerosol spraying using a 2mM solution in THF. After deposition and rinsing, the samples were characterized by DRIFT. (Figure 4.10) The position of the peaks

corresponding to ν_{CH2} after rinsing were $\nu_{CH2\ asym}$= 2918 cm^{-1} and $\nu_{CH2\ symm}$= 2848 cm^{-1}, indicating that an ordered film was present. (Figure 4.11a) The modifications were removed upon sonication in THF for 5- 10 minutes. The CO region of the heptadecanoic acid solid IR shows $\nu_{C=O}$= 1702 cm^{-1}, ν_{CH}= 1471 cm^{-1}, and ν_{C-O}= 1202 cm^{-1}(Figure 4.11b-black spectra). In contrast, the CO region of the bound heptadecanoic acid contained stretches at ν_{CO}= 1626 cm^{-1}, ν_{COH}= 1394 $cm^{-1}$and ν_{CO}= 1204 cm^{-1} (Figure 4.11b-red spectra). The CO region IR spectrum of the modified substrates indicates that heptadecanoic acid was hydrogen bonded to the surface, as evidenced by the shift of the ν_{CO}, ν_{COH} and ν_{CO} peaks. (Figure 4.11c)

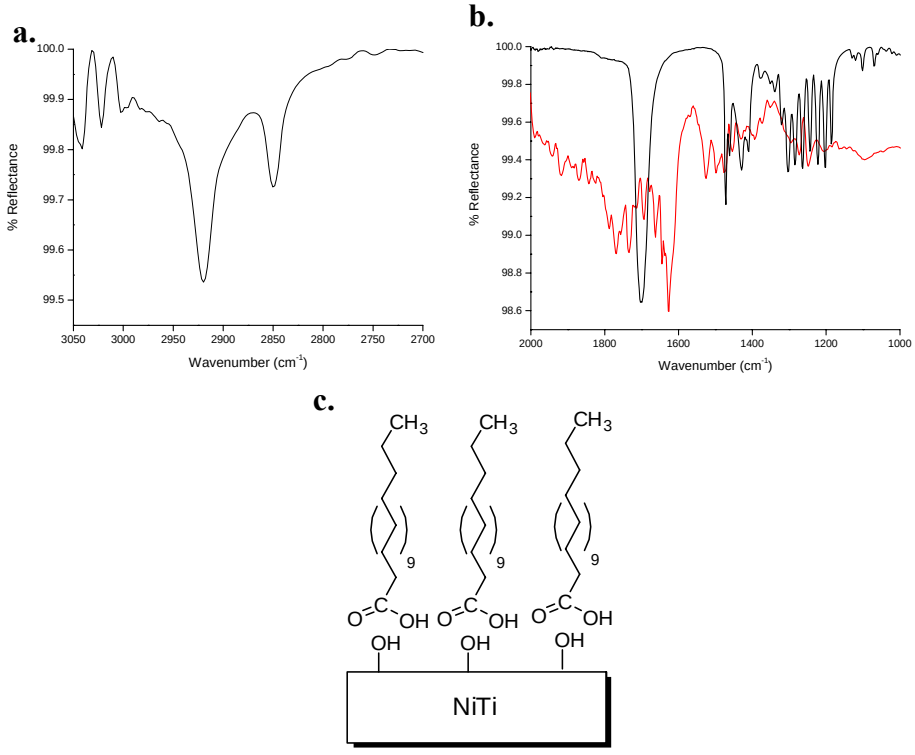

Figure 4.11 IR spectra of heptadecanoic acid on nitinol surface (a) CH region after rinsed, (b) CO region after modified, (red spectra) and the CO region of heptadecanoic acid solid (black spectra), (c) the IR spectra indicates a monodentate binding (structure A) or hydrogen bonding (structure B).

When the chain length was increased to C_{18} or C_{19} the modifications were not able to resist the rinse with THF and the molecules were removed from the surface. Usually, odd chain lengths are incapable of forming closely packed SAMs because the interaction between the molecules decreases.[248]

4.3.3.2.1 Tail Groups

SAM formation can be affected by tail group functionality, which can also be used to control the wettability of the surface.[35, 42, 44, 47] Hydrogen bonding between terminal groups in SAMs is thought to contribute to the stabilization of monolayers in amino, hydroxyl- and carboxylic acid-terminated monolayers.[49] Here, the stability of the organic films was increased by using hydroxyl and carboxylic acid -terminated monolayers but not bromo terminated monolayers. The bromo terminated monolayers form poor monolayers due to the large tail group leading to the repulsion of neighboring tails groups, and thus alkyl chains. Hydroxyl and carboxylic acid terminated monolayers can form hydrogen bonding interactions that stabilize the monolayers and that is not possible with the bromo terminated monolayers.

Nitinol samples were modified with tetradecanedioic acid (di-COOH-carboxylic acid terminated monolayer) using a 1.5mM solution in THF. After deposition, rinsing, and sonication, the samples were characterized by DRIFT. The position of the peaks corresponding to ν_{CH2} after sonication were $\nu_{CH2\ asym}$= 2913 cm^{-1} and $\nu_{CH2\ symm}$= 2846 cm^{-1}, indicating that an ordered and strong film is present (Figure 4.12a). The CO region of the di-COOH solid shows $\nu_{C=O}$= 1688 cm^{-1}, ν_{CH}= 1409 cm^{-1}, and ν_{C-O}= 1219 cm^{-1}(Figure 4.12b-black spectra). In contrast, the CO region of the bound di-COOH contained stretches at ν_{COsym}= 1444 cm^{-1}, and ν_{COH}= 1259 cm^{-1} and a peak appeared at 1584 cm^{-1}

which is assigned to ν_{COasym}. (Figure 4.12b-red spectra) The IR spectrum of the CO region of the modified substrates shows that di-COOH was bound to the nitinol surface in a bidentate manner, as evidenced by the appearance of ν_{COasym} and absence of $\nu_{C=O}$ peak. The difference between the asymmetric and symmetric band can indicate the binding to the metal oxide surface.[46, 104, 251] Here, the $\Delta\nu$ is 140 cm^{-1} which is considered to be the result of a bridging bidentate bond motif. (Figure 4,12c) However, Allara has postulated that when a hydrophilic tail and head group are present, both will adsorb onto the metal oxide surface creating looping structures[11]. (Figure 4.12c) As we have observed in diphosphonic acid, the di-COOH is strongly bound to the surface in a looping manner, increasing the stability of the molecules on the surface (Chapter 3).

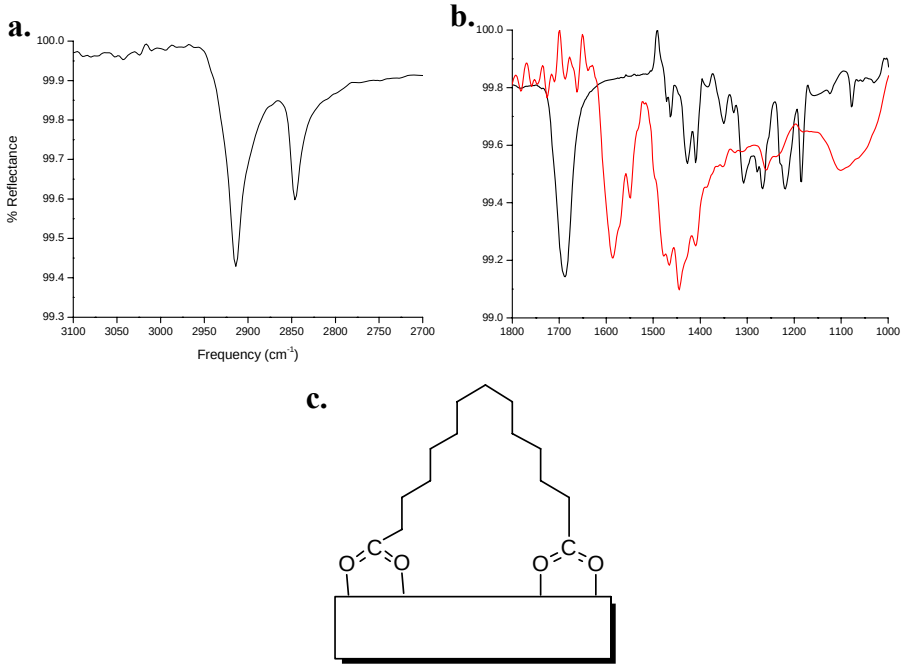

Figure 4.12 (a) IR spectra of tetradecanedioic acid (di-COOH) on nitinol surface after sonication in THF, (b) IR of PO region of the solid 1,12 dodecyldiphosphonic acid, (c) Structure proposed of tetradecanedioic acid (di-COOH) on the nitinol surface in a bridging binding with the oxide layer.

Analysis of the SAMs using MALDI-TOF (Figure 4.13) reveals a peak at *m/z* 281.162, corresponding to the sodiated tetradecanedioic acid (di-COOH) monomer on the nitinol surface. (Figure 4.13) Mass spectrometer analysis using the electrospray was performed on the ODSA solid (MW 258.18 g/mol) the spectrum contained the sodiated monomer at 281.176 *m/z* + Na^+.

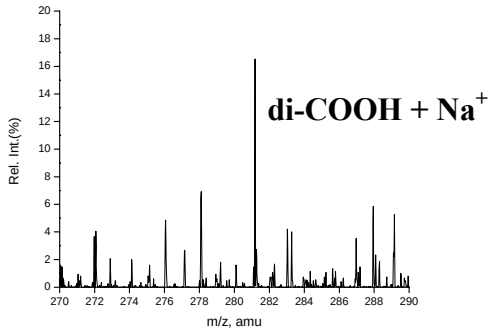

Figure 4.13 MALDI-TOF spectra of the monomer region of tetradecanedioic acid (di-COOH) SAMs on NiTi at *m/z* 281.162.

4.3.3.2.2 Perfluoroalkanoic

NiTi oxide samples were modified with perfluorooctadecanoic acid (PFA) by aerosol spraying using a 1mM solution in THF. After deposition and rinsing, the samples were characterized by DRIFT as seen in Figure 4.14. The asymmetric and symmetric CF_2 stretches are observed, $\nu_{CF2\ asym}$= 1208 and $\nu_{CF2\ symm}$= 1148 cm^{-1}, indicative of a bound film on the surface (Figure 4.14a). The modifications were removed upon sonication in THF for 5- 10 minutes. The perfluorooctadecanoic acid solid shows $\nu_{C=O}$= 1685 cm^{-1}, $\nu_{CF2\ asym}$= 1198 cm^{-1} and $\nu_{CF2\ sym}$= 1147 cm^{-1}. (Figure 4.14a-black spectra) In contrast, upon adsorption of perfluorooctadecanoic acid on the nitinol surface the stretch

for $\nu_{C=O}$ shifted to 1650 cm^{-1} and ν_{COsym} appeared at 1559 cm^{-1}. (Figure 4.14a-red spectra) The IR spectrum of the CO region of the modified substrates shows that PFA was bound to the nitinol surface in a monodentate manner or hydrogen bonded. (Figure 4.14b) The contact angle measurements of the modified surface are consistent with that of a hydrophobic surface, with a water contact angle of 99° ± 7, compared to the control sample's contact angle with water (46°). However, perfluorocarbon modifications have been shown to have a greater (>120º) contact angle with water than the methyl-terminated alkyl SAMs.[52, 68, 264-266] Contact angles are sensitive to the orientation of the organic film on the surface and therefore, in well-ordered SAMs the methyl terminated group of the alkyl chain is oriented outward, reducing the access of the water to the surface. The perfluorocarbon chains adopt a helical conformation and consequently larger cross sections compared to a simple alkyl chain. It has been observed that films consisting of a long backbone of CF_2 units might increase the stability shown by the chain-chain interactions.[268] Here, although the chains are strongly bound to the surface after rinsing with THF, the molecules formed aggregates or pinholes, in which the water can penetrate into the SAM and therefore the monolayers were removed after sonication. This leads to the low contact angle as well the high standard deviation.[68]

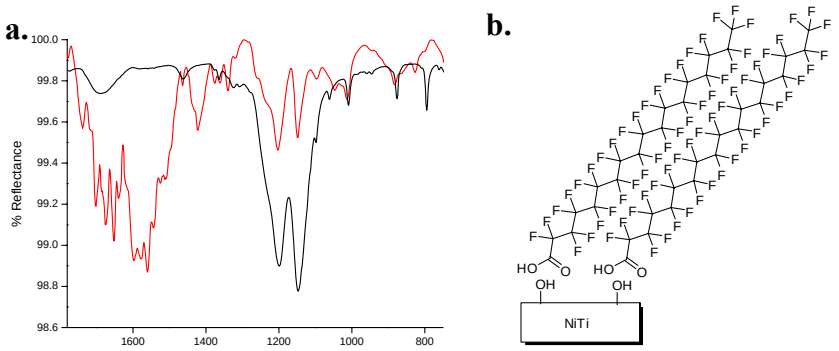

Figure 4.14 (a) IR spectra of perfluorooctadecanoic acid (PFA) on nitinol surface after rinsing with THF, (b) Structure proposed of perfluorooctadecanoic acid (PFA) on the nitinol surface hydrogen bonding with the oxide layer.

Other carboxylic acids with different terminal groups were used to modify the NiTi surface and the resulting data are summarized in Table 4.3. Hydroxyl and amino terminated monolayers were bound strongly and remained after rinsing with THF. To better understand the bonding affinity of the hydroxyl and amine group, octadecanol and octadecylamine were deposited on the NiTi surface. However, there was no evidence of organic moities on the surface after deposition. These terminal (hydroxyl and amine, bromo and carboxyl) groups can be further used to perform reactions at the interface for specific applications such as protein, cell adhesion and polymer grafting.[35, 174, 215, 288-293]

Table 4.3 Summary of results of modifications performed on the nitinol oxide surface.

Organic Acids	**Deposition (cm^{-1})**	**Rinsed (cm^{-1})**	**Sonication/ Taped (cm^{-1})**	**Contact angles (degrees)**	**Bonding**
Octanoic	Not formed				
Tetradecanoic	Not formed				
Pentadecanoic	Not formed				
Hexadecanoic	2922/ 2851	Removed			
Heptadecanoic	2915/ 2846	2918/ 2849	Removed		H bonding
Octadecanoic	2913/ 2849	Removed			
Nonadecanoic	2923/ 2851	Removed			
12-bromododecanoic	2913/ 2847	Removed			
12-aminododecanoic	2913/ 2846	2914/ 2846	Removed		Monodentate
12-hydroxydodecanoic	2911/ 2846	2911/ 2846	2910/ 2845	70 ± 3	Monodentate
16-hydroxyhexadecanoic	2913/ 2847	2913/ 2846	2916/ 2848	77 ± 4	Bidentate
Tetradecanedioic	2914/ 2846	2914/ 2846	2913/ 2846	73± 6	Bidentate/ Looping
Perfluorooctadecanoic	1201/ 1147	1202/ 1148	Removed		Bidentate

4.3.3.3 Nickel Oxide Surface

Nickel oxide samples were cleaned and modified with heptadecanoic acid (HDCA) using a 2mM solution in THF. After deposition and rinsing, the samples were characterized by DRIFT. The position of the peaks corresponding to ν_{CH2} stretches after rinsing were $\nu_{CH2\ asym}$= 2920 cm^{-1} and $\nu_{CH2\ symm}$= 2849 cm^{-1}, respectively, indicating that a

disordered film is present. The modifications were removed upon sonication in THF for 5- 10 minutes. The CO region of the bound heptadecanoic acid contained stretches at $\nu_{C=O}$= 1739 cm^{-1}, ν_{COH}= 1394 $cm^{-1}$and ν_{CO}= 1243 cm^{-1}. Additionally, a new peak appeared at 1569 cm^{-1} ν_{COsym}. The IR spectrum of the CO region of the modified substrates shows that heptadecanoic acid may be bound to the nickel oxide surface in a monodentate/ H-bonding manner, as evidenced by the appearance of ν_{COasym} and a shift to higher frequency values for the $\nu_{C=O}$ peak. The weak bonding is evidenced by the disordering of the film after rinsing with THF and removal after sonication.

The chain length was also increased to 18 and 19 carbons. The molecules were not able to remain after rinsing with THF using an18 carbon chain and were disordered using a 19 carbon chain.

4.3.3.3.1 Tail Groups

Nickel oxide samples were modified with 16-hydroxyhexadecanoic acid (16-OH) by aerosol spraying using a 1.5mM solution in THF. After deposition, rinsing, and sonication the samples were characterized by DRIFT. The position of the peaks corresponding to ν_{CH2} after sonication were $\nu_{CH2\ asym}$= 2915 cm^{-1} and $\nu_{CH2\ symm}$= 2848 cm^{-1}, shows that an ordered and strongly-bound film is present. The CO region of the 16-OH solid shows $\nu_{C=O}$= 1681 cm^{-1}, ν_{CH}= 1469 cm^{-1}, and ν_{OH} bend= 1309 cm^{-1}. In contrast, the CO region of the bound 16-OH contained stretches at $\nu_{C=O}$= 1630 cm^{-1} and ν_{CH}=1400 cm^{-1}. Here, the $\Delta\nu$ is 230 cm^{-1}, which is considered to be a monodentate binding to the nickel oxide surface.

4.3.3.3.2 Perfluoroalkanoic

The nickel oxide surface was modified using a 1mM solution of perfluorooctadecanoic acid (PFA) in THF. The asymmetric and symmetric CF_2 stretches are observed at $\nu_{CF2\ asym}$= 1208 and $\nu_{CF2\ symm}$= 1151 cm^{-1}, respectively, showing a strongly bound film, which remains after sonication in THF. The perfluorooctadecanoic acid solid shows $\nu_{C=O}$= 1685 cm^{-1}, $\nu_{CF2\ asym}$= 1198 and $\nu_{CF2\ symm}$= 1147 cm^{-1}(Figure 4.15a-black spectra). Upon adsorption of perfluorooctadecanoic acid on the nickel oxide surface, the stretch was shifted to $\nu_{C=O}$ = 1688 cm^{-1}(Figure 4.15a-red spectra). The $\Delta\nu$ (263 cm^{-1}) value measured is consistent with the formation of monodentate binding (> 200 cm^{-1}) on the nickel oxide surface. (Figure 4.15b) The contact angle measurements of the modified surface are consistent with that of a hydrophobic surface, with a water contact angle of 110° ± 8. It was observed that PFA is more strongly bound on the nickel oxide surface than the nitinol surface indicated by the fact that the films remained after sonication and the contact angles were hydrophobic as expected.

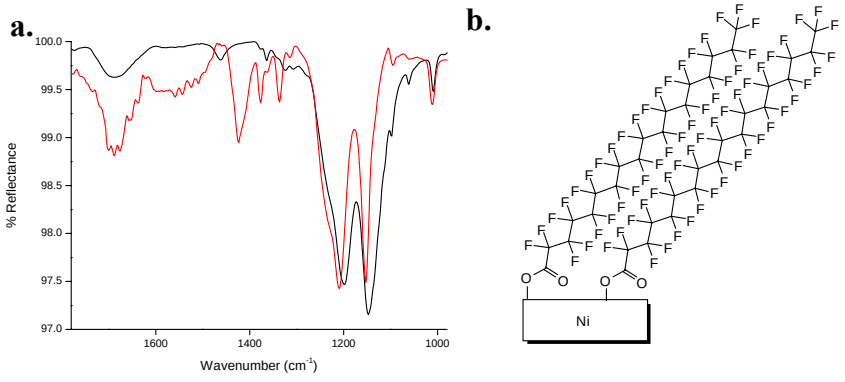

Figure 4.15 (a) IR spectra of perfluorooctadecanoic acid (PFA) on nickel oxide surface after sonication in THF, (b) Structure proposed perfluorooctadecanoic acid (PFA) on the nickel oxide surface in a monodentate binding with the oxide layer.

Table 4.4 Summary of results of modifications performed on the nickel oxide surface.

Organic Acids	**Deposition (cm^{-1})**	**Rinsed (cm^{-1})**	**Sonication/ Taped (cm^{-1})**	**Contact angles (degrees)**	**Binding**
Octanoic	Not formed				
Tetradecanoic	Not formed				
Pentadecanoic	Not formed				
Hexadecanoic	Not formed				
Heptadecanoic	2918/ 2848	2920/ 2849	Removed		Monodentate/ H bonding
Octadecanoic	2914/ 2848	Removed			
Nonadecanoic	2923/ 2852	2924/ 2852	Removed		
12-Bromododecanoic	2912/ 2847	2913/ 2849	Removed		Monodentate
12-Aminododecanoic	2914/ 2846	2915/ 2846	Removed		Monodentate
12-Hydroxydodecanoic	2911/ 2846	2912/ 2846	2913/ 2845	71 ± 4	Bidentate
16-Hydroxyhexadecanoic	2914/ 2848	2915/ 2849	2915/ 2848	77 ± 3	Bidentate
Tetradecanedioic	2915/ 28247	2914/ 2847	2914/ 2847	75 ± 1	Bidentate
Perfluorooctadecanoic	1203/ 1149	1205/ 1150	1208/ 1151	110 ± 8	Monodentate

4.3.3.4 Titanium Oxide Surface

Titanium oxide samples were cleaned and modified with heptadecanoic acid (HDCA) by aerosol spraying using a 2mM solution. After deposition and rinsing, the samples were characterized by DRIFT. The position of the peaks corresponding to ν_{CH2} after rinsing were $\nu_{CH2\ asym}$= 2918 cm^{-1} and $\nu_{CH2\ symm}$= 2849 cm^{-1}, showing a mostly heterogeneous film with gauche/ trans conformation and therefore, the films were

removed upon sonication in THF for 5- 10 minutes. The CO region of the bound heptadecanoic acid contained stretches at ν_{CO}= 1739 cm^{-1}, ν_{COH}= 1375$cm^{-1}$and ν_{CO}= 1239 cm^{-1}. The IR spectrum of the CO region of the modified substrates shows that heptadecanoic acid can be bound to the nickel oxide surface through physisorption or strong hydrogen bonding and is consequently removed by sonication.

4.3.3.4.1 Tail Groups

Titanium oxide samples were modified with tetradecanedioic acid (di-COOH) using a 1.5mM solution. After deposition, rinsing, and sonication the samples were characterized by DRIFT. The position of the peaks corresponding to ν_{CH2} rinsing were $\nu_{CH2\ asym}$= 2914 cm^{-1} and $\nu_{CH2\ symm}$= 2847 cm^{-1}, showing an ordered film is present. The modification is removed after sonication in THF solution. The CO region of the di-COOH solid shows $\nu_{C=O}$= 1688 cm^{-1}, ν_{CH}= 1409 cm^{-1}, and ν_{C-O}= 1219 cm^{-1}. In contrast, the CO region of the bound di-COOH contained stretches at $\nu_{C=O}$= 1658 cm^{-1}, and ν_{CH}= 1457 cm^{-1}. The IR spectrum of the CO region of the modified substrates shows that di-COOH was bound to the titanium oxide surface in a monodentate manner. Here, the $\Delta\nu$ is 199 cm^{-1} which is considered a monodentate binding. Other functionalized molecules did not form monolayers on the titanium oxide surface. (Table 4.5)

4.3.3.4.2 Perfluoroalkanoic

The titanium oxide surface was modified using a 1mM solution of perfluorooctadecanoic acid (PFA) in THF. The asymmetric and symmetric CF_2 stretches are observed $\nu_{CF2\ asym}$= 1205 and $\nu_{CF2\ symm}$= 1150cm^{-1}, respectively, showing it is bound after rinsing in THF. The modifications were removed upon sonication in THF for 5- 10

minutes. Upon adsorption of perfluorooctadecanoic acid on the titanium oxide surface the stretch was shifted to $\nu_{C=O}$ = 1688 cm^{-1}. The IR spectrum of the CO region of the modified substrates shows that PFA was bound to the titanium oxide surface in a monodentate manner, as evidenced by the shift of $\nu_{C=O}$. The $\Delta\nu$ (261 cm^{-1}) value measured is consistent with the formation of monodentate binding. The contact angle measurements of the modified surface are consistent with that of a hydrophobic surface, with a water contact angle of 116° ± 3. Reven et al. have previously modified the titanium oxide surface using perfluorocarbon compounds.[104] In their report, perfluorocarbons are shown to be weakly bound to the titanium oxide surface. Here, we also report that after rinsing the sample with solvent, almost all of the film is removed and further sonication completely removes the molecules. Moreover, Reven et al. reported a monodentate binding as compared with zirconia in which the perfluorocarbons bind via a bidentate bond.[104, 251]

Table 4.5 Summary of results of modifications performed on the titanium oxide surface.

Organic Acids	**Deposition (cm^{-1})**	**Rinsed (cm^{-1})**	**Sonication/ Taped (cm^{-1})**	**Contact angles (degrees)**	**Binding**
Octanoic	Not formed				
Tetradecanoic	Not formed				
Pentadecanoic	Not formed				
Hexadecanoic	Not formed				
Heptadecanoic	2917/ 2849	2918/ 2849	Removed		Monodentate/ H bonding
Octadecanoic	2915/ 2850	Removed			
Nonadecanoic	2915/ 2848				
12-Bromododecanoic	Not formed				
12-Aminododecanoic	2920/ 2850	2915/ 2848			
12-Hydroxydodecanoic	Not formed				
16-Hydroxyhexadecanoic	2910/ 2846	Removed			
Tetradecanedioic	2914/ 2847	2914/ 2847	Removed	75 ± 5	Monodentate
Perfluorooctadecanoic	1203/ 1149	1205/ 1150	Removed	106 ± 3	Monodentate

4.3.4 Comparison of the Stability Difference between the Metal Oxide Surfaces

One important variable in SAM formation is the effect of head group pKa. Here, several organic acids were evaluated with sulfonic (pKa 2), phosphonic (pKa 4.5), hydroxamic (pKa 9) and carboxylic acids (pKa= 9.5) head groups. Hydroxamic acid, which has a pKa of approximately 9[28, 279-281], is more strongly bound to the surface than

octadecanoic acid (pKa 9.5).[30, 31, 294] This may be related to the resonance structure that can be formed from the carbonyl, amine and hydroxyl groups. In our results, hydroxamic acid is bound to nitinol and nickel oxide in a bidentate manner compared to alkanoic acid, which mainly bound in a monodentate manner or by strong hydrogen bonding. (Figures 4.2c and 4.11c respectively) This chemical motif indicates that the hydroxamic acid is more strongly chemisorbed, because two oxygens are used to form covalent bonds with the surface in the hydroxamic case, which is greater energy than monodentate or hydrogen bonding interactions. (Table 4.6)

Table 4.6 Different head groups modification on nitinol, nickel oxide and titanium oxide surfaces after rinsed. Phosphonic acid data is shown in Chapter 3.

Metal Oxide Surfaces	**Octadecane sulfonic (cm^{-1})**	**Octadecyl phosphonic (cm^{-1})**	**Octadecane hydroxamic (cm^{-1})**	**Octadecanoic (cm^{-1})**
Nitinol	2915/ 2846	2913 / 2846	2916/ 2848	Removed
Nickel	2917 /2847	2914/ 2847	2916/ 2849	Removed
Titanium	2917/ 2845	2913/2847	2915/ 2848	removed

The phosphonic acid head group (Chapter 3) chemisorbs strongly on the metal oxide surfaces. This may be related to the fact that phosphonates have two acid groups from which to form bidentate bonds with hydroxyl sites on the metal oxide surfaces compared to alkanoic or hydroxamic acids. Organic acid monolayers, such as carboxylic and hydroxamic acids, can adsorb by hydrogen bonding, leading to weak binding on metal oxides surfaces.[295] For these oxide-methyl terminated monolayer combinations, phosphonic acid is the only modification that remains after sonication in THF for 5-10

minutes, heating and adhesion tests. (Table 4.7) Moreover, phosphonic acid (pKa 4.5) is more acidic than octadecanoic or octadecanehydroxamic acids. However, sulfonic acid is more acidic (pKa 2) than phosphonic acid and it does not survive the sonication/tape step.[296] Therefore head group pKa is not the only factor in creating a strong substrate-monolayer interaction.

If we compare the bond energy between the oxygen from the surface and sulfur from the sulfonic acid head group (S-O = 268 kJ/mol) and oxygen and phosphorus from the phosphonic acid head group (P-O = 335 kJ/mol), the monolayers formed with phosphonic acid would be stronger and therefore more stable on the surfaces.[223]

Table 4.7 Variable head groups on nitinol, nickel oxide and titanium oxide surfaces after sonication. Phosphonic acid data is shown in Chapter 3.

Metal Oxide Surfaces	**Octadecane sulfonic (cm^{-1})**	**Octadecane hydroxamic (cm^{-1})**	**Octadecyl phosphonic (cm^{-1})**	**Octadecanoic (cm^{-1})**
Nitinol	removed	removed	2913 / 2846	removed
Nickel	removed	removed	2915 / 2848	removed
Titanium	removed	removed	2913/2847	removed

Table 4.8 Chemical motif of the different head group on metal oxide surfaces after deposition.

Metal Oxide Surfaces	Octadecane sulfonic	Octadecane hydroxamic	Octadecyl Phosphonic	Octadecanoic
Nitinol	bidentate	bidentate	Monodentate	bidentate
Nickel	bidentate	bidentate	Bidentate	Bi/ monodentate
Titanium	monodentate	Hydrogen bonding	Bidentate	Monodentate/ H bonding

Another variable analyzed was the metal oxide surface that was modified. The titanium oxide surface has previously been modified using alkylphosphonic, alkanoic acid and hydroxamic acids.[15, 16, 24, 28, 42, 46, 263] Researchers have correlated the reactivity of surfaces and organics with the isoelectric point (IEP)of the metal.[28, 69, 263] The IEP is also known as the zero point charge (ZPC) which represents the pH at which an immersed solid oxide surface has both a zero net charge and electrically equivalent concentrations of positive and negative complexes in a system of hydroxo complexes.[297, 298] The pKa of the organic acid has to be lower than the IEP to be capable of forming strong SAMs on the metal oxide surfaces. Here, the IEP of titanium oxide has been reported to be 4-6.[28, 297, 299, 300] Therefore, under this theory, sulfonic and phosphonic acid are the only acids capable of forming strong and stable interactions on the titanium oxide surface.

For nickel oxide, which is more reactive than titanium oxide, the IEP has been previously reported to be 10-11.[297, 298, 300] Therefore, the nickel oxide surface can theoretically be modified using carboxylic, hydroxamic, sulfonic and/or phosphonic

acids. These acids remained after rinsing with THF and have formed a bidentate bond with the nickel oxide surface, which is considered to be stronger than monodentate because, the organic acid is deprotonated and has formed a bond. (Table 4.8)

The final metal oxide used was nitinol which is a nickel -titanium alloy. Phosphonic and sulfonic acids were strongly bound to the nitinol surface. However, carboxylic and hydroxamic acids were not successfully chemisorbed on the surface. Hydroxamic acid formed micelles that were removed after sonication. The IEP of nitinol is unknown and is difficult to determine because one would need a salt of the alloy, which is not available.[297, 298]

Another factor which may affect the formation of SAMs is the structure of the surface and the hydroxyl content. For example, it has been demonstrated that titanium oxide is not well-suited to form SAMs using alkanoic or hydroxamic acid, due to the weak interaction of the molecules on the surface. The hydroxyl content of titanium oxide is lower than other metal oxides such as aluminum and iron, which appears to increase the difficulty of forming monolayers on the surface.[26, 301] Here, metallic films of nickel, nitinol and titanium, which spontaneously oxidize the surface under ambient conditions, are used.[179, 223, 302, 303] The crystal structure of nickel oxide is face-centered cubic.[304-307] By ion scattering spectroscopy (ISS) the surface consists of 70% nickel oxide ions and 30% oxygen.[308] Thirty percent of the surface oxygens are hydroxyl groups.[308, 309] The titanium dioxide surface is mainly known to be a rutile crystal structure (tetragonal unit cell) which has less accessible oxygens on the surface and the amount of hydroxyl content was calculated to be 16% of the total surface oxygen; the rest is in μ-oxo groups.[303, 306, 307, 310] Titanium dioxide has a higher affinity towards oxygen than nickel

oxide and this may decrease the conversion of the oxygen to hydroxyl groups.[195] The nitinol surface has two crystal structures depending on the temperature as explained in Chapter 1. The low temperature martensite structure, which is monoclinic, was used here. At high temperatures the austenite structure which is a body-centered cubic structure (CsCl) is observed. (Table 4.9)[178, 179, 311] However, there are not many reports about the oxygen content on the surface.[185, 195, 202] Some researchers have reported that the oxide layer is mainly composed of titanium oxide and the oxygen composition on the surface was calculated to be 28-34% using X-ray photoelectron spectroscopy (XPS) and Auger electron spectroscopy (AES) analysis.[185, 198] The atomic fraction of chemisorbed water on nitinol surface was calculated to be 35-40%, which is higher than that of the titanium oxide surface.[195, 303] The martensite structure offers the more defective surface, and consequently, more reactive surface with a higher hydroxyl content.[195] This nitinol crystal structure may allow for more accessible oxygens and/or hydroxyl groups that can react with an organic acid may make this alloy more reactive than the pure titanium or nickel oxide surface. (Figure 4.16)

Table 4.9 Unit cell and structures of NiTi and its constituents nickel oxide and titanium oxide.

Unit Cell	**Crystal Structure**	**Cell volume/ nm^3**
Nickel oxide	Face-centered cubic (fcc)	0.044
Rutile-TiO_2	Tetragonal	0.062
Austenite NiTi	Body-center cubic (bcc)	0.027
Matensite NiTi	Monoclinic	0.055

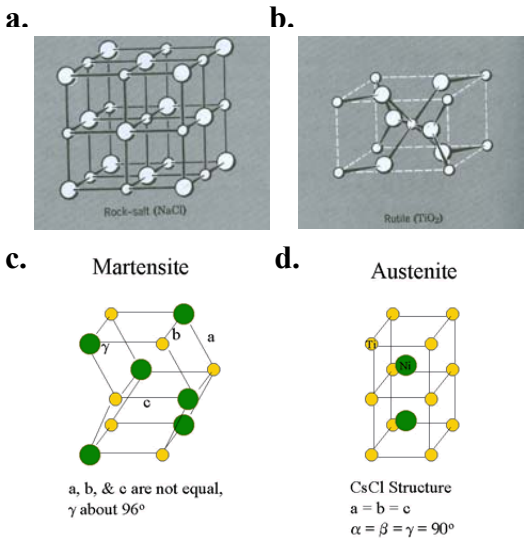

Figure 4.16 Crystal structures of (a) nickel oxide, (b) titanium dioxide), nitinol structures at (c) low temperature (martensite) and (d) high temperature (austenite).[192, 310]

4.3.5 Variations of Head Group, Backbone, Chain Length, and Tail Groups

The alkyl chain can affect the stability of the monolayer through variation of length and functionalized group. For example, in perfluoroalkanoic acid the alkyl chain was fluorinated, which changed not only the interchain interactions, but also the acidity of the molecules. Perfluorooctadecanoic acid has a pKa lower than 1 and octadecanoic acid is the least acidic of the molecules used here with a pKa of approximately 9.5.[30, 31, 286, 296] This difference of acidity between the octadecanoic and perfluorooctadecanoic acids is due to the fact that as the fluorination of the alkyl chain increases the acidity by stabilizing the deprotonated molecule. Fluorine is much electronegative than carbon, which makes the backbone of the monolayer electron withdrawing.[223, 302] The effect of

this is seen in the stability difference of the SAMs; octadecanoic acid did not form organic films on the metal oxides studied here whereas, perfluorooctadecanoic acid was strongly bound to the all surfaces. Both of these organic acids have the same head group, but its pKa is altered and the backbone interactions among the perfluorocarbons are stronger than the alkyl chain interactions due to dipole-dipole interactions between the chains.

The chain length was varied for all of the different organic acid head groups from 8, 11, to 18 carbons. As the chain length of the backbone of the monolayers was increased the intermolecular interactions were enhanced and consequently, an ordering effect is expected during the adsorption of the molecules on the metal oxide surfaces. Therefore, short chains lead to low conformation order, resulting from the presence of gauche defects and can lead to low quality monolayers and the formation of physisorbed molecules that can be removed from the surface by rinsing and/or sonication in THF.[245, 246, 312] Moreover, if an odd number of carbons in the alkyl chain is used, a steric repulsion effect is observed and, therefore, a heterogeneous mixture of trans/gauche conformation of the molecules is produced.[248] Here, monolayers using 17 carbon alkyl chain lengths were able to form monolayers and remain after rinsing with THF. However, the molecules were removed after sonication.

When the terminal group of the octadecanoic acid was changed to carboxyl or hydroxyl groups, the SAMs were more strongly bound to the surface than the methyl terminated films. This is due to the hydrogen bonding that stabilizes the molecules on the surface. The energy related to hydrogen bonding ranges from 2 to 10 kcal/mol and is known to be the strongest of the intermolecular forces.[19, 223, 313] Therefore, although the

acidity of the organic acid is an important aspect of the SAMs formation, the intermolecular forces are also relevant in the molecular packing and chemisorption on the surfaces.

4.4 Conclusion

SAMs using short and long alkyl chains of organic acids were formed on the native oxides of the titanium, nitinol and nickel surfaces. Hydroxamic, sulfonic and alkanoic acids were used as head groups to modify the surface. Phosphonic acid monolayers were compared to the organic acids used here and they are more reactive and stable toward monolayer formation on metal oxides. However, functionalized phosphonic acids are difficult to synthesize and there are many commercially available carboxylic acid compounds which can form monolayers.

The hydrophilicity of the surfaces was controlled using hydroxyl (OH), carboxylic acid, amino, bromo and methyl tail groups. DRIFT, contact angle, AFM and MALDI-TOF were used to characterize the unmodified and modified surfaces. There is not one controlling factor in monolayer formation, but a number of factors that affect formation and stability of the monolayers.

Chapter 5

Polystyrene Formation on Monolayer-Modified Nitinol Effectively Controls Corrosion

5.1 Introduction

Nitinol has very desirable mechanical properties such as super-elasticity and the shape memory effect, but is also expensive. Furthermore, current knowledge of the corrosion behavior of nitinol inside the body is very limited and comes from studies of dental arch wires under *in vitro* conditions.[167, 198] An ongoing concern with nitinol is the release of nickel ions into the body through corrosion, which may lead to allergic, toxic and carcinogenic effects associated with the biological properties of nickel.[166, 178, 179, 202] The native nickel oxide (NiO), which makes up 50% of the nitinol surface, is also much more likely to dissolve in the human body than the native TiO_2 titanium (which makes up 50%) because it is not as stable.[167, 179] Therefore, it is essential to characterize nitinol's corrosion resistance in the aqueous environment of the body.[201]

Surface modifications of materials may be utilized to reduce the electrochemical activity on the implant surface.[194] Previously, biomaterial surfaces have been modified by various methods, including simple polymer adsorption and covalent grafting.[8, 14, 16, 24, 74, 75, 102, 163, 178, 179, 193, 230, 301] In this report, nitinol and nickel oxide surfaces were modified using a SAM as the platform for *in-situ* formation and attachment of

polystyrene on the oxide surface. Surface polymerization is a versatile means for the molecular design of polymer surfaces to enhance their physical and chemical properties for specific applications.[314] Polymer coating is an interesting direction to explore because polymer elasticity is compatible with that of nitinol.[197] The use of monolayers as surface-immobilized azo-initiators for *in situ* polymer synthesis is a significant advance in the technology of solid surface modification and has been reported using SAMs of thiols on gold.[88, 314, 315]

Here, polystyrene was synthesized on the carboxylic terminated phosphonic acid monolayer by surface-initiated free radical polymerization (SIP) using azo-initiators on the nitinol and nickel oxide surfaces. These polystyrene films have the potential to be barrier layers for corrosion control.[88] The modified surfaces were characterized by infrared spectroscopy (IR), atomic force microscopy (AFM), matrix-assisted laser desorption ionization (MALDI) mass spectrometry, and water contact angles. The reduction-oxidation reaction at the surface was measured and compared with the bare surface, monolayers and polymers by cyclic voltammetry (CV) and electrochemical impedance spectroscopy (EIS).

5.2 Experimental Section

5.2.1 Methods and Materials

Octadecylphosphonic acid (ODPA, 99.0% purity) was purchased from Alfa Aesar. 12-bromododecanoic acid (97%), acetyl chloride (>99%,), triethyl phosphite (98%), [24, 49, 76, 240, 241] 2,2'-Azobis(2-amidinopropane) dihydrochloride (ABAP, 97%),1-ethyl-3-(3-

dimethylamino) propylcarbodiimide hydrochloride (EDC, 98%) and pentafluorophenol (PFP, 99%) were purchased from Aldrich, and hydrochloric acid (Certified ACS Plus) was purchased from Fisher Scientific. All were used without further purification. (12-carboxydodecyl)phosphonic acid was synthesized as previously described.[49, 76] Styrene (99%) was purchased from Acros and was purified by extracting it three times with 0.1 M aqueous sodium hydroxide (NaOH) and twice with Millipore water (18 MΩ·cm) and dried over anhydrous sodium sulfate (Na_2SO_4) before polymerization. Nitinol foils (51% nickel: 49 % titanium; 0.008" thickness, >99.0 % purity) were purchased from Johnson Matthey, Inc. Nickel foils (0.25mm thickness, > 99.0 % purity) were purchased from Goodfellow Inc.

5.2.2 Preparation of the Substrates

Substrates were cut into 1 x 1 cm squares, sanded (220, 320 and 400 grit sandpaper) and then polished (Buehler Ecomet 4 mechanical polisher) using sandpaper of 400, 800, 1200 grits and 1μm diamond suspension. The substrates were rinsed with acetone and methanol and cleaned by ultrasonication in acetone for 1 hour. The substrates were then rinsed with acetone and stored in the oven at 90° C for 30 minutes – 1 hour. The substrates were rinsed again and stored under vacuum overnight (0.1 Torr).

5.2.3 Formation of Monolayers

Monolayers were formed by spraying a solution of phosphonic acid in dry tetrahydrofuran (THF) (distilled over Na and stored under argon) using a thin layer chromatography (aerosol; Sigma-Aldrich) sprayer with a nitrogen gas stream. A 0.50mM solution of (12-carboxydodecyl) phosphonic acid was used to spray the samples. The

substrates were allowed to dry at room temperature and then rinsed with THF for 15 minutes. The samples were stored under vacuum overnight (0.1 Torr). Octadecylphosphonic acid (ODPA) monolayers were prepared as previously explained[14] (Chapter 3).

5.2.4 Covalent Immobilization of Free Radical Initiator onto a Reactive SAM on the Surfaces

Carboxylic acid-terminated phosphonic monolayers were treated with 0.1 M 1-ethyl-3-(3-dimethylamino) propylcarbodiimide (EDC) and 0.2 M pentafluorophenol (PFP) in methanol for 45 minutes to convert the carboxylic acid groups to pentafluorophenyl esters.[88] Then, the samples were treated with a 10 mM solution of 2,2'-Azobis(2-amidinopropane) dihydrochloride(ABAP) in methanol for 2.5 hours.

5.2.5 Surface-Initiated Polymerization of Polystyrene

The ABAP grafted samples were placed in a deoxygenated Schlenk tube. A degassed mixture of styrene and toluene (1:1 v/v) was transferred into the Schlenk tube. Polymerization was carried out by heating the Schlenk tube (90 °C), under nitrogen atmosphere, for 24 hours. Afterwards, the samples were rinsed in toluene for 22 hours and then put under vacuum overnight (0.1 Torr).

5.2.6 Characterization of the Monolayers

5.2.6.1 DRIFT

The substrates were studied using Diffuse Reflectance Infrared Fourier Transform

Spectroscopy (DRIFT). DRIFT was used to analyze the alkyl chain ordering bonding mode of the molecules and monitor the reaction on the surface.

5.2.6.2 Contact Angle

The contact angle measurements were used to analyze the hydrophobicity of the surface. Advancing angle measurements were taking on the monolayer and the polystyrene film.

5.2.6.3 AP MALDI-TOF MS

Atmospheric pressure matrix-assisted laser desorption/ionization time-of-flight mass spectrometry (AP MALDI-TOF MS) was used to characterize each step of the surface modification. MALDI-TOF MS has been used has been used to characterize polymers and for characterization of interfacial reactions on SAMs.[96] MALDI preparation was done by dried-drop method in which a 1μL aliquot of the matrix solution was dropped onto each of the metal surfaces previously modified with organic thin films and then dried at room temperature as explained previously[95] (Chapter 2).

5.2.6.4 AFM

Atomic force microscopy (AFM) was used to analyze the surface before and after the formation of the polymer film. AFM imaging (Molecular Imaging, Pico SPM) of the samples was performed in non-contact mode at ambient conditions using silicon tips with a resonance frequency of 182-195 kHz and a force constant of 42-48 N/m.

5.2.6.5 Electrochemical Characterization

Electrochemical measurements were carried out on a Bioanalytical Systems (BAS) model CV-50W. Voltammograms were recorded with a standard three-electrode

system consisting of nitinol as the working electrode with a 0.8 cm^2 exposed area, a saturated calomel electrode (SCE) as the reference electrode and a Pt-wire auxiliary electrode. Characterization was performed in a 0.1M NaOH aqueous solution after the samples were in solution 30 minutes with a potential scan ranging from -0.3 to +0.7 V at 50 mV s^{-1}scan rate for the nitinol substrates and scan ranging from -0.3 to +0.6 V for the nickel oxide substrates. Using the same three-electrode system, the current density was measured using an EG&G Princeton Applied Research scanning potentiostat Model 362 and was plotted using an EG&G Princeton Applied Research (Houston Model RE0074) X-Y recorder and a 169 Keithley multimeter with y scale 2.5 mA, a current at 10mA at 10 mV s^{-1}scan rate.

The Electrochemical Impedance Spectroscopy (EIS) measurements were performed at the corrosion potentials in the frequency range from 0.1 Hz to 300 kHz with 5 points per decade. The sinusoidal perturbation signal's amplitude was 10 mV at corrosion potential. The impedance data were analyzed with Gamry Framework v5.30 software using a Gamry Instruments FAS2 Femtostat potentiostat.

5.3 Results and Discussion

Functionalized carboxylic acid-terminated phosphonic acid monolayers (COOH-PA) were used to immobilize styrene on nitinol and nickel oxide surfaces as shown in Figure 5.1.

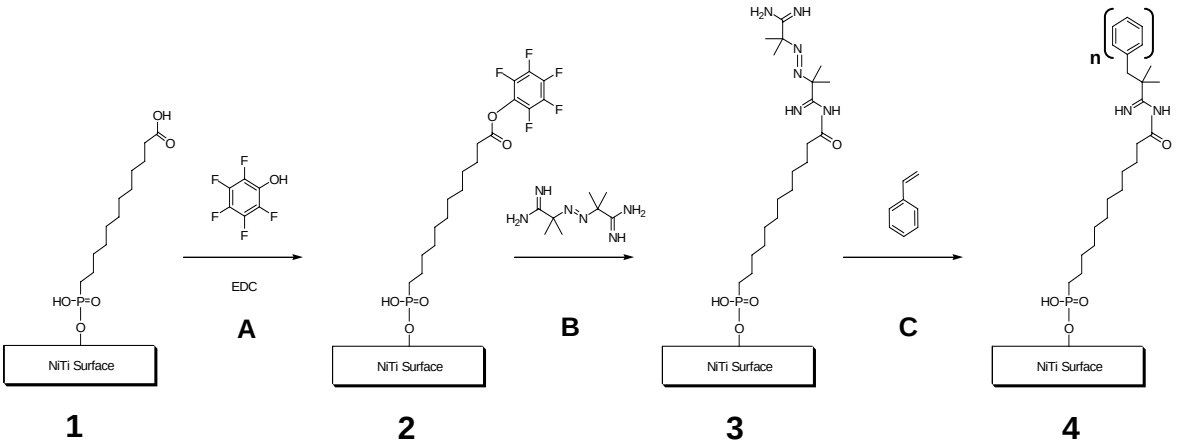

Figure 5.1 Schematic of surface-initiated free radical polymerization of styrene on nitinol and nickel oxide surfaces.

The nitinol surface was modified with carboxylic acid-terminated phosphonic acid monolayers and characterized by IR, MALDI-TOF and contact angles as reported previously.[14] First, the nitinol surface was modified with carboxylic acid-terminated phosphonic acid monolayers and characterized by IR, MALDI-TOF and contact angles as reported previously (Chapter 3).[14] The monolayers were ordered on the nitinol surface with peaks corresponding to $\nu_{CH2\ asym} = 2910\ cm^{-1}$) and $\nu_{CH2\ sym} = 2846\ cm^{-1}$ indicating that the monolayers are highly ordered to the surface.[14] The carbonyl region in the IR was analyzed and a peak at 1691 cm^{-1}, which corresponds to the $\nu_{C=O}$ of free carboxylic acid was observed.[49, 76] The carbonyl peak of the solid compound is seen at 1684 cm^{-1} (Figure 5.2a-black spectra). To study the reactivity of the carboxylic acid moiety towards nitinol and rule out any possibility of looping (both carboxylate and phosphonate groups chelating tothe surface), octadecylcarboxylic acid was deposited under the same conditions, and no evidence of film formation was seen in the IR spectrum. Therefore, a looping reaction between the carboxylic acid tail and the surface was ruled out due to the

observation of the free carboxylic acid peak in the IR spectrum and the lack of reactivity between octadecylcarboxylic acid and nitinol.

The modification of the nitinol surface was also studied by MALDI-TOF. For the MALDI-TOF analysis, the samples were spotted with the matrix CHCA by the dried drop method and let them dry at room temperature. This procedure leads to the formation of uniform crystals on the sample which makes it easier to desorb and ionize the matrix and the analyte.[95] The positive ion spectra of COOH-PA monolayers reveals a peak at *m/z* 303.137 corresponding to a sodiated COOH-PA monomer.[14] Moreover, the dimer peak was not detected by MALDI-TOF and therefore, a monolayer was formed on the nitinol surface.[15]

The carboxylic acid tail group was then allowed to react with pentafluorophenol (PFP) in 1-ethyl-3-(3-dimethylamino) propylcarbodiimide (EDC) (step A). The carbodiimide is used to activate the carboxylic acid towards an amide formation. Then, (step B) the azo initiator 2,2'-Azobis(2-amidinopropane) (ABAP) was allowed to react with pentafluorophenol as a nucleophile forming an amide bond. Finally, in step C, styrene is added to the solution and polymerized by free radical polymerization.[88] The organic were analyzed by IR and MALDI-TOF. The resulting polystyrene on the surfaces was also analyzed by IR, AFM images and contact angles measurements.

5.3.1 Nitinol Surface

The carboxylic acid tail group was then treated with pentafluorophenol (PFP) in 1-ethyl-3-(3-dimethylamino) propylcarbodiimide (EDC) (Step A). The carbodiimide is used to activate the carboxylic acid towards an amide formation for 45 minutes at room

temperature to form a pentafluorophenyl ester. PFP was chosen over N-hydroxysuccinimide ester because previous reports have suggested that the pentafluorophenyl esters are more reactive.[88, 316] The PFP/ EDC reaction on the monolayers was analyzed by IR (Figure 5.1, Structure 2). Peaks in the spectra were attributed to $\nu_{C=O}$ = 1689 cm^{-1}, ν_{C-C} = 1624 (which are characteristic of an aromatic ring), ν_{C-O} = 1283 cm^{-1}, and ν_{C-F} = 992 cm^{-1} (Figure 5.2b).

The pentafluorophenyl ester phosphonic acid monolayer was then treated in Step B (Figure 5.1) with 10mM 2,2'-azobis(2-amidinopropane) dihydrochloride (ABAP) solution for 2.5 hours at room temperature. This reaction leads to the formation of an amide bond between the ester and the amine and an azo radical initiator at the terminus of the monolayer. Figure 5.2c shows the IR spectrum for this modification. The ABAP formation on the nitinol surface is indicated by peaks corresponding to ν_{NH2} = 3147 cm^{-1} and $\nu_{-C=NH}$ at 3051 cm^{-1}. A peak at 1689 cm^{-1} is attributed to $\nu_{C=O}$, and a $\nu_{C-H\ bend}$ at 1406 $cm^{-1}$and ν_{C-N} at 1202 cm^{-1} can also be observed. The peak characteristic of C-F stretching around 1000 cm^{-1} has disappeared from the IR spectra as expected due to the immobilization of ABAP on the surface (Figure 5.1, Step 3).

MALDI-TOF analysis of the resulting monolayer showed a peak at *m/z* 463.250 (Figure 5.3). The new peak represents the protonated form of Structure 3 (Figure 5.1) (MW of Structure 3 = 462.31 g/mol).

The ABAP modified monolayers were used to polymerize styrene on the nitinol surface in Step C. The ABAP samples were transferred to a tube with styrene and toluene heating the reaction up to 90ºC to initiate the polymerization. After 24 hours of reaction, the samples were rinsed with toluene for 20-22 hours to eliminate physisorbed

polymer from the surface and then stored under vacuum overnight. The polystyrene modified substrates were analyzed by IR and the spectra contained peaks corresponding to $\nu_{C\text{-}H\ aromatic\ ring}$ = 3025 cm^{-1}, methylene $\nu_{C\text{-}H\ asym}$ = 2923 cm^{-1} and $\nu_{C\text{-}H\ sym}$ = 2849 cm^{-1}, $\nu_{C\text{-}C\ aromatic\ ring}$ = 1600 cm^{-1} and 1491 cm^{-1}, $\nu_{C\text{-}H\ bend}$ = 1449 cm^{-1}, and $\nu_{C\text{-}H}$ aromatic combination bands between 2000-1660 cm^{-1} (Figure 5.2d). These peaks are characteristic of styrene on a modified surface and have been reported on iron oxide nanoparticles and gold substrates.[88, 317-319] Therefore, it was concluded that a carboxylic acid-terminated phosphonic acid monolayer was formed on the nitinol surface and used as a platform for the polymerization of styrene by azo radical initiator as observed by infrared spectroscopy. As a control, unmodified nitinol surfaces were placed in the polymerization reaction with styrene and toluene. Subsequently, the adsorbed polystyrene film was removed by rinsing with toluene, as confirmed by IR.

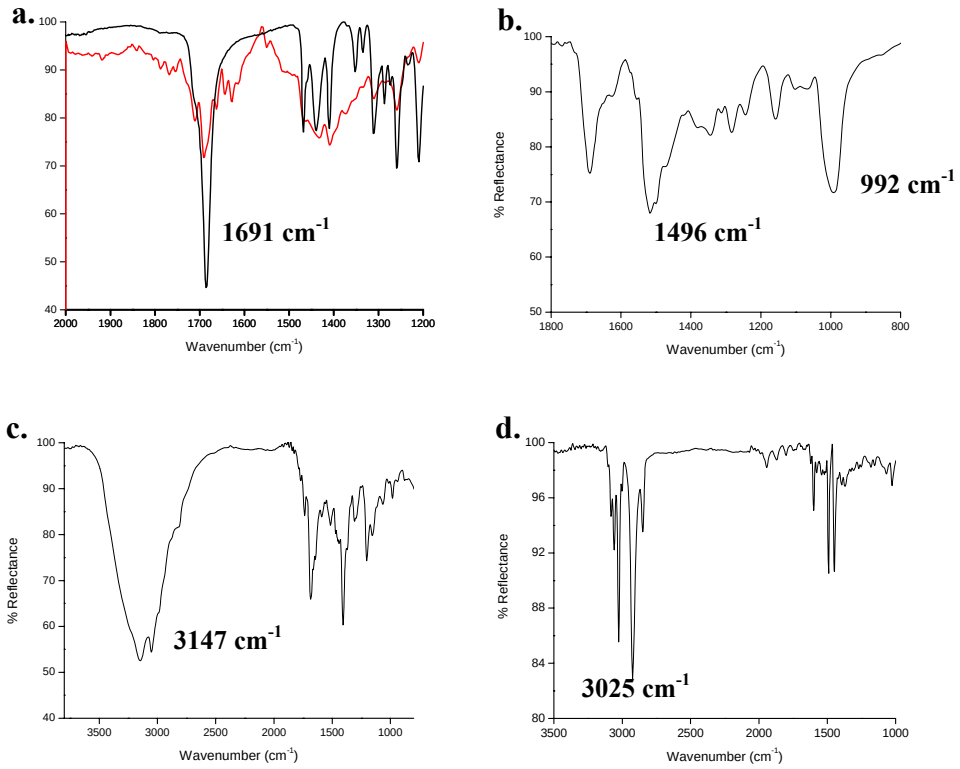

Figure 5.2 IR spectra of the modifications steps in SIP on Nitinol: a) IR of carboxylic acid region of the carboxylic-terminated phosphonic acid modified sample (red spectra) and the solid 12-carboxydodecylphosphonic acid (black spectra) (1) b) PFP/EDC on the monolayer (2), c) ABAP radical initiator formation on the monolayer (3), d) Polystyrene film formation by SIP after 24 hours and then rinsed with toluene for 20-22 hours (4).

Table 5.1 Summary of IR data of all the modifications on the NiTi surface

Frequencies (ν) cm^{-1}	Functional groups/assignments	Modification
1662, 1689	Carbonyl group, C=O	PFP/EDC, ABAP
992	C-F	PFP/EDC
1283	C-O	PFP/EDC
1624, 1496	C-C aromatic ring	PFP/EDC, PS
3025, 2000-1660	C-H aromatic ring	PS
1201	C-N	ABAP
3266, 3147	NH amine/amide	ABAP
3147	C=NH	ABAP
1689	(-C=N-)	ABAP
1689	(-N=N-)	ABAP
2923 and 2849	$-CH_2$ asym/sym	PS

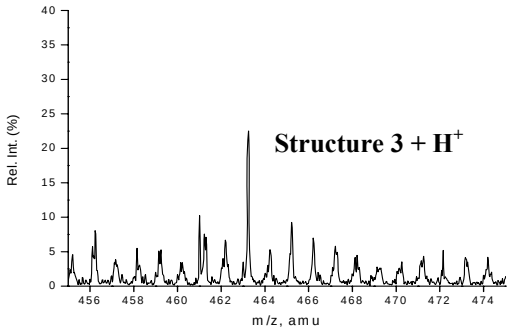

Figure 5.3 Sample MALDI-TOF spectra of structure 3 on the nitinol surface shows mass peaks at *m/z* 463.250

AFM images were collected of the surface before and after the polymerization with styrene. The samples were scanned over $1\mu m^2$ region. The morphology of the

surface changed noticeably. It was observed that the control sample had lines on the surface created by the polishing. However, the modified polystyrene surface was covered by organic and the lines are no longer visible. The polymer surface did contain holes as previously observed in this type of polymerization due to benzene ring packing.[116] The nitinol control sample had an average rms roughness of 14Å (Figure 5.4a). The polystyrene samples had a smaller rms roughness than the bare surface with an rms roughness of 4Å (Figure 5.4b).

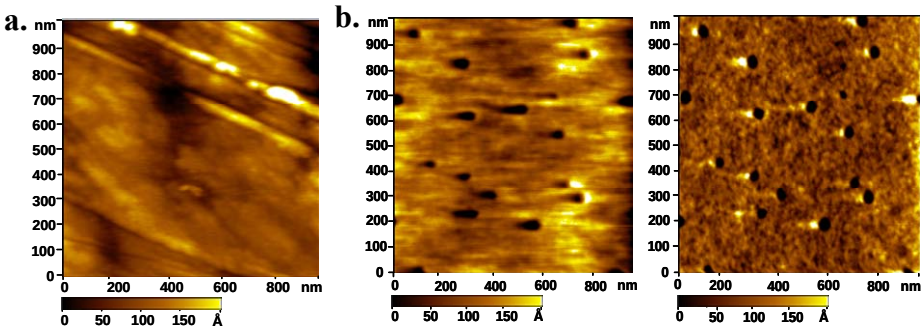

Figure 5.4 (a) AFM image of clean Nitinol (rms roughness =14Å), (b) after modified with polystyrene coating and rinsed with toluene (rms roughness = 4Å) in topography and amplitude

Wettability is a critical factor for applications such as coatings, sensors and biomedical implants because this may increase the biocompatibility by decreasing the cell and protein adhesion on the material surfaces.[116, 320, 321] Sessile water contact angles of the advanced angle were measured and the resulting averages with their standard deviation. Carboxylic acid-terminated phosphonic acid monolayers yielded a hydrophilic surface with a value of 42 ± 2º.[14] When the surface was polymerized using styrene a hydrophobic surface was achieved with a contact angle value of 103 ± 4º. (Figure 5.5) As expected, the wettability of the surface was varied from a hydrophilic to a

hydrophobic surface by the SIP technique in which styrene was immobilized on the surface.

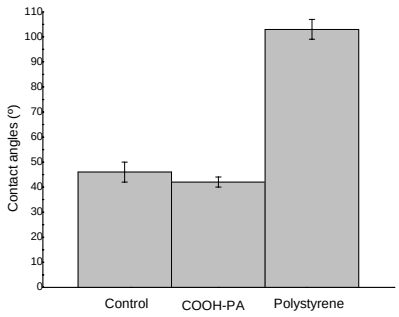

Figure 5.5 Contact angle values of the primary modifications on the nitinol surface

5.3.2 Nickel Oxide Surface

The nickel oxide surface, a major component of the nitinol oxide surface (49%) was modified with carboxylic acid-terminated phosphonic acid monolayers. A DRIFT spectrum of 12-carboxydodecanephosophonic acid is shown in supporting information. The monolayers were ordered on the nickel oxide surface with peaks corresponding to $\nu_{CH2\ asym}$ = 2916 cm^{-1} and $\nu_{CH2\ sym}$ = 2848 cm^{-1} after rinsing with THF, indicating that the monolayer is strongly bound. (Figure 5.6a) There was no evidence in the IR of looping by the carboxylic acid tail group. The carbonyl area of the COOH-PA was analyzed by IR showing a peak at 1703 cm^{-1} corresponding to the carbonyl peak (C=O) of the carboxylic acid tail group. Furthermore, MALDI-TOF was used to characterize this functionalized surface. Analysis of the SAMs using MALDI-TOF reveals a peak at *m/z* 303.143 corresponding to the sodiated (12-carboxydodecyl) phosphonic acid monomer. (Figure 5.7a) The inclusion of this peak and the lack of dimer peak indicate that a monolayer is present on the surface. Then SIP of styrene was then successfully

performed on the monolayers as above.

The carboxylic acid terminated monolayers were allowed to react with pentafluorophenol (PFP) using EDC (Figure 5.1, structure 2). The PFP immobilization on the monolayers was analyzed by IR and the spectrum contained peaks at $\nu_{C=O}$ = 1662 cm^{-1}, ν_{C-C} = 1561 and 1495 cm^{-1} (characteristic of aromatic ring), ν_{C-O} = 1252 cm^{-1}, and aliphatic ν_{C-F} = 979 cm^{-1} (Figure 5.6b).

The ABAP was treated with the pentafluorophenyl ester monolayer and spectral results of this modification step can be seen in the Figure 5.2c. The ABAP formation on the nickel oxide surface shows the appearance of the peaks corresponding to $-NH_2$ stretch at 3128 cm^{-1}, a -C=NH stretch at 3045 cm^{-1}, a peak at 1681 cm^{-1} that can be attributed to open-chain imino (-C=N-) stretch, a carbonyl stretch, a secondary amine N-H bend or an open-chain azo (-N=N-) based on the structure of ABAP. Also, a methylene bend at 1481 $cm^{-1}$and a C-N stretch at 1202 cm^{-1} appeared in the spectrum (Figure 5.2). The peak characteristic of the C-F bond around 1000 cm^{-1} has disappeared from the IR spectra as expected due to the further reaction with ABAP on the surface (Figure 5.1, structure 3). MALDI-TOF analysis on the modification shows a peak at *m/z* 463.250 which corresponds to protonated ABAP (Figure 5.7b).

The ABAP modified monolayers were used to further form polystyrene on the nickel oxide surface by surface-initiated polymerization in step C. The polystyrene synthesis was analyzed by IR after rinsing with toluene for 20-22 hours showing peaks corresponding to ν_{C-H} aromatic ring at 3058 cm^{-1}, methylene $\nu_{C-H\ asym}$ at 2921 cm^{-1} and $\nu_{C-H\ asym}$ at 2849 cm^{-1}, ν_{C-C} from aromatic ring at 1600 cm^{-1} and 1491 cm^{-1}, methylene ν_{C-H} bend at 1449 cm^{-1}, and ν_{C-H} aromatic combination bands at 2000-1660 cm^{-1}(Figure 5.2d).

Based on these spectral results, carboxylic acid-terminated phosphonic acid monolayers were formed on the nickel oxide surface and used as a platform for the polymerization of styrene by an azo radical initiator as observed by infrared spectroscopy.

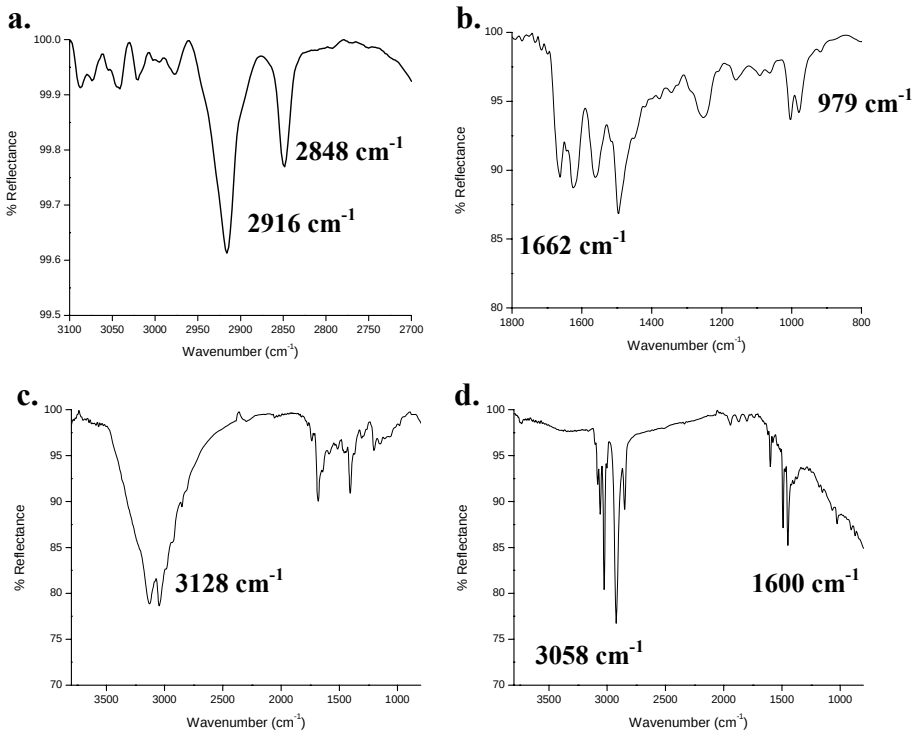

Figure 5.6 IR spectra of the steps in SIP on the nickel oxide surface: a) IR spectra of (12-carboxydodecyl)phosphonic acid on nickel oxide surface after rinsing with THF b) PFP/EDC on the monolayer, c) ABAP radical initiator formation on the monolayer, d) Polystyrene film formation by SIP after 24 hours and then rinsed with toluene.

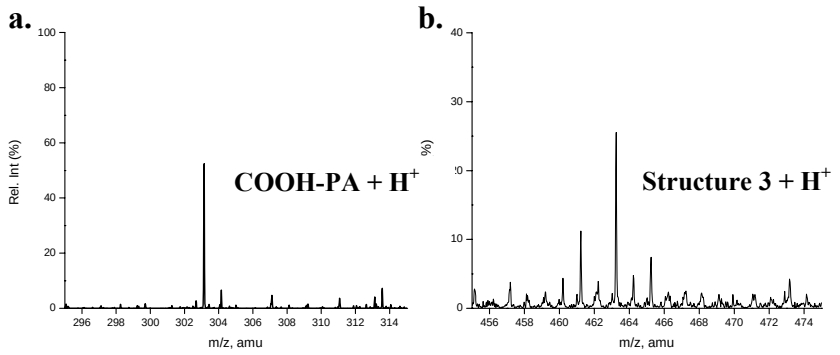

Figure 5.7 (a) MALDI-TOF spectra of the monomer region of (12-carboxydodecyl)phosphonic acid SAMs on nickel oxide surface at *m/z* 303.143, (b) MALDI-TOF spectra of the ABAP on nickel oxide surface shows mass peaks at *m/z* 463.250

The contact angles of the bare nickel oxide surface, COOH-PA SAMs and the polystyrene were compared. Carboxylic acid-terminated phosphonic acid monolayers yielded a hydrophilic surface with a value of 59 ± 8º. When the surface was polymerized to styrene a hydrophobic surface was achieved with value of 103 ± 6º (Figure 5.8).

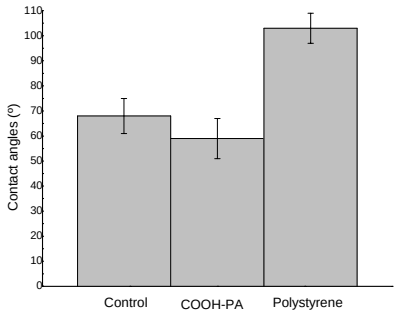

Figure 5.8 Contact angle values of the primary modifications on the nickel oxide surface.

5.3.3 Electrochemical Stability

The capability of the modifications to reduce electrochemical activity on the

surface was studied. Electrochemical techniques such as electrochemical impedance spectroscopy (EIS) and cyclic voltammetry (CV) are suitable techniques for monitoring electrochemical reactions at the modified surfaces and both were utilized here.[62, 63] The results of these techniques are always based on the comparison of the results obtained with unmodified and modified electrode substrates.[62, 63, 139, 322] The nitinol substrates were placed in a 0.1M NaOH solution and the potential was scanned from -300 to +700 mV at a scan rate of 50 $mV \cdot s^{-1}$ in solution, which are typical conditions for these studies. Nickel oxide substrates were scanned from -300 to +600 mV in solution using the same conditions as nitinol surface.[154, 203, 237] For comparison, the cyclic voltammogram (CV) of a cleaned but atmospherically oxidized nitinol surface (Figure 5.9a, black line) is superimposed on those of a COOH-PA modified surface (Figure 5.9a, red line), octadecylphosphonic acid (ODPA) monolayers (green line), and a polystyrene film (Figure 5.9a, blue line). During the anodic potential sweep, the clean nitinol and nickel oxide surfaces have a peak at a potential of +0.4 to +0.5 V assigned to the oxidation of the nickel oxide and nickel hydroxide.[203, 237] Compared with the cyclic voltammetry of the bare nitinol surface, the oxidative peak height of the cyclic voltammograms for the nitinol modified with the monolayer is reduced and the height is dramatically reduced for polystyrene modified substrates (Figure 5.9a). This indicates that the oxidation process is inhibited by the self-assembled monolayers and this reduction is enhanced with the polymer film formation on the surface of nitinol. The samples were scanned five times with no change in the size of the oxidation peak indicating that the films are stable and resistant to electrochemical oxidation. The decreased height observed in the peak current for the oxidation/reduction reaction is related to the fractional coverage of the

modifications, θ^{i}_{CV}. Assuming that diffusion to uncovered parts of the electrode is linear:[7, 63, 323]

$$\theta^{i}_{CV} = 1 - \left(\frac{i_p^{\text{modification}}}{i_p^{\text{bare}}} \right) \quad (1)$$

were i_p^{bare} is the peak current measured at the bare surface and $i_p^{\text{modification}}$ is the peak current measured in the same conditions at the modified samples. The surface coverage of the COOH-PA monolayers was θ^{i}_{CV}=0.66, ODPA monolayers θ^{i}_{CV}=0.67 and for the polystyrene coating was θ^{i}_{CV}=0.97.

Based on the cyclic voltammograms collected, the calculated current-potential intensity relations are presented. The bare nitinol surface reached a current density of bare nitinol surface was measured to be 0.11 mA/cm^2. The maximum current density reached for the modified surfaces were 0.06 mA/cm^2 for COOH-PA and ODPA monolayers and 0.01 mA/cm^2 for the polystyrene modified surface (Figure 5.9b). Voltammetry of the latter consists mainly of charging current indicating that this film effectively blocks electron transfer at the electrode interface.

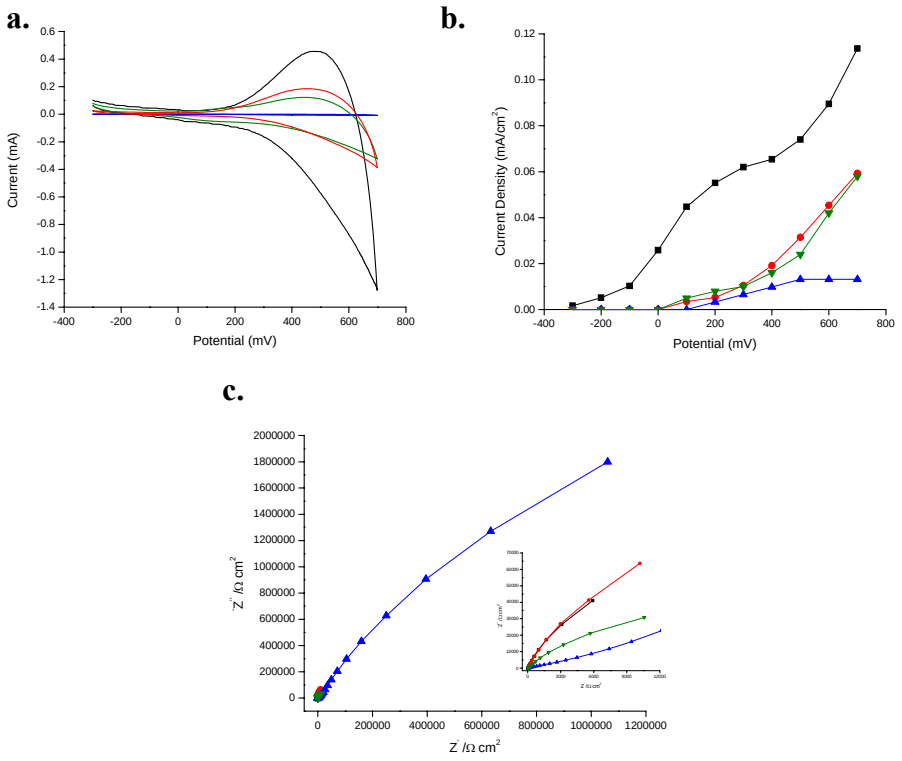

Figure 5.9 (a) Cyclic voltammograms for the bare nitinol electrode (black line), modified with COOH-PA monolayers (red line), ODPA monolayers (green line) and modified with polystyrene film (blue line) (b) Current density measurements for the bare nitinol electrode (black line), modified with COOH-PA monolayers (red line), ODPA monolayers (green line) and modified with polystyrene film (blue line) (c) Nyquist plot of bare nitinol surface (black line) modified with COOH-PA monolayers (red line), ODPA monolayers (green line) and modified with polystyrene film (blue line).

Electrochemical impedance spectroscopy (EIS) provides an effective method for measuring the resistance against the transfer of ionic species to the underlying metal surface and has been widely used to evaluate the barrier properties of SAMs.[62, 135-139, 146, 149, 151, 260, 262, 324] The charge-transfer resistance (R_{CT}) of a coating on the substrate is a measure of the coating's ability to act as a barrier to the corrosion process, and its magnitude is approximately equal to the diameter of the capacitive loop.[136, 151, 260, 324]

The Nyquist plots of bare nitinol and nitinol modified with COOH-PA, ODPA and polystyrene film in 0.1 M NaOH solution are shown in Figure 5.9c. When comparing the modifications to the bare nitinol surface, the size of the Nyquist impedance semicircles of the polystyrene film coated nitinol electrodes were larger than those of the COOH-PA or ODPA modified nitinol. This indicates that the polystyrene modification forms a better barrier to surfa oxidation-reduction reactions than the monolayers for the nitinol surface.[151] Here, the value of $R_{CT\ control}$ of the bare nitinol surface was $5.9 \times 10^3\ \Omega\ cm^2$ (Figure 5.9c black line). As shown in Table 5.2, the average R_{CT} for the polystyrene film is 10^2 times greater than the COOH-PA monolayer and has an excellent capacity for blocking electrode reactions.

The magnitude of the charge-transfer resistance can be related to the coverage of the electrode by assuming that electron-transfer reactions occur only at bare spots on the electrode surface and that diffusion to these defect sites is planar.[63] The protection efficiency (PE) of a film can be calculated by comparing the R_{CT} of the bare surface ($R_{CT\ bare)}$ and of the modified surfaces ($R_{CT\ mod}$) in corrosive solution. Using a 0.1 mM NaOH aqueous solution,[136, 260] a PE value was calculated using the following equation:[136, 139, 260]

$$PE\ (\%) = \frac{R_{CT\ mod} - R_{CTbare}}{R_{CT\ mod}} \times 100\% \qquad (2)$$

where $R_{CT\ mod}$ was the transfer resistance of electrons of the modified surfaces and $R_{CT\ bare}$ the charge-transfer resistance for the bare surface in a corrosive solution. Table 5.2 lists the R_{CT} and PE values of COOH-PA, ODPA monolayers and polystyrene film. This data shows that the PE significantly increased to 99.4% for the polystyrene modified the nitinol surface. The polystyrene film on the nitinol surface is effectively blocking the

electron transfer and therefore protecting the surface. The PE value of COOH-PA and ODPA monolayers is 42% and 46% respectively.

Similar results were obtained for nickel oxide and its modified substrates. The protection efficiency of COOH-PA and ODPA monolayers on nickel oxide were calculated to be 27% and 45%,[10] respectively, by EIS. The polymer modified substrate had a PE of 71% and a θ^{i}_{CV}=0.96 (Figure 5.10, Table 5.2). Previously, a phosphonic acid modified iron surface was reported to have slightly higher (51%) PE than the monolayers reported here. However, diphosphonic acid molecules were used which can increase the corrosion barrier due to the formation of a multilayers on the iron surface.[137, 262] Polystyrene grafted onto a gold surface, without using SAM linkers, was shown to have a surface fraction coverage of $\theta = 0.91$.[325] Therefore, our protection efficiency values of the monolayer and polystyrene films on nitinol and nickel oxide are comparable to or better than those reported by others.[325]

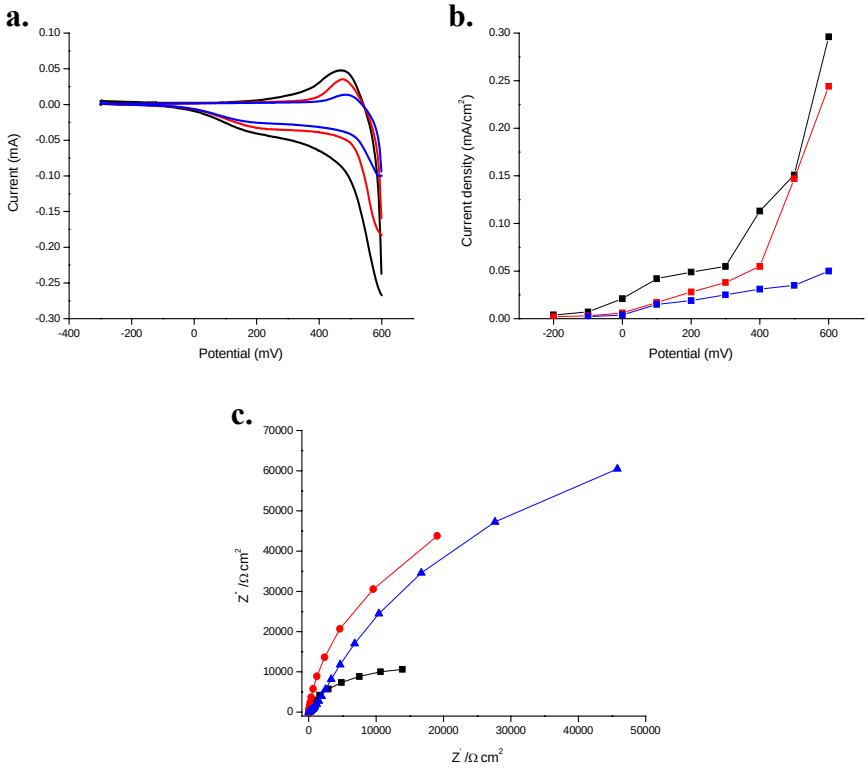

Figure 5.10 (a) Cyclic voltammograms for the bare nickel oxide electrode (black line), modified with COOH-PA monolayers (red line), and modified with polystyrene film (blue line) (b) Current density measurements for the bare nickel oxide electrode (black line), modified with COOH-PA monolayers (red line) and modified with polystyrene film (blue line) (c) Nyquist plot of bare nickel oxide surface (black line) modified with COOH-PA monolayers (red line) and modified with polystyrene film (blue line)

Table 5.2 Summary of impedance parameters obtained by nitinol and nickel oxide modified

	R_{CT} (Ω cm^2)	PE (%)	θ^i_{CV} (%)
Bare nitinol	5.9×10^3	—	—
COOH-PA on nitinol	1.0×10^4	42.0	66.0
ODPA on nitinol	1.1×10^4	46.0	67.0
Polystyrene on nitinol	1.0×10^6	99.4	99.0
Bare nickel oxide	1.3×10^4	—	—
COOH-PA on nickel oxide	1.9×10^4	27.0	11.0
Polystyrene on nickel oxide	4.6×10^4	71.0	96.0

The study carried out here demonstrated that the polystyrene film forms an excellent, stable barrier to electrochemical oxidation of the surface, most likely due to its ability to act as a hydrophobic barrier.[117, 322, 326] However, it is interesting to compare the fractional coverage estimated by the two techniques, EIS (PE) and CV (θ^i_{CV}). Although the estimation of the fractional surface coverage follows the same qualitative trend using both techniques, the actual values varied. The low values estimated by cyclic voltammetry can be attributed to the dominance of radial diffusion near each defect site.[63, 323] According to assumptions of the microarray model, [55, 142] if the radial diffusion to micropores is occurring, then the peak current observed is not a simple function of the exposed area of the SAM-coated electrode, as is assumed in Equation 1.[55, 142] Further, Finklea has established that pinholes that nonuniform radii and separation of the pinholes affects the accuracy of the value obtained from Equation 1.[55, 142] Due to the limitations of cyclic voltammetry, the protection efficiency calculated by impedance spectroscopy is the most widely used method to estimate the fractional coverage at the equilibrium

potential by measuring the charge-transfer resistance.[7, 63, 134-136, 139] The charge transfer resistance is a function of both the coverage and the pinhole parameters.[62, 63, 144, 323, 327]

5.4 Conclusions

A polystyrene film was synthesized on the nitinol and nickel oxide surfaces utilizing carboxylic acid terminated phosphonic acid monolayers as covalent linkers between the polymer and oxide surfaces. This was achieved through surface-initiated free radical polymerization using an azo-initiator. The modifications on the surfaces were characterized by IR, MALDI, AFM and contact angle measurements. The integrity and properties of the polystyrene and monolayer modifications have been evaluated by electrochemical characterization. Results obtained support the conclusion that polystyrene behaves as a better insulator and corrosion barrier than the methyl and carboxyalkylphosphonic acid monolayers. The excellent protection efficiency and stability of this system may allow it to serve as a model system for future corrosion inhibition and/or layered film studies on alloys. The holes in the polystyrene film may limit the use of the film as a long term corrosion barrier because the holes may serve as points of entry for water or other deleterious chemicals to the surface which could cause removal or deterioration of the film.

References

1. Blodgett, K. B., Films Built by Depositing Successive Monomolecular Layers on a Solid Surface. *J. Am. Chem. Soc.* **1935,** 57, (6), 1007-1022.

2. Lee, H.; Kepley, L. J.; Hong, H. G.; Mallouk, T. E., Inorganic analogs of Langmuir-Blodgett films: adsorption of ordered zirconium 1,10-decanebisphosphonate multilayers on silicon surfaces. *J. Am. Chem. Soc.* **1988,** 110, (2), 618-620.

3. Byrd, H.; Whipps, S.; Pike, J. K.; Ma, J.; Nagler, S. E.; Talham, D. R., Role of the template layer in organizing self-assembled films: zirconium phosphonate monolayers and multilayers at a Langmuir-Blodgett template. *J. Am. Chem. Soc.* **1994,** 116, (1), 295-301.

4. Azzam, R. M. A.; Bashara, N. M., *Ellipsometry and polarized light*. 4th ed.; North-Holland Pub. Co.: Amsterdam, 1977.

5. Ulman, A., *An Introduction to Ultrathin Organic Films from Langmui-Blodgett to Self-Assembly*. Academic Press: San Diego, California, 1991; p 442.

6. Gole, A.; Orendorff, C. J.; Murphy, C. J., Immobilization of Gold Nanorods onto Acid-Terminated Self-Assembled Monolayers via Electrostatic Interactions. *Langmuir* **2004,** 20, (17), 7117-7122.

7. Shervedani, R. K.; Hatefi-Mehrjardi, A.; Babadi, M. K., Comparative electrochemical study of self-assembled monolayers of 2-mercaptobenzoxazole, 2-mercaptobenzothiazole, and 2-mercaptobenzimidazole formed on polycrystalline gold electrode. *Electrochimica Acta* **2007,** 52, (24), 7051-7060.

8. Raman, A.; Dubey, M.; Gouzman, I.; Gawalt, E. S., Formation of Self-Assembled Monolayers of Alkylphosphonic acid on the Native Oxide Surface of SS316L. *Langmuir*

2006, 22, (15), 6469-6472.

9. Raman, A.; Gawalt, E. S., Self-Assembled Monolayers of Alkanoic Acids on the Native Oxide Surface of SS316L by Solution Deposition. *Langmuir* **2007,** 23, (5), 2284-2288.

10. Quiñones, R.; Raman, A.; Gawalt, E. S., Functionalization of Nickel Oxide using Alkylphosphonic Acid Self-Assembled Monolayers. *Thin Solid Films* **2008,** accepted.

11. Allara, D. L.; Atre, S. V.; Elliger, C. A.; Snyder, R. G., The formation of a crystalline monolayer of folded molecules by solution self-assembly of .alpha.,.omega.-alkanedioic acids on silver. *J. Am. Chem. Soc.* **1991,** 113, (5), 1852-1854.

12. Rodriguez, L. M.; Gayone, J. E.; Sanchez, E. A.; Grizzi, O.; Blum, B.; Salvarezza, R. C., Room Temperature Kinetics of Short-Chain Alkanethiol Film Growth on Ag(111) from the Vapor Phase. *J. Phys. Chem. B.* **2006,** 110, 7095-7097.

13. Siqueira Petri, D. F.; Wenz, G.; Schunk, P.; Schimmel, T., An Improved Method for the Assembly of Amino-Terminated Monolayers on SiO2 and the Vapor Deposition of Gold Layers. *Langmuir* **1999,** 15, (13), 4520-4523.

14. Quiñones, R.; Gawalt, E. S., Study of the Formation of Self-Assembled Monolayers on Nitinol. *Langmuir* **2007,** 23, (20), 10123-10130.

15. Quiñones, R.; Raman, A.; Gawalt, E. S., An approach to differentiating between multi- and monolayers using MALDI-TOF MS. *Surf. Interface Anal.* **2007,** 39, (7), 593-600.

16. Gawalt, E. S.; Avaltroni, M. J.; Koch, N.; Schwartz, J., Self-Assembly and Bonding of Alkanephosphonic Acids on the native Oxide Surface of Titanium. *Langmuir* **2001,** 17, (19), 5736-5738.

17. Allara, D. L.; Nuzzo, R. G., Spontaneously organized molecular assemblies. 1. Formation, dynamics, and physical properties of n-Alkanoic acids adsorbed from solution on an oxidized aluminum surface. *Langmuir* **1985,** 1, 45-52.

18. Touwslager, F. J.; Sondag, A. H. M., Order and disorder in n-Alkylcarboxylic acid monolayers. Chain-length dependence and lateral interaction effects. *Langmuir* **1994,** 10, 1026-1033.

19. Cooper, E.; Leggett, G. J., Influence of Tail-Group Hydrogen Bonding on the Stabilities of Self-Assembled Monolayers of Alkylthiols on Gold. *Langmuir* **1999,** 15, 1024-1032.

20. Bain, C. D.; Evall, J.; Whitesides, G. M., Formation of monolayers by the coadsorption of thiols on gold: variation in the head group, tail group, and solvent. *J. Am. Chem. Soc.* **1989,** 111, (18), 7155-7164.

21. Laibinis, P. E.; Whitesides, G. M.; Allara, D. L.; Tao, Y.-T.; Parikh, A. N.; Nuzzo, R. G., Comparison of the Structures and Wetting Properties of Self-Assembled Monolayers of n-Alkanethiols on the Coinage Metal Surfaces, Cu, Ag, Au. *J. Am. Chem. Soc.* **1991,** 113, 7152-7167.

22. Deng, H.; Nanjo, H.; Qian, P.; Xia, Z.; Ishikawa, I.; Suzuki, T. M., Corrosion prevention of iron with novel organic inhibitor of hydroxamic acid and UV irradiation. *Electrochimica Acta* **2008,** 53, (6), 2972-2983.

23. Sung, M. M.; Sung, K.; Kim, C. G.; Lee, S. S.; Kim, Y., Self-Assembled Monolayers of Alkanethiols on Oxidized Copper Surfaces. *J. Phys. Chem. B* **2000,** 104, (10), 2273-2277.

24. Adden, N.; Gamble, L. J.; Castner, D. G.; Hoffmann, A.; Gross, G.; Menzel, H.,

Phosphonic Acid Monolayers for Binding of Bioactive Molecules to Titanium Surfaces. *Langmuir* **2006,** 22, (19), 8197-8204.

25. Fiurasek, P.; Reven, L., Phosphonic and Sulfonic Acid-Functionalized Gold Nanoparticles: A Solid-State NMR Study. *Langmuir* **2007,** 23, (5), 2857 - 2866.

26. Gawalt, E. S.; Lu, G.; Bernasek, S. L.; Schwartz, J., Enhanced Bonding of Alkenephosphonic Acids to Oxidized Titanium using Surface-Bound Alkoxyzirconium Complex interfaces. *Langmuir* **1999,** 15, 8929-8933.

27. Yee, C.; Kataby, G.; Ulman, A.; Prozorov, T.; White, H.; King, A.; Rafailovich, M.; Sokolov, J.; Gedanken, A., Self-Assembled Monolayers of Alkanesulfonic and -phosphonic Acids on Amorphous Iron Oxide Nanoparticles. *Langmuir* **1999,** 15, (21), 7111-7115.

28. Folkers, J. P.; Gorman, C. B.; Laibinis, P. E.; Buchholz, S.; Whitesides, G. M.; Nuzzo, R. G., Self-Assembled Monolayers of Long-Chain Hydroxamic Acids on the Native Oxide of Metals. *Langmuir* **1995,** 11, (3), 813-824.

29. Telegdi, J.; Rigo, T.; Kalman, E., Molecular layers of hydroxamic acids in copper corrosion inhibition. *Journal of Electroanalytical Chemistry* **2005,** 582, (1-2), 191-201.

30. Gershevitz, O.; Sukenik, C. N., In Situ FTIR-ATR Analysis and Titration of Carboxylic Acid-Terminated SAMs. *J. Am. Chem. Soc.* **2004,** 126, (2), 482-483.

31. Winter, N.; Vieceli, J.; Benjamin, I., Hydrogen-Bond Structure and Dynamics at the Interface between Water and Carboxylic Acid-Functionalized Self-Assembled Monolayers. *j. phys. Chem. B* **2008,** 112, (2), 227-231.

32. Allara, D. L.; Nuzzo, R. G., Spontaneously organized molecular assemblies. 2. Quantitative infrared spectroscopic determination of equilibrium structures of solution-

adsorbed n-alkanoic acids on an oxidized aluminum surface. *Langmuir* **1985,** 1, (1), 52-66.

33. Ederth, T.; Claesson, P.; Liedberg, B., Self-Assembled Monolayers of Alkanethiolates on Thin Gold Films as Substrates for Surface Force Measurements. Long-Range Hydrophobic Interactions and Electrostatic Double-Layer Interactions. *Langmuir* **1998,** 14, 4782-4789.

34. Myers, D., *Surfaces, Interfaces and Colloids: principles and applications*. 2nd ed.; John Wiley & Sons: USA, 1999; p 501.

35. Chirakul, P.; Perez-Luna, V. H.; Owen, H.; Lopez, G. P.; Hampton, P. D., Synthesis and Characterization of Amine-Terminated Self-Assembled Monolayers Containing Diethylene Glycol Linkages. *Langmuir* **2002,** 18, 4324-4330.

36. Cheng, F.; Gamble, L. J.; Grainger, D. W.; Castner, D. G., X-ray Photoelectron Spectroscopy, Time-of-Flight Secondary Ion Mass Spectrometry, and Principal Component Analysis of the Hydrolysis, Regeneration, and Reactivity of N-Hydroxysuccinimide-Containing Organic Thin Films. *Anal. Chem.* **2007,** 79, (22), 8781-8788.

37. Evans-Nguyen, K. M.; Tolles, L. R.; Gorkun, O. V.; Lord, S. T.; Schoenfisch, M. H., Interactions of Thrombin with Fibrinogen Adsorbed on Methyl-, Hydroxyl-, Amine-, and Carboxyl-Terminated Self-Assembled Monolayers. *Biochemistry* **2005,** 44, (47), 15561-15568.

38. Gole, A.; Sainkar, S. R.; Sastry, M., Electrostatically Controlled Organization of Carboxylic Acid Derivatized Colloidal Silver Particles on Amine-Terminated Self-Assembled Monolayers. *Chem. Mater.* **2000,** 12, (5), 1234-1239.

39. Wang, H.; Chen, S.; Li, L.; Jiang, S., Improved Method for the Preparation of Carboxylic Acid and Amine Terminated Self-Assembled Monolayers of Alkanethiolates. *Langmuir* **2005,** 21, (7), 2633-2636.

40. Frutos, A. G.; Brockman, J. M.; Corn, R. M., Reversible Protection and Reactive Patterning of Amine- and Hydroxyl-Terminated Self-Assembled Monolayers on Gold Surfaces for the Fabrication of Biopolymer Arrays. *Langmuir* **2000,** 16, (5), 2192-2197.

41. Van Stipdonk, M. J.; English, R. D.; Schweikert, E. A., Sputtering of Tetrafluoro- and Tetraphenylborate Anions Adsorbed to an Amine-Terminated Self-Assembled Monolayer Surface. *J. Phys. Chem. B* **1999,** 103, (37), 7929-7934.

42. Zwahlen, M.; Tosatti, S.; Textor, M.; Hahner, G., Orientation in methyl- and hydroxyl-terminated Self-Assembled Alkanephosphonate monolayers on titanium oxide surfaces investigated with soft X-ray Adsorption. *Langmuir* **2002,** 18, 3957-3962.

43. Vogt, A. D.; Beebe, T. P., Jr., Interactions of Alcohols with Hydroxyl- and Methyl-Terminated Self-Assembled Monolayer Surfaces Studied by Temperature-Programmed Desorption. *J. Phys. Chem. B.* **1999,** 103, (40), 8482-8489.

44. Venkataraman, N. V.; Zurcher, S.; Spencer, N. D., Order and Composition of Methyl-Carboxyl and Methyl-Hydroxyl Surface-Chemical Gradients. *Langmuir* **2006,** 22, (9), 4184-4189.

45. Colorado, R., Jr.; Villazana, R. J.; Lee, T. R., Self-Assembled Monolayers on Gold Generated from Aliphatic Dithiocarboxylic Acids. *Langmuir* **1998,** 14, (22), 6337-6340.

46. Pawsey, S.; Yach, K.; Halla, J.; Reven, L., Self-Assembled Monolayers of Alkanoic acids: A Solid-State NMR study. *Langmuir* **2000,** 16, (7), 3294-3303.

47. Tosatti, S.; Michael, R.; Textor, M.; Spencer, N. D., Self-Assembled Monolayers of

dodecyl and hydroxy-dodecyl phosphates on both smooth and rough titanium and titanium oxide surfaces. *Langmuir* **2002,** 18, 3537-3548.

48. Auletta, T.; van Veggel, F. C. J. M.; Reinhoudt, D. N., Self-Assembled Monolayers on Gold of Ferrocene-Terminated Thiols and Hydroxyalkanethiols. *Langmuir* **2002,** 18, (4), 1288-1293.

49. Pawsey, S.; McCormick, M.; De Paul, S.; Graf, R.; Lee, Y. S.; Reven, L.; Spiess, H. W., 1H Fast MAS NMR Studies of Hydrogen-Bonding Interactions in Self-Assembled Monolayers. *J. Am. Chem. Soc.* **2003,** 125, (14), 4174-4184.

50. Howell, S.; Kuila, D.; Kasibhatla, B.; Kubiak, C. P.; Janes, D.; Reifenberger, R., Molecular Electrostatics of Conjugated Self-Assembled Monolayers on Au(111) Using Electrostatic Force Microscopy. *Langmuir* **2002,** 18, (13), 5120-5125.

51. Jiang, J.; Krauss, T. D.; Brus, L. E., Electrostatic Force Microscopy Characterization of Trioctylphosphine Oxide Self-assembled Monolayers on Graphite. *J. Phys. Chem. B* **2000,** 104, (50), 11936-11941.

52. Ramon Colorado, J.; Lee, T. R., Physical organic probes of interfacial wettability reveal the importance of surface dipole effects. *j. Phys. Org. Chem.* **2000,** 13, 796-807.

53. Schreiber, F., Structure and growth of self-assembling monolayers. *Progress in Surface Science* **2000,** 65, 151-256.

54. Nuzzo, R. G.; Allara, D. L., Adsorption of bifunctional organic disulfides on gold surfaces. *J. Am. Chem. Soc.* **1983,** 105, (13), 4481-4483.

55. Finklea, H. O. Self-Assembled Monolayers on Electrodes.

56. Weinstein, R. D.; Moriarty, J.; Cushnie, E.; Colorado, R.; Lee, T. R.; Patel, M.; Alesi, W. R.; Jennings, G. K., Structure, Wettability, and Electrochemical Barrier Properties of

Self-Assembled Monolayers Prepared from Partially Fluorinated Hexadecanethiols. *J. Phys. Chem. B* **2003,** 107, (42), 11626-11632.

57. Badia, A.; Lennox, R. B.; Reven, L., A Dynamic view of Self-Assembled Monolayers. *Acc. Chem. Res.* **2000,** 33, 475-481.

58. Ulman, A., Formation and Structure of Self-Assembled Monolayers. *Chem. Rev.* **1996,** 96, 1533-1554.

59. Frederix, F.; Bonroy, K.; Laureyn, W.; Reekmans, G.; Campitelli, A.; Dehaen, W.; Maes, G., Enhanced Performance of an Affinity Biosensor Interface Based on Mixed Self-Assembled Monolayers of Thiols on Gold. *Langmuir* **2003,** 19, 4351-4357.

60. Brewer, S. H.; Allen, A. M.; Lappi, S. E.; Chasse, T. L.; Briggman, K. A.; Gorman, C. B.; Franzen, S., Infrared Detection of a Phenylboronic acid Terminated Alkane Thiol Monolayer on Gold Surfaces. *Langmuir* **2004,** 13, (20), 5512-5520.

61. Dillmore, W. S.; Yousaf, M. N.; Mrksich, M., A Photochemical Method for Patterning the Immobilization of Ligands and Cells to Self-Assembled Monolayers. *Langmuir* **2004,** 20, 7223-7231.

62. Ganesh, V.; Pal, S. K.; Kumar, S.; Lakshminarayanan, V., Self-assembled monolayer (SAMs) of alkoxycyanobiphenyl thiols on gold- A study of electron transfer reaction using cyclic voltammetry and electrochemical impedance spectroscopy. *Journal of Colloid and Interface Science* **2006,** 296, 195-203.

63. Campuzano, S.; Pedrero, M.; Montemayor, C.; Fatas, E.; Pingarron, J. M., Characterization of alkanethiol-self-assembled monolayers-modified gold electrodes by electrochemical impedance spectroscopy. *journal of Electrochemistry* **2006,** 586, 112-121.

64. Porter, M. D.; Bright, T. B.; Allara, D. L.; Chidsey, C. E. D., Spontaneously organized molecular assemblies. 4. Structural characterization of n-alkyl thiol monolayers on gold by optical ellipsometry, infrared spectroscopy, and electrochemistry. *J. Am. Chem. Soc.* **1987,** 109, (12), 3559-3568.

65. Graham, D. J.; Ratner, B. D., Multivariate Analysis of TOF-SIMS Spectra from Dodecanethiol SAM Assembly on Gold: Spectral Interpretation and TOF-SIMS Fragmentation Processes. *Langmuir* **2002,** 18, (15), 5861 -5868.

66. Nuzzo, R. G.; Dubois, L. H.; Allara, D. L., Fundamental Studies of Microscopic Wetting on Organic Surfaces. 1. Formation and Structural Characterization of a Self-Consistent Series of Polyfunctional Organic Monolayers. *J. Am. Chem. Soc.* **1990,** 112, 558-569.

67. Damos, F. S.; Luz, R. C. S.; Kubota, L. T., Determination of Thickness, Dielectric Constant of Thiol Films, and Kinetics of Adsorption Using Surface Plasmon Resonance. *Langmuir* **2005,** 21, (2), 602-609.

68. Brukman, M. J.; Oncins, G.; Dunbar, T. D.; Boardman, L. D.; Carpick, R. W., Nanotribological Properties of Alkanephosphonic Acid Self-Assembled Monolayers on Aluminum Oxide: Effects of Fluorination and Substrate Crystallinity. *Langmuir* **2006,** 22, (9), 3988-3998.

69. Sonnenschein, M. F.; Cheatham, C. M., Effect of Interfacial Energetics on the Protection of Steel and Aluminum Surfaces by Alkyl Acid Coatings. *Langmuir* **2002,** 18, (9), 3578-3584.

70. van den Brand, J.; Blajiev, O.; Beentjes, P. C. J.; Terryn, H.; de Wit, J. H. W., Interaction of Anhydride and Carboxylic Acid Compounds with Aluminum Oxide

Surfaces Studied Using Infrared Reflection Absorption Spectroscopy. *Langmuir* **2004,** 20, (15), 6308-6317.

71. Mutin, P. H.; Lafond, V.; Popa, A. F.; Granier, M.; Markey, L.; Dereux, A., Selective Surface Modification of SiO_2-TiO_2 Supports with Phosphonic Acids. *Chem. Mater.* **2004,** 16, 5670-5675.

72. Lin, S.-Y.; Tsai, T.-K.; Lin, C.-M.; Chen, C.-h., Structures of Self-Assembled Monolayers of n-Alkanoic Acids on Gold Surfaces Modified by Underpotential Deposition of Silver and Copper: Odd-Even Effect. *Langmuir* **2002,** 18, 5473-5478.

73. Lim, M. S.; Feng, K.; Chen, X.; Wu, N.; Raman, A.; Nightingale, J.; Gawalt, E. S.; Korakakis, D.; Hornak, L. A.; Timperman, A. T., Adsorption and Desorption of Stearic Acid Self-Assembled Monolayers on Aluminum Oxide. *Langmuir* **2007,** 23, (5), 2444-2452.

74. Mahapatro, A.; Johnson, D. M.; Patel, D. N.; Feldman, M. D.; Ayon, A. A.; Agrawal, C. M., Surface Modification of Functional Self-Assembled Monolayers on 316L Stainless Steel via Lipase Catalysis. *Langmuir* **2006,** 22, (3), 901-905.

75. Shustak, G.; Domb, A. J.; Mandler, D., Preparation and Characterization of n-Alkanoic Acid Self-Assembled Monolayers Adsorbed on 316L Stainless Steel. *Langmuir* **2004,** 20, (18), 7499-7506:.

76. Pawsey, S.; Yach, K.; Reven, L., Self-Assembly of Carboxyalkylphosphonic Acids on Metal Oxide Powders. *Langmuir* **2002,** 18, (13), 5205-5212.

77. Zhao, B., A Combinatorial Approach to Study Solvent-Induced Self-Assembly of Mixed Poly(methyl methacrylate)/Polystyrene Brushes on Planar Silica Substrates: Effect of Relative Grafting Density. *Langmuir* **2004,** 20, (26), 11748-11755.

78. Weinstein, R. D.; Richards, J.; Thai, S. D.; Omiatek, D. M.; Bessel, C. A.; Faulkner, C. J.; Othman, S.; Jennings, G. K., Characterization of Self-assembled Monolayers from Lithium Dialkyldithiocarbamate Salts. *Langmuir* **2007,** 23, (5), 2887-2891.

79. Lee, J. K.; Chi, Y. S.; Choi, I. S., Reactivity of Acetylenyl-Terminated Self-Assembled Monolayers on Gold: Triazole Formation. *Langmuir* **2004,** 20, (10), 3844-3847.

80. Wen, Y.; Yi, W.; Meng, L.; Feng, M.; Jiang, G.; Yuan, W.; Zhang, Y.; Gao, H.; Jiang, L.; Song, Y., Photochemical-Controlled Switching Based on Azobenzene Monolayer Modified Silicon (111) Surface. *J. Phys. Chem. B* **2005,** 109, (30), 14465-14468.

81. Shaporenko, A.; Cyganik, P.; Buck, M.; Terfort, A.; Zharnikov, M., Self-Assembled Monolayers of Aromatic Selenolates on Noble Metal Substrates. *J. Phys. Chem. B* **2005,** 109, (28), 13630-13638.

82. Mamdouh, W.; Uji-i, H.; Gesquiere, A.; DeFeyter, S.; Amabilino, D. B.; Abdel-Mottaleb, M. M. S.; Veciana, J.; DeSchryver, F. C., A Nanoscale View of Supramolecular Stereochemistry in Self-Assembled Monolayers of Enantiomers and Racemates. *Langmuir* **2004,** 20, (22), 9628-9635.

83. Kosbar, L.; Srinivasan, C.; Afzali, A.; Graham, T.; Copel, M.; Krusin-Elbaum, L., Self-Assembled Multilayers of Transition-Metal-Terpyridinyl Complexes; Formation, and Characterization. *Langmuir* **2006,** 22, (18), 7631-7638.

84. Blomberg, E.; Claesson, P. M.; Konradsson, P.; Liedberg, B., Globotriose- and Oligo(ethylene glycol)-Terminated Self-Assembled Monolayers: Surface Forces, Wetting, and Surfactant Adsorption. *Langmuir* **2006,** 22, (24), 10038-10046.

85. Revell, D. J.; Knight, J. R.; Blyth, D. J.; Haines, A. H.; Russell, D. A., Self-Assembled Carbohydrate Monolayers: Formation and Surface Selective Molecular Recognition. *Langmuir* **1998,** 14, (16), 4517-4524.

86. Zhang, Y.; Luo, S.; Tang, Y.; Yu, L.; Hou, K.-Y.; Cheng, J.-P.; Zeng, X.; Wang, P. G., Carbohydrate-Protein Interactions by "Clicked" Carbohydrate Self-Assembled Monolayers. *Anal. Chem.* **2006,** 78, (6), 2001-2008.

87. Heitzman, C. E.; Tu, H.; Braun, P. V., Two-Dimensional Diffusion of Prodan on Self-Assembled Monolayers Studied by Fluorescence Recovery after Photobleaching. *J. Phys. Chem. B* **2004,** 108, (36), 13764-13770.

88. Hyun, J.; Chilkoti, A., Surface-Initiated Free Radical Polymerization of Polystyrene Micropatterns on a Self-Assembled Monolayer on Gold. *Macromolecules* **2001,** 34, (16), 5644-5652.

89. Brandani, P.; Stroeve, P., Kinetics and Equilibria of Adsorption of PEO-PPO-PEO Triblock Copolymers on a Hydrophilic Self-Assembled Monolayer on Gold. *Macromolecules* **2004,** 37, (17), 6640-6643.

90. Ejaz, M.; Yamamoto, S.; Tsujii, Y.; Fukuda, T., Fabrication of Patterned High-Density Polymer Graft Surfaces. 1. Amplification of Phase-Separated Morphology of Organosilane Blend Monolayer by Surface-Initiated Atom Transfer Radical Polymerization. *Macromolecules* **2002,** 35, (4), 1412-1418.

91. Li, J.; Zhu, L. H.; Wu, Y. H.; Harima, Y.; Zhang, A. Q.; Tang, H. Q., Hybrid composites of conductive polyaniline and nanocrystalline titanium oxide prepared via self-assembling and graft polymerization. *Polymer* **2006,** 47, (21), 7361-7367.

92. Senaratne, W.; Andruzzi, L.; Ober, C. K., Self-assembled monolayers and polymer

brushes in biotechnology: Current applications and future perspectives. *Biomacromolecules* **2005,** 6, (5), 2427-2448.

93. Tai, Y.; Shaporenko, A.; Eck, W.; Grunze, M.; Zharnikov, M., Depth Distribution of Irradiation-Induced Cross-Linking in Aromatic Self-Assembled Monolayers. *Langmuir* **2004,** 20, (17), 7166-7170.

94. Brockman, A. H.; Dodd, B. S.; Orlando, R., A Desalting Approach for MALDI-MS Using On-Probe Hydrophobic Self-Assembled Monolayers. *Anal. Chem.* **1997,** 69, 4716-4720.

95. Griesser, H. J.; Kingshott, P.; McArthur, S. L.; McLean, K. M.; Kinsel, G. R.; Timmons, R. B., Surface-MALDI mass spectrometry in biomaterials research. *Biomaterials* **2004,** 25, 4861-4875.

96. Su, J.; Mrksich, M., Using MALDI-TOF Mass Spectrometry to Characterize interfacial reactions on Self-Assembled Monolayers. *Langmuir* **2003,** 19, (12), 4867-4870.

97. Francis, J. T.; Nie, H.-Y.; McIntyre, N. S.; Briggs, D., ToF-SIMS Investigation of Octadecylphosphonic Acid Monolayers on a Mica Substrate. *Langmuir* **2006,** 22, (22), 9244-9250.

98. Wolf, K. V.; Cole, D. A.; Bernasek, S. L., High-Resolution TOF-SIMS Study of Varying Chain Length Self-Assembled Monolayer Surfaces. *Anal. Chem.* **2002,** 74, (19), 5009-5016.

99. Gouzman, I.; Dubey, M.; Carolus, M. D.; Schwartz, J.; Bernasek, S. L., Monolayer vs. Multilayer self-assembled alkylphosphonate films: X-ray photoelectron spectroscopy studies. *Surface Science* **2006,** 600, 773-781.

100. Wolf, K. V.; Cole, D. A.; Bernasek, S. L., Chain Length Effects for Cluster Ion Formation during High Energy Ion/Surface Collisions with Self-Assembled Monolayer Surfaces. *J. Phys. Chem. B.* **2002,** 106, (40), 10382-10387.

101. Keszthelyi, T.; Paszti, Z.; Rigo, T.; Hakkel, O.; Telegdi, J.; Guczi, L., Investigation of Solid Surfaces Modified by Langmuir-Blodgett Monolayers Using Sum-Frequency Vibrational Spectroscopy and X-ray Photoelectron Spectroscopy. *J. Phys. Chem. B* **2006,** 110, (17), 8701-8714.

102. Sinapi, F.; Naji, A.; Delhalle, J.; Mekhalif, Z., Assessment by XPS and electrochemical techniques of two molecular organosilane films prepared on stainless-steel surfaces. *Suf. Interface. Anal.* **2004,** 36, 1484-1490.

103. Mrksich, M., Mass Spectrometry of Self-Assembled Monolayers: A New Tool for Molecular Surface Science. *ACS Nano* **2008,** 2, (1), 7-18.

104. Pawsey, S.; Reven, L., ^{19}F Fast Magic-Angle Spinning NMR Studies of Perfluoroalkanoic acid Self-Assembled Monolayers. *Langmuir* **2006,** 22, 1055-1062.

105. La, Y.-H.; Jung, Y. J.; Kim, H. J.; Kang, T.-H.; Ihm, K.; Kim, K.-J.; Kim, B.; Park, J. W., Sub-100-nm Pattern Formation through Selective Chemical Transformation of Self-Assembled Monolayers by Soft X-ray Irradiation. *Langmuir* **2003,** 19, (10), 4390-4395.

106. Snyder, R. G.; Struss, H. L.; Elliger, C. A., C-H Stretching modes and Structure of n-Alkyl Chains. 1. Long, Disordered Chains. *J. Phys. Chem* **1982,** 86, 5145-5150.

107. Snyder, R. G.; Maroncelli, M.; Strauss, H. L.; Hallmark, V. M., Temperature and phase behavior of infrared intensities: the poly(methylene) chain. *J. Phys. Chem.* **1986,** 90, (22), 5623-5630.

108. Hahner, G.; Hofer, R.; Klingenfuss, I., Order and orientation in Self-Assembled long chain Alkanephosphate monolayers adsorbed on metal oxide surfaces. *Langmuir* **2001,** 17, 7047-7052.

109. Creager, S. E.; Clarke, J., Contact-Angle Titrations of Mixed w-Mercaptoalkanoic Acid/Alkanethiol Monolayers on Gold. Reactive vs Nonreactive Spreading, and Chain Length Effects on Surface pKa Values. *Langmuir* **1994,** 10, (10), 3675-3683.

110. Liakos, I. L.; Newman, R. C.; McAlpine, E.; Alexander, M. R., Study of the Resistance of SAMs on Aluminium to Acidic and Basic Solutions Using Dynamic Contact Angle Measurement. *Langmuir* **2007,** 23, (3), 995-999.

111. Extrand, C. W., Contact Angles and their Hysteresis as a measure of liquid-solid adhesion. *Langmuir* **2004,** 20, 4017-4021.

112. Tadmor, R., Line Energy and the relation between advancing, receding, anf Young contact angles. *Langmuir* **2004,** 20, 7659-7664.

113. Extrand, C. W., Model for Contact Angles and hysteresis on rough and ultraphobic surfaces. *Langmuir* **2002,** 18, 7991-7999.

114. Extrand, C. W., Criteria for Ultralyophobic Surfaces. *Langmuir* **2004,** 20, (12), 5013-5018.

115. Gao, L.; McCarthy, T. J., A Perfectly Hydrophobic Surface (A/R = 180/180). *J. Am. Chem. Soc.* **2006,** 128, (28), 9052-9053.

116. Kawai, T.; Suzuki, M.; Kondo, T., Fabrication of Flexible Gold Films with Periodic Sub-Micrometer Roughness and Their Wettability Control by Modification of SAM. *Langmuir* **2006,** 22, (24), 9957-9961.

117. Matarredona, O. M.; Mach, K.; Rieger, M. M.; O'Rear, E. A., Alteration of

wettability and inhibition of corrosion in narrow aluminum 7075 by thin polymer films. *Corrosion Science* **2003,** 45, 2541-2562.

118. Anderson, J. C.; Leaver, K. D.; Rawlings, R. D.; M., A. J., *Materials Science*. 4th ed.; Chapman and Hall.

119. Berim, G. O.; Ruckenstein, E., Microscopic Interpretation of the Dependence of the Contact Angle on Roughness. *Langmuir* **2005,** 21, (17), 7743-7751.

120. Cappella, B.; Dietler, G., Force-distance by atomic force microscopy. *Surface Science Reports* **1999,** 34, (1-3), 5-104.

121. Al-Taher, F.; Telegdi, J.; Kalman, E., Effect of divalent cations in Langmuir-Blodgett films on the protection of copper against corrosion. *Materials Science Forum* **2007,** 537-538, 9-16.

122. McQuaw, C. M.; Sostarecz, A. G.; Zheng, L.; Ewing, A. G.; Winograd, N., Lateral Heterogeneity of Dipalmitoylphosphatidylethanolamine-Cholesterol Langmuir-Blodgett Films Investigated with Imaging Time-of-Flight Secondary Ion Mass Spectrometry and Atomic Force Microscopy. *Langmuir* **2005,** 21, (3), 807-813.

123. Imanishi, A.; Suzuki, M.; Nakato, Y., In Situ AFM Studies on Self-Assembled Monolayers of Adsorbed Surfactant Molecules on Well-Defined H-Terminated Si(111) Surfaces in Aqueous Solutions. *Langmuir* **2007,** 23, (26), 12966-12972.

124. Lee, D. H.; Kim, D.; Oh, T.; Cho, K., Phase State Effect on Adhesion Behavior of Self-Assembled Monolayers. *Langmuir* **2004,** 20, (19), 8124-8130.

125. Adenier, A.; Cabet-Deliry, E.; Lalot, T.; Pinson, J.; Podvorica, F., Attachment of Polymers to Organic Moieties Covalently Bonded to Iron Surfaces. *Chem. Mater.* **2002,** 14, (11), 4576-4585.

126. Thierry, B.; Winnik, F. M.; Merhi, Y.; Silver, J.; Tabrizian, M., Bioactive coatings of endovascular stents based on polyelectrolyte multilayers. *Biomacromolecules* **2003,** 4, (6), 1564-1571.

127. Sonnenberg, L.; Parvole, J.; Borisov, O.; Billon, L.; Gaub, H. E.; Seitz, M., AFM-Based Single Molecule Force Spectroscopy of End-Grafted Poly(acrylic acid) Monolayers. *Macromolecules* **2006,** 39, 281-288.

128. Cacciafesta, P.; Humphris, A. D. L.; Jandt, K. D.; Miles, M. J., Human Plasma Fibrinogen Adsorption on Ultraflat Titanium Oxide Surfaces Studied with Atomic Force Microscopy. *Langmuir* **2000,** 16, (21), 8167-8175.

129. Phang, T.-L.; Franses, E. I., Physically Self-Assembled Monolayers (PSAMs) of Lecithin Lipids at Hydrophilic Silicon Oxide Interfaces. *Langmuir* **2006,** 22, (4), 1609-1618.

130. Wang, M. S.; Palmer, L. B.; Schwartz, J. D.; Razatos, A., Evaluating Protein Attraction and Adhesion to Biomaterials with the Atomic Force Microscope. *Langmuir* **2004,** 20, (18), 7753-7759.

131. Sibilia, J. P., *A Guide to Materials Characterization and Chemical Analysis*. 2nd ed.; Wiley-VCH: 1996.

132. McGuire, G. E.; Weiss, P. S.; Kushmerick, J. G.; Johnson, J. A.; Simko, S. J.; Nemanich, R. J.; Parikh, N. R.; Chopra, D. R., Surface characterization. *Analytical Chemistry* **1997,** 69, (12), R231-R250.

133. McGuire, G. E.; Swanson, M. L.; Parikh, N. R.; Simko, S.; Weiss, P. S.; Ferris, J. H.; Nemanich, R. J.; Chopra, D. R.; Chourasia, A. R., Surface Characterization. *Analytical Chemistry* **1995,** 67, (12), R199-R220.

134. Zhang, H.; Baldelli, S., Alkanethiol Monolayers at Reduced and Oxidized Zinc Surfaces with Corrosion Protection: A Sum Frequency Generation and Electrochemistry Investigation. *J. Phys. Chem. B* **2006,** 110, 24062-24069.

135. Hintze, P. E.; Calle, L. M., Electrochemical properties and corrosion protection of organosilane self-assembled monolayers on aluminum 2024-T3. *Electrochimica Acta* **2006,** 51, 1761-1766.

136. Liu, Y.; Yu, Z.; Zhou, S.; Wu, L., Self-assembled monolayers on magnesium alloy surfaces from carboxylate ions. *Applied Surface Science* **2006,** 252, (10), 3818-3827.

137. Felhosi, I.; Telegdi, J.; Palinkas, G.; Kalman, E., Kinetics of self-assembled layer formation on iron. *Electrochimica Acta* **2002,** 47, (13-14), 2335-2340.

138. Zhao, M.; Zhou, Y.; Bruening, M. L.; Bergbreiter, D. E.; Crooks, R. M., Inhibition of Electrochemical Reactions at Gold Surfaces by Grafted, Highly Fluorinated, Hyperbranched Polymer Films. *Langmuir* **1997,** 13, (6), 1388-1391.

139. Ma, H. F.; Chen, S. H.; Liu, G. Z.; Xu, J.; Zhou, M., Inhibition effect of self-assembled films formed by gold nanoparticles on iron surface. *Applied Surface Science* **2006,** 252, (12), 4327-4334.

140. Henke, C.; Steinem, C.; Janshoff, A.; Steffan, G.; Luftmann, H.; Sieber, M.; Galla, H.-J., Self-Assembled Monolayers of Monofunctionalized Cyclodextrins onto Gold: A Mass Spectrometric Characterization and Impedance Analysis of Host-Guest interaction. *Anal. Chem.* **1996,** 68, 3158-3165.

141. Noda, H.; Tai, Y.; Shaporenko, A.; Grunze, M.; Zharnikov, M., Electrochemical Characterizations of Nickel Deposition on Aromatic Dithiol Monolayers on Gold Electrodes. *J. Phys. Chem. B* **2005,** 109, (47), 22371-22376.

142. Finklea, H. O.; Snider, D. A.; Fedyk, J.; Sabatani, E.; Gafni, Y.; Rubinstein, I., Characterization of octadecanethiol-coated gold electrodes as microarray electrodes by cyclic voltammetry and ac impedance spectroscopy. *Langmuir* **1993,** 9, (12), 3660-3667.

143. Sanchez-Pomales, G.; Rodriguez, L. S.-.; Velez, N. E. R.-.; Cabrera, C. R., Control of DNA self-assembled monolayers surface coverage by electrochemical desorption. *Journal of Electroanalytical Chemistry* **2007,** 611, 80-86.

144. Widrig, C. A.; Chung, C.; Porter, M. D., The electrochemical desorption of n-alkanethiol monolayers from polycrystalline Au and Ag electrodes. *J. Electroanal. Chem.* **1991,** 310, 335-359.

145. Fleming, B. D.; Praporski, S.; Bond, A. M.; Martin, L. L., Electrochemical Quartz Crystal Microbalance Study of Azurin Adsorption onto an Alkanethiol Self-Assembled Monolayer on Gold. *Langmuir* **2008,** 24, (1), 323-327.

146. Paszternak, A.; Stichleutner, S.; Felhosi, I.; Keresztes, Z.; Nagy, F.; Kuzmann, E.; Vertes, A.; Homonnay, Z.; Peto, G.; Kalman, E., Surface modification of passive iron by alkyl-phosphonic acid layers. *Electrochimica Acta* **2007,** 53, 337-345.

147. Telegdi, J.; Otmaèiæ, H.; Tadic, K.; Al-Taher, F.; Stupnišek-Lisac, E.; Kalman, E., Inhibition of copper corrosion by self assembled amphiphiles. *Chem. Biochem. Eng.* **2007,** 21, (1), 77-82.

148. Telegdi, J.; Rigo, T.; Kalman, E., Nanolayer barriers for inhibition of copper corrosion. *Corrosion Engineering, Science and Technology* **2004,** 39, (1), 65-70.

149. Karman, F. H.; Felhosi, I.; Kalman, E.; Cserny, I.; Kover, L., The role of oxide layer formation during corrosion inhibition of mild steel in neutral aqueous media. *Electrochimica Acta* **1998,** 43, (1-2), 69-75.

150. Laibinis, P. E.; Whitesides, G. M., Self-assembled monolayers of n-alkanethiolates on copper are barrier films that protect the metal against oxidation by air. *J. Am. Chem. Soc.* **1992,** 114, (23), 9022-9028.

151. Ma, H. Y.; Yang, C.; Chen, S. H.; Jiao, Y. L.; Huang, S. X.; Li, D. G.; Luo, J. L., Electrochemical investigation of dynamic interfacial processes at 1-octadecanethiol-modified copper electrodes in halide-containing solutions. *Electrochimica Acta* **2003,** 48, 4277-4289.

152. Cecchet, F.; DeMeersman, B.; Demoustier-Champagne, S.; Nysten, B.; Jonas, A. M., One Step Growth of Protein Antifouling Surfaces: Monolayers of Poly(ethylene oxide) (PEO) Derivatives on Oxidized and Hydrogen-Passivated Silicon Surfaces. *Langmuir* **2006,** 22, (3), 1173-1181.

153. Mekhalif, Z.; Lazarescu, A.; Hevesi, L.; Pireaux, J.-J.; Delhalle, J., Self-assembled monolayers of n-hexanethiol and 6-[2',5'-di(2''-thienyl)pyrrol-1'-yl] hexanethiol on polycrystalline nickel substrates. *J. Mater. Chem.* **1998,** 8, (3), 545-551.

154. Lee, Y.; Morales, G. M.; Yu, L., Self-Assembled Monolayers of Isocyanides on Nickel Electrodes. *Angew. Chem. Int. Ed.* **2005,** 44, 2-5.

155. Mekhalif, Z.; Delhalle, J.; Pireaux, J.-J. N., S.; Houze, F.; Boyer, L., Surface modifications of nickel substrates with self-assembled monolayers of alkanethiols for electrical contact applications. *Surface & coating technology* **1998,** 100-101, 463-468.

156. Fendler, J. H., Chemical Self-Assembly for Electronic Applications. *Chem. Mater.* **2001,** 13, 3196-3210.

157. Tivanski, A. V.; Walker, G. C., Ferrocenylundecanethiol Self-Assembled

Monolayer Charging Correlates with Negative Differential Resistance Measured by Conducting Probe Atomic Force Microscopy. *J. Am. Chem. Soc.* **2005,** 127, 7647-7653.

158. Martin, P.; Marsaudon, S.; Thomas, L.; Desbat, B.; Aime, J.-P.; Bennetau, B., Liquid Mechanical Behavior of Mixed Monolayers of Amino and Alkyl Silanes by Atomic Force Microscopy. *Langmuir* **2005,** 21, (15), 6934 -6943.

159. Chan, Y.-H. M.; Schweiss, R.; Werner, C.; Grunze, M., Electrokinetic Characterization of Oligo- and Poly(ethylene glycol)-Terminated Self-Assembled Monolayers on Gold and Glass Surfaces. *Langmuir* **2003,** 19, (18), 7380-7385.

160. Higashi, N.; Takahashi, M.; Niwa, M., Immobilization of DNA through Intercalation at Self-Assembled Monolayers on Gold. *Langmuir* **1999,** 15, (1), 111-115.

161. Lee, C.-Y.; Gong, P.; Harbers, G. M.; Grainger, D. W.; Castner, D. G.; Gamble, L. J., Surface Coverage and Structure of Mixed DNA/Alkylthiol Monolayers on Gold: Characterization by XPS, NEXAFS, and Fluorescence Intensity Measurements. *Anal. Chem.* **2006,** 78, (10), 3316-3325.

162. D.F., W.; Black, J.; Doherty, P. J., Consensus report of second conference on definitions in biomaterials. Biomaterial-tissue interfaces. In ed.; Elsevier: Amsterdam, 1992; Vol. 10, p 525-533.

163. McPherson, T. B.; Shim, H. S.; Park, K., Grafting of PEO to glass, nitinol, and pyrolytic carbon surfaces by gamma irradiation. *Journal of Biomedical Materials Research* **1997,** 38, (4), 289-302.

164. Jon, S. Y.; Seong, J. H.; Khademhosseini, A.; Tran, T. N. T.; Laibinis, P. E.; Langer, R., Construction of nonbiofouling surfaces by polymeric self-assembled monolayers. *Langmuir* **2003,** 19, (24), 9989-9993.

165. Wynblatt, P., Rohrer, G.S., Papillon, F., Grain Boundary Segregation in Oxide Ceramics. *Journal of European Ceramic Society* **2003,** 23, 2841-2848.

166. Filip, P.; Lausmaa, J.; Musialek, J.; Mazanec, K., Structure and surface of TiNi human implants. *Biomaterials* **2001,** 22, (15), 2131-2138.

167. Huang, H. H., Surface characterizations and corrosion resistance of nickel-titanium orthodontic archwires in artificial saliva of various degrees of acidity. *Journal of Biomedical Materials Research Part A* **2005,** 74A, (4), 629-639.

168. Van Alsten, J. G., Self-Assembled Monolayers on Engineering Metals: Structure, Derivatization, and Utility. *Langmuir* **1999,** 15, (22), 7605-7614.

169. Helses, J. A.; Breme, H. J., Metals as Biomaterials. In ed.; Engineering, W. S. i. B. S. a., England, 1998; p 1-3, 26-31.

170. Rondelli, G., Corrosion resistance tests on NiTi shape memory alloy. *Biomaterials* **1996,** 17, (20), 2003-2008.

171. Bogdanski, D.; Köller, M.; Müller, D.; Muhr, G.; Bram, M.; Buchkremer, H. P.; Stöver, D.; Choi, J.; Epple, M., Easy assessment of the biocompatibility of Ni–Ti alloys by in vitro cell culture experiments on a functionally graded Ni–NiTi–Ti. *Biomaterials* **2002,** 23, 4549-4555.

172. Chen, M. F.; Yang, X. J.; Hu, R. X.; Cui, Z. D.; Man, H. C., Bioactive NiTi shape memory alloy used as bone bonding implants. *Materials Science & Engineering C-Biomimetic and Supramolecular Systems* **2004,** 24, (4), 497-502.

173. Kidane, A. G.; Salacinski, H.; Tiwari, A.; Bruckdorfer, K. R.; Seifalian, A. M., Anticoagulant and Antiplatelet Agents: Their Clinical and Device Application(s) Together with Usages to Engineer Surfaces. *Biomacromolecules* **2004,** 5, (3), 798-813.

174. Chapman, R. G.; Ostuni, E.; Liang, M. N.; Meluleni, G.; Kim, E.; Yan, L.; Pier, G.; Warren, H. S.; Whitesides, G. M., Polymeric Thin Films That Resist the Adsorption of Proteins and the Adhesion of Bacteria. *Langmuir* **2001,** 17, (4), 1225-1233.

175. Lestelius, M.; Liedberg, B.; Tengvall, P., In Vitro Plasma Protein Adsorption on ù-Functionalized Alkanethiolate Self-Assembled Monolayers. *Langmuir* **1997,** 13, (22), 5900-5908.

176. Dee, K. C.; Puleo, D. A.; Bizios, R., *An Introduction to Tissue-Biomaterial Interactions*. John Wiley & Sons, Inc: New Jersey, 2002; p 228.

177. Kapanen, A.; Ryhänen, J.; Danilov, A.; Tuukkanen, J., Effect of nickel-titanium shape memory metal alloy on bone formation. *Biomaterials* **2001,** 22, (18), 2475-2480.

178. Shabalovskaya, S. A., Physicochemical and biological aspects of Nitinol as a biomaterial. *International Materials Reviews* **2001,** 46, (5), 233-250.

179. Shabalovskaya, S. A., Surface, corrosion and biocompatibility aspects of Nitinol as an implant material. *Bio-Medical Materials and Engineering* **2002,** 12, (1), 69-109.

180. Trepanier, C.; Pelton, A. R. *Biocompatibility and corrosion resistance of NiTi*; Cordis-NDc: Fremont, CA, p 9.

181. Ryhänen, J. Biocompatibility evaluation nickel-titanium shape metal alloy. University hospital of Oulu, Oulu, 1999.

182. Ryhänen, J.; Kallioinen, M.; Tuukkanen, J.; Lehenkari, P.; Junila, J.; Niemela, E.; Sandvik, P.; Serlo, W., Bone modeling and cell-material interface responses induced by nickel-titanium shape memory alloy after periosteal implantation. *Biomaterials* **1999,** 20, (14), 1309-1317.

183. Ryhänen, J.; Niemi, E.; Serlo, W.; Niemela, E.; Sandvik, P.; Pernu, H.; Salo, T.,

Biocompatibility of nickel-titanium shape memory metal and its corrosion behavior in human cell cultures. *Journal of Biomedical Materials Research* **1997,** 35, (4), 451-457.

184. Shih, C. C.; Lin, S. J.; Chen, Y. L.; Su, Y. Y.; Lai, S. T.; Wu, G. J.; Kwok, C. F.; Chung, K. H., The cytotoxicity of corrosion products of nitinol stent wire on cultured smooth muscle cells. *Journal of Biomedical Materials Research* **2000,** 52, (2), 395-403.

185. Firstov, G. S.; Vitchev, R. G.; Kumar, H.; Blanpain, B.; Humbeeck, J. V., Surface oxidation of NiTi shape memory alloy. *Biomaterials* **2002,** 23, 4863-4871.

186. Dieter Stöckel, C. *Nitinol - Material with Unusual Properties*; Johnson & Johnson Company: p 7.

187. Trigwell, S.; Hayden, R. D.; Nelson, K. F.; Selvaduray, G., Effects of surface treatment on the surface chemistry of NiTi alloy for biomedical applications. *Surf. Interface Anal.* **1998,** 26, (7), 483-489.

188. Tietze, H.; Muellner, M.; Selgert, P., Temperature-induced precipitations in the memory alloy nickel-titanium. *Journal of Physics D: Applied Physics* **1984,** 17, (7), 1391-8.

189. Robertson, S. W.; Imbeni, V.; Wenk, H. R.; Ritchie, R. O., Crystallographic texture for tube and plate of the superelastic/shape-memory alloy Nitinol used for endovascular stents (vol 41, pg 621, 2006). *Journal of Biomedical Materials Research Part A* **2006,** 78A, (2), 432-432.

190. Plant, S. D.; Grant, D. M.; Leach, L., Behaviour of human endothelial cells on surface modified NiTi alloy. *Biomaterials* **2005,** 26, (26), 5359-5367.

191. Ryhänen, J., Biocompatibility of Nitinol. *Minimally Invasive Therapy & Allied Technologies* **2000,** 9, (2), 99-105.

192. Robertson, S. W.; Imbeni, V.; Wenk, H.-R.; Ritchie, R. O., Crystallographic texture for tube and plate of the superelastic/shape-memory alloy nitinol used for endovascular stents. *Journal of Biomedical Materials Research Part A* **2005,** 72A, (2), 190-199.

193. Dai, Z.; Liu, M.; Xing, L.; Yue, X.; Ma, F.; Ren, N., Stabilized Hemocompatible Coating of Nitinol Devices Based on Photo-Cross-Linked Alginate/Heparin Multilayer. *Langmuir* **2007,** 23, (18), 9378-9385.

194. Richert, L.; Boulmedais, F.; Lavalle, P.; Mutterer, J.; Ferreux, E.; Decher, G.; Schaaf, P.; Voegel, J.-C.; Picart, C., Improvement of Stability and Cell Adhesion Properties of Polyelectrolyte Multilayer Films by Chemical Cross-Linking. *Biomacromolecules* **2004,** 5, 284-294.

195. Green, S. M.; Grant, D. M.; Wood, J. V., XPS Characterization of surface modified Ni-Ti shape memory alloy. *Materials Science & Engineering A* **1997,** 224, (1-2), 21-26.

196. Lipscomb, I. P.; Nokes, L. D. M., *The Application of Shape Memory Alloys in Medicine*. 1st ed.; Paston Press Ltd: London, Norfolk, 1996; p 153.

197. Shabalovskaya, S.; Rondelli, G.; Anderegg, J.; Simpson, B.; Budko, S., Effect of Chemical Etching and Aging in Boiling Water on the Corrosion Resistance of Nitinol Wires with Black Oxide Resulting
from Manufacturing Process. *J Biomed Mater Res Part B: Appl Biomater* **2003,** 66B, 331–340.

198. Clarke, B.; Carroll, W.; Rochev, Y.; Hynes, M.; Bradley, D.; Plumley, D., Influence of nitinol wire surface treatment on oxide thickness and composition and its subsequent effect on corrosion resistance and nickel release. *Journal of Biomedical Materials Research Part A* **2006,** 79A, 61-70.

199. Shevchenko, N.; Pham, M. T.; Maitz, M. F., Studies of surface modified NiTi alloy. *Applied Surface Science* **2004,** 235, (1-2), 126-131.

200. Cheng, Y.; Zheng, Y. F., Effect of N-2/Ar gas flow ratio on the deposition of TiN/Ti coatings on NiTi shape memory alloy by PIIID. *Materials Letters* **2006,** 60, (17-18), 2243-2247.

201. Michiardi, A.; Aparicio, C.; Planell, J. A.; Gil, F. J., Electrochemical behavior of oxidized NiTi shape memory alloys for biomedical applications. *Surface & Coatings Technology* **2007,** 201, 6484-6488.

202. Armitage, D. A.; Grant, D. M., Characterisation of surface-modified nickel titanium alloys. *Materials Science & Engineering A* **2003,** 349, (1-2), 89-97.

203. Luo, P. F.; Kuwana, T.; Paul, D. K.; Sherwood, P. M. A., Electrochemical and XPS Study of the Nickel-Titanium Electrode Surface. *Anal. Chem.* **1996,** 68, (19), 3330-3337.

204. Hoffmann, E. d.; Stroobant, V., *Mass Spectrometry. Principles and Applications*. 2nd ed.; John Wiley & Sons, ltd: 2002; p 407.

205. Shen, J.; Ahmed, T.; Vogt, A.; Wang, J.; Severin, J.; Smith, R.; Dorwin, S.; Johnson, R.; Harlan, J.; Holzman, T., Preparation and characterization of nitrilotriacetic-acid-terminated Self-Assembled Monolayers on gold surfaces for matrix-assisted laser desorption ionization-time of flight-mass spectrometry analysis of proteins and peptides. *Anal. Biochem.* **2005,** 345, 258-269.

206. Xu, Y.; Bruening, M. L.; Watson, J. T., Use of Polymer-modified MALDI-MS probes to improve analyses of protein digests and DNA. *Anal. Chem.* **2004,** 76, 3106-3111.

207. Xu, Y.; Watson, T.; Bruening, M. L., Patterned Monolayer/Polymer films for

analysis of dilute or salt-contaminated protein samples by MALDI-MS. *Anal. Chem.* **2003,** 75, 185-190.

208. Hanley, L.; Kornienko, O.; Ada, E. T.; Fuoco, E.; Trevor, J. L., Surface Mass Spectrometry of Molecular Species. *Journal of Mass Spectrometry* **1999,** 34, 705-723.

209. Xu, P.; Kumar, J.; Samuelson, L.; Cholli, A. L., Monitoring the Enzymatic Polymerization of 4-Phenylphenol by Matrix-Assisted Laser Desorption Ionization Time-of-Flight Mass Spectrommetry: A novel approach. *Biomacromolecules* **2002,** 2, 889-893.

210. Su, J.; Mrksich, M., Using Mass Spectrometry to Characterize Self-Assembled Monolayers presenting peptides, proteins and carbohydrates. *Angew. Chem. Int. Ed* **2002,** 41, (24), 4715-4718.

211. Guo, Z.; Zhang, Q.; Zou, H.; Guo, B.; Ni, J., A Method for the Analysis of Low-Mass Molecules by MALDI-TOF Mass Spectrometry. *Anal. Chem.* **2002,** 74, 1637-1641.

212. Jun, Y.; Zhu, X.-Y.; Hsu, J. W. P., Formation of alkanethiol and alkanedithiol monolayers on GaAs(001). *Langmuir* **2006,** 22, (8), 3627-3632.

213. Haga, M.-a.; Hong, H.-G.; Shiozawa, Y. K., Y. ; Monjushiro, H.; Fukuo, T.; Arakawa, R., Synthesis and Proton-Coupled Electron-Transfer Reaction of Self-Assembled Monolayers of a Ruthenium(II) Complex Containing Tridentate 2,6-Bis(benzimidazol-2-yl)pyridine on a Gold Surface: Comparison of Acid/Base Chemistry with Bulk Solution Chemistry. *Inorg. Chem.* **2000,** 39, 4566-4573.

214. Hortin, G. L., The MALDI TOF Mass Spectrometric View of the Plasma Proteome and Peptidome. *Clinical Chemistry* **2006,** 52:7, 1-13.

215. Chechik, V.; Crooks, R. M.; Stirling, C. J. M., Reactions and Reactivity in Self-Assembled Monolayers. *Advanced Materials* **2000,** 12, (16), 1161 - 1171.

216. McCafferty, E.; Wightman, J. P., Determination of the Concentration of Surface Hydroxyl groups on metal oxide films by a Quantitative XPS method. *Surf. Interface Anal.* **1998,** 26, 549-564.

217. Yan, C.; Zharnikov, M.; Gölzhäuser, A.; Grunze, M., Preparation and Characterization of Self-Assembled Monolayers on Indium Tin Oxide. *Langmuir* **2000,** 16, 6208-6215.

218. Han, S. W.; Ha, T. H.; Kim, C. H.; Kim, K., Self-Assembly of Anthraquinone-2-carboxylic Acid on Silver: Fourier Transform Infrared Spectroscopy, Ellipsometry, Quartz Crystal Microbalance, and Atomic Force Microscopy Study. *Langmuir* **1998,** 14, (21), 6113-6120.

219. Mark, S. S.; Sandhyarani, N.; Zhu, C.; Campagnolo, C.; Batt, C. A., Dendrimer-Functionalized Self-Assembled Monolayers as a Surface Plasmon Resonance Sensor Surface. *Langmuir* **2004,** 20, (16), 6808-6817.

220. Dubey, M.; Gouzman, I.; Bernasek, S. L.; Schwartz, J., Characterization of Self-Assembled Organic Films Using Differential Charging in X-ray Photoelectron Spectroscopy. *Langmuir* **2006,** 22, (10), 4649-4653.

221. Beulen, M. W. J.; Huisman, B.-H.; van der Heijden, P. A.; van Veggel, F. C. J. M.; Simons, M. G.; Biemond, E. M. E. F.; de Lange, P. J.; Reinhoudt, D. N., Evidence for Nondestructive Adsorption of Dialkyl Sulfides on Gold. *Langmuir* **1996,** 12, (26), 6170-6172.

222. Wong, S. C. C.; Lockyer, N. P.; Vickerman, J. C., Mechanisms of secondary ion emission from self-assembled monolayers and multilayers. *Surf. Interface Anal.* **2005,** 37, (9), 721-730.

223. Bruice, P. Y., *Organic Chemistry*. 2nd ed.; Upper Saddle River, NJ, 1998.

224. Li, J.; Thiara, P. S.; Mrksich, M., Rapid Evaluation and Screening of Interfacial Reactions on Self-Assembled Monolayers. *Langmuir* **2007,** 23, (23), 11826-11835.

225. Helmy, R.; Fadeev, A. Y., Self-Assembled Monolayers supported on TiO_2: Comparison of $C_{18}H_{37}SiX_3$ (X=H, Cl, OCH_3), $C_{18}H_{37}Si(CH_3)_2Cl$ and $C_{18}H_{37}PO(OH)_2$. *Langmuir* **2002,** 18, 8924-8928.

226. Marcinko, S.; Fadeev, A. Y., Hydrolytic Stability of Organic Monolayers supported on TiO_2 and ZrO_2. *Langmuir* **2004,** 20, (6), 2270-2273.

227. Sayago, D. I.; Polcik, M.; Lindsay, R.; Toomes, R. L.; Hoeft, J. T.; Kittel, M.; Woodruff, D. P., Structure determination of Formic acid reaction products on TiO_2 (110). *J. Phys. Chem. B* **2004,** 108, 14316-14323.

228. Ramachandran, S.; Tsai, B.-L.; Blanco, M.; Chen, H.; Tang, Y.; Goddard, W. A., III, Self-Assembled Monolayer Mechanism for Corrosion Inhibition of Iron by Imidazolines. *Langmuir* **1996,** 12, (26), 6419-6428.

229. Shustak, G.; Domb, A. J.; Mandler, D., n-Alkanoic Acid Monolayers on 316L Stainless Steel Promote the Adhesion of Electropolymerized Polypyrrole Films. *Langmuir* **2006,** 22, (12), 5237-5240.

230. Griep-Raming, N.; Karger, M.; Menzel, H., Using Benzophenone-Functionalized Phosphonic Acid to Attach thin polymer films to Titanium surfaces. *Langmuir* **2004,** 20, 11811-11814.

231. Brovelli, D.; Hahner, G.; Ruiz, L.; Hofer, R.; Kraus, G.; Waldner, A.; Schlosser, J.; Oroszlan, P.; Ehrat, M.; Spencer, N. D., Highly Oriented, Self-Assembled Alkanephosphate Monolayers on Tantalum(V) Oxide Surfaces. *Langmuir* **1999,** 15, (13),

4324-4327.

232. Adams, K. M.; Johnson, M. E. In *Detection of Fatty Amides and Fatty Acids with MALDI and Electrospray Mass Spectrometry*, Pittcon, Orlando, Fl, 03/14/2006. Orlando, Fl, 2006.

233. Dinca, V. C.; Soare, S.; Barbalat, A.; Dinu, C. Z.; Moldovan, A.; Stoica, I.; Vassu, T.; Purice, A.; Scarisoareanu, N.; al., R. B. e., Nickel–titanium alloy: Cytotoxicity evaluation on microorganism culture. *Applied Surface Science* **2006,** 252, 4619-4624.

234. Gabet, Y.; Mueller, R.; Levy, J.; Dimarchi, R.; Chorev, M.; Bab, I.; Kohavi, D., Parathyroid hormone 1-34 enhances titanium implant anchorage in low-density trabecular bone: a correlative micro-computed tomographic and biomechanical analysis. *Bone* **2006,** 39, (2), 276-282.

235. Bain, C. D.; Whitesides, G. M., Molecular-Level Control over Surface Order in Self-Assembled Monolayer Films of Thiols on Gold. *Science* **1987,** 40, 62-63.

236. Aqua, T.; Cohen, H.; Vilan, A.; Naaman, R., Long-Range Substrate Effects on the Stability and Reactivity of Thiolated Self-Assembled Monolayers. *J. Phys. Chem. C* **2007,** 111, (44), 16313-16318.

237. Mekhalif, Z.; Riga, J.; Pireaux, J.-J.; Delhalle, J., Self-Assembled Monolayers of n-Dodecanethiol on Electrochemically Modified Polycrystalline Nickel Surfaces. *Langmuir* **1997,** 13, 2285-2290.

238. Wanunu, M.; Livne, S.; Vaskevich, A.; Rubinstein, I., Assembly of Coordination Nanostructures via Ligand Derivatization of Oxide Surfaces. *Langmuir* **2006,** 22, (5), 2130-2135.

239. Pellerite, M. J.; Dunbar, T. D.; Boardman, L. D.; Wood, E. J., Effects of

Fluorination on Self-Assembled Monolayer Formation from Alkanephosphonic Acids on Aluminum: Kinetics and Structure. *J. Phys. Chem. B.* **2003,** 107, (42), 11726-11736.

240. Putvinski, T. M.; Schilling, M. L.; Katz, H. E.; Chidsey, C. E. D.; Mujsce, A. M.; Emerson, A. B., Self-assembly of organic multilayers with polar order using zirconium phosphate bonding between layers. *Langmuir* **1990,** 6, (10), 1567-1571.

241. Bakiamoh, S. B.; Blanchard, G. J., Surface Second Harmonic Generation from Asymmetric Multilayer Assemblies: Gaining Insight into Layer-Dependent Order. *Langmuir* **2001,** 17, (11), 3438-3446.

242. Hanson, E.; Schwartz, J.; Nickel, B.; N., K.; Danisman, M. F., Bonding Self-Assembled, Compact Organophosphate Monolayers to the Native Oxide. *J. Am. Chem. Soc.* **2003,** 125, 16074-16080.

243. Jerome Workman, J.; Koch, M.; Veltkamp, D. J., Process Analytical chemistry. *Anal. Chem.* **2003,** 75, 2859-2876.

244. Faucheux, A.; Gouget-Laemmel, A. C.; Villeneuve, C. H. d.; Boukherroub, R.; Ozanam, F.; Allongue, P.; Chazalviel, J.-N., Well-Defined Carboxyl-Terminated Alkyl Monolayers Grafted onto H-Si(111): Packing Density from a combined AFM and Quantitative IR Study. *Langmuir* **2006,** 22, 153-162.

245. Voue, M.; Rioboo, R.; Adao, M. H.; Conti, J.; Bondar, A. I.; Ivanov, D. A.; Blake, T. D.; DeConinck, J., Contact-Line Friction of Liquid Drops on Self-Assembled Monolayers: Chain-Length Effects. *Langmuir* **2007,** 23, (9), 4695-4699.

246. Ishizaki, T.; Saito, N.; SunHyung, L.; Ishida, K.; Takai, O., Study of Alkyl Organic Monolayers with Different Molecular Chain Lengths Directly Attached to Silicon. *Langmuir* **2006,** 22, 9962-9966.

247. Xiao, X.; Hu, J.; Charych, D. H.; Salmeron, M., Chain Length Dependence of the Frictional Properties of Alkylsilane Molecules Self-Assembled on Mica Studied by Atomic Force Microscopy. *Langmuir* **1996,** 12, 235-237.

248. Tao, F.; Goswami, J.; Bernasek, S. L., Self-Assembly and Odd-Even Effects of cis-Unsaturated Carboxylic Acids on Highly Oriented Pyrolytic Graphite. *J. Phys. Chem. B.* **2006,** 110, 4199-4206.

249. Saupe, G. B.; Mallouk, T. E.; Kim, W.; Schmehl, R. H., Visible Light Photolysis of Hydrogen Iodide Using Sensitized Layered Metal Oxide Semiconductors: The Role of Surface Chemical Modification in Controlling Back Electron Transfer Reactions. *J. Phys. Chem. B.* **1997,** 101, 2508-2513.

250. Jennings, G. K. M., Jeffrey C.; Yong, Tesh-Hwan; Laibinis, Paul E., Effect of Chain Length on the Protection of Copper by n-Alkanethiols. *Langmuir* **1998,** 14, (11), 6130-6139.

251. O'Donnell, A.; Yach, K.; Reven, L., Particle-Particle Interactions and Chain Dynamics of Fluorocarbon and Hydrocarbon Functionalized ZrO2 Nanoparticles. *Langmuir* **2008,** 24, (6), 2465-2471.

252. Skulason, H. F., C. D., Detection of Discrete Interactions upon Rupture of Au Microcontacts to Self-Assembled Monolayers Terminated with -S(CO)CH3 or -SH. *J. Am. Chem. Soc.* **2000,** 122, (40), 9750-9760.

253. Coates, J., *Interpretation of Infrared Spectra, A Practical Approach*. ed.; John Wiley 7 Sons Ltd: Netown, USA.

254. Danahy, M. P.; Avaltroni, M. J.; Midwood, K. S.; Schwarzbauer, J. E.; Schwartz, J., Self-assembled Monolayers of α,ω−Diphosphonic Acids on Ti Enable Complete or

Spatially Controlled Surface Derivatization. *Langmuir* **2004,** 20, (13), 5333-5337.

255. Noel, O.; Brogly, M.; Castelein, G.; Schultz, J., In Situ Determination of the Thermodynamic Surface Properties of Chemically Modified Surfaces on a Local Scale: An Attempt with the Atomic Force Microscope. *Langmuir* **2004,** 20, (7), 2707-2712.

256. Mingyan, H.; Blum, A. S.; Aston, E.; Buenviaje, C.; Overney, R. M.; Luginbuhl, R., Critical phenomena of water bridges in nanoasperity contacts. *J. Chem. Phys.* **2001,** 114, 1355-1360.

257. Neves, B. R. A.; Salmon, M. E.; Russell, P. E.; E. B. Troughton, J., Spread coating of OPA on Mica: From Multilayers to Self-Assembled Monolayers. *Langmuir* **2001,** 17, 8193-8198.

258. Taylor, C. E.; Schwartz, D. K., Octadecanoic Acid Self-Assembled Monolayer Growth at Sapphire Surfaces. *Langmuir* **2003,** 19, (7), 2665-2672.

259. Gao, L.; McCarthy, T. J., Contact Angle Hysteresis Explained. *Langmuir* **2006,** 22, 6234-6237.

260. Li, D.; Chen, S.; Zhao, S.; Ma, H., The corrosion inhibition of the self-assembled Au, and Ag nanoparticles films on the surface of copper. *Colloid and Surfaces A: Physicochem. Eng. Aspects* **2006,** 273, 16-23.

261. Whitesides, C. D. B. G. M., Molecular-Level Control over Surface Order in Self-Assembled Monolayer Films of Thiols on Gold. *Science* **1987,** 40, 62-63.

262. Poczik, P.; Felhosi, I.; Telegdi, J.; Kalaji, M.; Kalman, E., Layer formation by 1,7-diphosphono-heptane. *J.Serb.Chem.Soc.* **2001,** 66, (11–12), 859–870.

263. Gao, W.; Dickinson, L.; Grozinger, C.; Morin, F. G.; Reven, L., Self-Assembled Monolayers of Alkylphosphonic Acids on Metal Oxides. *Langmuir* **1996,** 12, 6429-6435.

264. Hoque, E.; DeRose, J. A.; Hoffmann, P.; Mathieu, H. J.; Bhushan, B.; Cichomski, M., Phosphonate self-assembled monolayers on aluminum surfaces. *Journal of Chemical Physics* **2006,** 124, (17), 174710/1-174710/6.

265. Bhushan, B.; Cichomski, M.; Hoque, E.; DeRose, J. A.; Hoffmann, P.; Mathieu, H. J., Nanotribological characterization of perfluoroalkylphosphonate self-assembled monolayers deposited on aluminum-coated silicon substrates. *Microsyst. Technol* **2006,** 12, 588-596.

266. Hoque, E.; DeRose, J. A.; Hoffmann, P.; Bhushan, B.; Mathieu, H. J., Alkylperfluorosilane Self-Assembled Monolayers on Aluminum: A Comparison with Alkylphosphonate Self-Assembled Monolayers. *J. Phys. Chem. C* **2007,** 111, (10), 3956-3962.

267. Mekhalif, Z.; Laffineur, F.; Couturier, N.; Delhalle, J., Elaboration of Self-Assembled Monolayers of n-Alkanethiols on Nickel Polycrystalline Substrates: Time, Concentration and Solvent Effects. *Langmuir* **2003,** 19, 637-645.

268. Wallace, R. M.; Chen, P. J.; Henck, S. A.; Webb, D. A., Adsorption of perfluorinated n-alkanoic acids on native aluminum oxide surfaces. *J. Vac. Sci. Technol. A* **1995,** 13, (3), 1345-1350.

269. Smith, D. A.; Wallwork, M. L.; Zhang, J.; Kirkham, J.; Robinson, C.; Marsh, A.; Wong, M., The Effect of Electrolyte Concentration on the Chemical Force Titration Behavior of ω-Functionalized SAMs: Evidence for the Formation of Strong Ionic Hydrogen Bonds. *J. Phys. Chem. B* **2000,** 104, (37), 8862-8870.

270. Zhang, J.; Kirkham, J.; Robinson, C.; Wallwork, M. L.; Smith, D. A.; Marsh, A.; Wong, M., Determination of the Ionization State of 11-Thioundecyl-1-phosphonic Acid

in Self-Assembled Monolayers by Chemical Force Microscopy. *Anal. Chem.* **2000,** 72, (9), 1973-1978.

271. Liakos, I. L.; Newman, R. C.; McAlpine, E.; Alexander, M. R., Comparative study of self-assembly of a range of monofunctional aliphatic molecules on magnetron-sputtered aluminium. *Surf.Interface Anal.* **2004,** 36, 347-354.

272. Reichelt, A.; Gaul, C.; Frey, R. R.; Kennedy, A.; Martin, S. F., Design, Synthesis, and Evaluation of Matrix Metalloprotease Inhibitors Bearing Cyclopropane-Derived Peptidomimetics as P1' and P2' Replacements. *J. Org. Chem.* **2002,** 67, (12), 4062-4075.

273. De Luca, L.; Giacomelli, G.; Taddei, M., An Easy and Convenient Synthesis of Weinreb Amides and Hydroxamates. *J. Org. Chem.* **2001,** 66, (7), 2534-2537.

274. Xue, C.-B.; Voss, M. E.; Nelson, D. J.; Duan, J. J.-W.; Cherney, R. J.; Jacobson, I. C.; He, X.; Roderick, J.; Chen, L.; Corbett, R. L.; Wang, L.; Meyer, D. T.; Kennedy, K.; DeGrado, W. F.; Hardman, K. D.; Teleha, C. A.; Jaffee, B. D.; Liu, R.-Q.; Copeland, R. A.; Covington, M. B.; Christ, D. D.; Trzaskos, J. M.; Newton, R. C.; Magolda, R. L.; Wexler, R. R.; Decicco, C. P., Design, Synthesis, and Structure-Activity Relationships of Macrocyclic Hydroxamic Acids That Inhibit Tumor Necrosis Factor α Release in Vitro and in Vivo. *J. Med. Chem.* **2001,** 44, (16), 2636-2660.

275. Farkas, E.; Enyedy, E. A.; Csoka, H., Some factors affecting metal ion-monohydroxamate interactions in aqueous solution. *J. Inorg. Chem.* **2000,** 79, (1-4), 205-211.

276. Sreenivas, T.; Padmanabhan, N. P. H., Surface chemistry and flotation of cassiterite with alkyl hydroxamates. *Colloids and Surfaces, A: Physicochemical and Engineering Aspects* **2002,** 205, (1-2), 47-59.

277. Wirgau, J. I.; Crumbliss, A. L., Carrier-facilitated bulk liquid membrane transport of iron(III) hydroxamate complexes utilizing a labile recognition agent and amine recognition in the second coordination sphere. *Dalton Transactions* **2003,** 19, 3680-3685.

278. Morroni, L.; Secco, F.; Venturini, M.; Garcia, B.; Leal, J. M., Kinetics and Equilibria of the Interactions of Hydroxamic Acids with Gallium(III) and Indium(III). *Inorg. Chem.* **2004,** 43, (9), 3005-3012.

279. Bordwell, F. G.; Fried, H. E.; Hughes, D. L.; Lynch, T. Y.; Satish, A. V.; Whang, Y. E., Acidities of carboxamides, hydroxamic acids, carbohydrazides, benzenesulfonamides, and benzenesulfonohydrazides in DMSO solution. *J. Org. Chem.* **1990,** 55, (10), 3330-3336.

280. Bohm, S.; Exner, O., Acidity of hydroxamic acids and amides. *Org. Biomol. Chem.* **2003,** 1, 1176-1180.

281. Ventura, O. N.; Rama, J. B.; Turi, L.; Dannenberg, J. J., Acidity of hydroxamic acids: an ab initio and semiempirical study. *J. Am. Chem. Soc.* **1993,** 115, (13), 5754-61.

282. Kudelski, A., Raman and Electrochemical Characterization of 2-Mercaptoethanesulfonate Monolayers on Silver: A Comparison with Monolayers of 3-Mercaptopropionic Acid. *Langmuir* **2002,** 18, (12), 4741-4747.

283. Shon, Y.-S.; Wuelfing, W. P.; Murray, R. W., Water-Soluble, Sulfonic Acid-Functionalized, Monolayer-Protected Nanoparticles and an Ionically Conductive Molten Salt Containing Them. *Langmuir* **2001,** 17, (4), 1255-1261.

284. Langner, R.; Zundel, G., FT-IR Investigation of Polarizable, Strong Hydrogen Bonds in Sulfonic Acid Sulfoxide, Phosphine Oxide, and Arsine Oxide Complexes in the Middle- and Far-Infrared Region. *J. Phys. Chem.* **1995,** 99, (32), 12214-12219.

285. Boehner, U.; Zundel, G., Sulfonic acid-oxygen base systems as a function of the .Δ.pKa. *J. Phys. Chem.* **1985,** 89, (8), 1408-1413.

286. Kanicky, J. R.; Shah, D. O., Effect of degree, type, and position of unsaturation on the pKa of long-chain fatty acids. In *Submitted to special JCIS issue in honor of Prof. Somasundaran*, Gainesville, FL, 2000; p 2-14.

287. Yang, J.; Bremer, P. J.; Lamont, I. L.; McQuillan, J., Infrared Spectroscopic Studied of Siderophore-Related Hydroxamic Acid Ligands Adsorbed on Titanium Dioxide. *Langmuir* **2006,** 22, (24), 10109-10117.

288. Montalbetti, C. A. G. N.; Falque, V., Amide bond fromation and peptide coupling. *Tetrahedron* **2005,** 61, 10827 - 10852.

289. Sullivan, T. P.; Huck, W. T. S., Reactions on Monolayers: Organic synthesis in two dimensions. *Eur. J. Org. Chem.* **2003**, 17-29.

290. Ren, S.-L.; Yang, S.-R.; Wang, J.-Q.; Liu, W.-M.; Zhao, Y.-P., Preparation and Tribological Studies of Stearic Acid Self-Assembled Monolayers on Polymer-Coated Silicon Surface. *Chem. Mater.* **2004,** 16, (3), 428-434.

291. Lahiri, J.; Ostuni, E.; Whitesides, G. M., Patterning Ligands on Reactive SAMs by Microcontact Printing. *Langmuir* **1999,** 15, (6), 2055-2060.

292. Solanki, P. R.; Arya, S. K.; Nishimura, Y.; Iwamoto, M.; Malhotra, B. D., Cholesterol Biosensor Based on Amino-Undecanethiol Self-Assembled Monolayer Using Surface Plasmon Resonance Technique. *Langmuir* **2007,** 23, (13), 7398-7403.

293. Holzl, M.; Tinazli, A.; Leitner, C.; Hahn, C. D.; Lackner, B.; Tampe, R.; Gruber, H. J., Protein-Resistant Self-Assembled Monolayers on Gold with Latent Aldehyde Functions. *Langmuir* **2007,** 23, (10), 5571-5577.

294. Hu, K.; Bard, A. J., Use of Atomic Force Microscopy for the Study of Surface Acid-Base Properties of Carboxylic Acid-Terminated Self-Assembled Monolayers. *Langmuir* **1997,** 13, (19), 5114-5119.

295. Bernasek, S. L.; Schwartz, J., Monolayer Stabilization on Hydroxylated Aluminum Surfaces. *Langmuir* **1998,** 14, (6), 1367-1370.

296. Nakamura, R.; Takeuchi, R.; Kuramochi, K.; Mizushina, Y.; Ishimaru, C.; Takakusagi, Y.; Takemura, M.; Kobayashi, S.; Yoshida, H.; Sugawara, F.; Sakaguchi, K., Chemical properties of fatty acid derivatives as inhibitors of DNA polymerases. *Org. Biomol. Chem* **2007,** 5, 3912 - 3921.

297. Parks, G. A. *The isoelectric points of solid oxides, solid hydroxides, and aqueous hydroxo complex systems*; Department of Mineral Engineering, Stanford University: Stanford, CA, September 9, 1964, 1964; p 177-197.

298. Kallay, N.; Torbie, Z.; Golie, M.; Matijevie, E., Determination of the Isoelectric point of Several Metals by Adhesion Methos. *J. Phys. Chem.* **1991,** 95, 7028-7032.

299. Moriwaki, H.; Yoshikawa, Y.; Morimoto, T., Oxide films on iron and nickel ultrafine particles studied with zero point of charge measurements. *Langmuir* **1990,** 6, (4), 847-850.

300. Parks, G. A.; Bruyn, P. L. d., THE ZERO POINT OF CHARGE OF OXIDES. *J. Phys. Chem.* **1962,** 66, (6), 967-973.

301. Purvis, K. L.; Lu, G.; Schwartz, J.; Bernasek, S. L., Reaction of Tetra (tert-Butoxy) Tin or-Zirconium with Hydroxylated Titanium in Ultrahigh Vacuum: Contrasting Reactivity with Hydroxylated Aluminum Substrate. *Langmuir* **1999,** 15, 7092-7096.

302. Brown, T. L.; H. Eugene LeMay, J.; Bursten, B. E., *Chemistry: The central science*.

7th ed.; Prentice Hall: Upper Saddle River, NJ, 1997; p 982.

303. Schwartz, J.; Bernasek, S. L.; Lu, G., Oxidation of polycrystalline titanium surface by oxygen and water. *Surface Science* **2000,** 458, 80-90.

304. Everhart, J. L., *Engineering properties of nickel and nickel alloys*. Plenum Press: New York, 1971.

305. Guglielminotti, E.; Cerruti, L.; Borello, E., An infrared study of surface properties of nearly stoichiometric nickel oxide. I. Adsorption of water, carbon dioxide, pyridine and nitric oxide. *Gazzetta Chimica Italiana* **1977,** 107, 447-454.

306. Tsyganenko, A. A.; Filimonov, V. N., Infrared spectra of surface hydroxyl groups and crystalline structure of oxides. *Journal of Molecular Structures* **1973,** 19, 579-589.

307. Cotton, F. A.; Wilkinson, G.; Gaus, P. L., *Basic Inorganic Chemistry*. 3rd ed.; John Wiley & Sons, Inc: Canada, 1995; p 838.

308. Cappus, D.; Xu, C.; Ehrlich, D.; Dillman, B.; Jr., C. A. V.; Shamery, K. A., Hydroxyl groups on oxide surfaces: NiO (100), NiO (111) and Cr_2O_3 (111). *Chemical Physics* **1993,** 177, 533-546.

309. Langell, M. A.; Berrie, C. L.; Nassir, M. H.; Wulser, K. W., Adsorption of acetic acid on hydrolyzed NiO(111) thin films. *Surface Science* **1994,** 320, 25-38.

310. Massa, W., *Crystal Structure Determination*. 2nd ed.; Springer: Germany, 2004; p 210.

311. Jackson, C. M.; Wagner, H. J.; Wasilewski, R. J. *55-Nitinol-The alloy with a memory: Its Physical Metallurgy, Properties, and Applications*; NASA: Washington D. C, 1972; p 86.

312. Spori, D. M.; Venkataraman, N. V.; Tosatti, S. G. P.; Durmaz, F.; Spencer, N. D.;

Zurcher, S., Influence of Alkyl Chain Length on Phosphate Self-Assembled Monolayers. *Langmuir* **2007,** 23, (15), 8053-8060.

313. Levine, I. N., *Physical Chemistry*. 4th ed.; Mc Graw- Hill Co.: 1994; p 1002.

314. Yu, W. H.; Kang, E. T.; Neoh, K. G., Controlled Grafting of Comb Copolymer Brushes on Poly(tetrafluoroethylene) Films by Surface-Initiated Living Radical Polymerizations. *Langmuir* **2005,** 21, (1), 450-456.

315. Ista, L. K.; Mendez, S.; Perez-Luna, V. H.; Lopez, G. P., Synthesis of Poly(N-isopropylacrylamide) on Initiator-Modified Self-Assembled Monolayers. *Langmuir* **2001,** 17, (9), 2552-2555.

316. Roux, S.; Duwez, A.-S.; Demoustier-Champagne, S., Surface Initiated Polymerization of Styrene from a Carboxylic Acid Functionalized Polypyrrole Coated Electrode. *Langmuir* **2003,** 19, (2), 306-313.

317. Li, G.; Fan, J.; Jiang, R.; Gao, Y., Cross-linking the Linear Polymeric Chains in the ATRP Synthesis of Iron Oxide/Polystyrene Core/Shell Nanoparticles. *Chem. Mater.* **2004,** 16, (10), 1835-1837.

318. Prucker, O.; Ruhe, J., Synthesis of Poly(styrene) Monolayers Attached to High Surface Area Silica Gels through Self-Assembled Monolayers of Azo Initiators. *Macromolecules* **1998,** 31, (3), 592-601.

319. Schmidt, R.; Zhao, T.; Green, J.-B.; Dyer, D. J., Photoinitiated Polymerization of Styrene from Self-Assembled Monolayers on Gold. *Langmuir* **2002,** 18, (4), 1281-1287.

320. Zhang, J.; Han, Y., A Topography/ Chemical Composition Gradient Polystyrene Surface: Toward the Investigation of the Relationship between Surface Wettability and Surface Structure and Chemical Composition. *Langmuir* **2008,** 24, 796-801.

321. Takeshita, N.; Paradis, L. A.; Oner, D.; McCarthy, T. J.; Chen, W., Simultaneous Tailoring of Surface Topography and Chemical Structure for Controlled Wettability. *Langmuir* **2004,** 20, 8131-8136.

322. Bouafsoun, A.; Helali, S.; Mebarek, S.; Zeiller, C.; Prigent, A.-F.; Othmane, A.; Kerkeni, A.; Renault, N. J.; Ponsonnet, L., Electrical probing of endothelial cell behavior on a fibronectin/polystyrene/thiol/gold electrode by Faradaic electrochemical impedance spectroscopy (EIS). *Bioelectrochemistry* **2007,** 70, 401-407.

323. Janek, R. P.; Fawcett, W. R.; Ulman, A., Impedance Spectroscopy of Self-Assembled Monolayers on Au(111): Sodium Ferrocyanide Charge Transfer at Modified Electrodes. *Langmuir* **1998,** 14, (11), 3011-3018.

324. Abelev, E.; Starosvetsky, D.; Ein-Eli, Y., Enhanced Copper Surface Protection in Aqueous Solutions Containing Short-Chain Alkanoic Acid Potassium Salts. *Langmuir* **2007,** 23, (22), 11281-11288.

325. Xia, S. J.; Liu, G.; Birss, V. I., Properties of Thin Polystyrene Films Prepared on Gold Electrodes by the Dip-Coating Method. *Langmuir* **2000,** 16, 1379-1387.

326. Wang, W.; Malkinski, L.; Tang, J., Enhanced spin-dependent tunneling magnetoresistance in magnetite films coated by polystyrene. *Journal of Applied Physics* **2007,** 101, 09J504-1,09J504 -3.

327. Kulkarni, S. A.; Mulla, I. S.; Vijayamohanan, K., Electrochemical Characterization of Self-Assembled Monolayers on Semiconducting Substrates for MEMS Applications. *Journal of Physics: Conference Series* **2006,** 34, 322-329.

LIST OF ABBREVIATIONS

ABAP 2,2'-Azobis(2-Amidinopropane) Dihydrochloride

AFM Atomic Force Microscopy

Ag Silver

AP MALDI-TOF MS Atmospheric Pressure Matrix Assisted Laser Desorption Ionization-Time of Flight Mass Spectrometry

Au Gold

Auger Electron Spectroscopy AES

BPA Butylphosphonic Acid

CHCA α-Cyano-4-Hydroxycinnamic Acid

COOH-PA 12-Carboxydodecylphosphonic Acid

CV Cyclic Voltammetry

Da Daltons

di-COOH Tetradecanedioic acid

di-PA 1,12 Dodecyldiphosphonic Acid

DRIFT Diffuse Reflectance Infrared Fourier Transform Spectroscopy

EDC 1-Ethyl-3-(3-dimethylamino) Propylcarbodiimide

EI MS Electron Ionization Mass Spectrometry

EIS Electrochemical Impedance Spectroscopy

FTIR Fourier Transform Infrared Spectroscopy

HDCA Heptadecanoic Acid

IR Infrared Spectroscopy

ISS Ion Scattering Spectroscopy

LB Langmuir-Blodgett films

NiO Nickel Oxide

NiTi Nitinol

NMR Nuclear Magnetic Resonance Spectroscopy

ODHA Octadecanehydroxamic Acid

ODPA Octadecylphosphonic acid

ODSA Octadecanesulfonic Acid

16-OH 16-Hydroxyhexadecanoic Acid

OH-PA 11-Hydroxyundecylphosphonic Acid

OPA Octylphosphonic acid

OTS Octadecyltrichhlorosilane

PE Protection Efficiency

PEO Poly(ethylene Oxide)

PFA Perfluorooctadecanoic Acid

PFP Pentafluorophenol

R_{ct} Charge Transfer Resistance

rms root-mean-square-roughness

SAMs Self-Assembled Monolayers

SIP Surface-Initiated Free Radical Polymerization

SPR Surface Plasma Resonance

STM Scanning Tunneling Microscope

THF Tetrahydrofuran

TiO_2 Titanium dioxide

TOF-SIMS Time-of-flight secondary ion mass spectrometry

UPA Undecylphosphonic Acid

XPS X-ray Photoelectron Spectroscopy